Chapter 1

Introduction

The antenna or the aerial is a device for radiating or receiving electromagnetic waves. There is little fundamental difference between transmitting and receiving antennas, since very often the same antenna is used for both purposes as in radar [1].

A good antenna design would ensure that the antenna transmits maximum power in the direction of the intended receiver. However, this is usually not the case due to losses in power caused by lossy transmission line and the impedance of the antenna. Therefore impedance matching is one of the critical factors that need to be considered in antenna design.

1.1 Literature Survey

The concept of microstrip antennas was originally proposed by Deschamps in 1953[2]. However, it takes more than twenty years until Munson realized the first microstrip antenna [3]. In 1979 an antenna symposium held in New Mexico concerning the microstrip antennas. A collection of papers presented at this meeting appeared in a spatial issue of the IEEE Transactions on Antennas and Propagation [4]. One of the books that summarized the topic of microstrip antennas, and which is still a standard reference, was written by Bahl and Bhartia [5]. Other books that described the microstrip antenna are R.C. Johnson [6] and T. A. Milligan [7].

The above mentioned sources provide a broad knowledge in printed antennas, while the following publications focus on bandwidth enhancement techniques.

Two chapters (3 and 6) in Handbook of microstrip antennas [8] have described a part of the bandwidth enhancement. Chapter 3 has been reported by K.F. Lee and J.S.Dahele, which describes the characteristic of microstrip patch antennas and some methods of improving frequency agility and bandwidth. Chapter 6 has been reported by D.H. Schaubert, which describes the multilayer and parasitic configurations.

The recent trends in improving the impedance bandwidth of microstrip patch antennas can be broadly divided into the following categories [9]:

(i) Various geometries and perturbations to introduce multiple resonances as well as input impedance matching,

(ii) Genetic Algorithm (GA) based optimization of antenna geometries,

(iii) Photonic Band Gap (PBG) structures used as printed antenna substrates,

(iv) Frequency Selective Surfaces (FSS) used as multilayered substrate or ground plane.

The first category is the leading of all four categories in numbers and varieties and it.

Recently, a variety of suspended plate antennas (SPAs) has been presented and extensively investigated as alternatives for low profile, broadband applications. In general, the plate of a SPA is suspended over a ground plane at a height of ~0.1 times operating wavelength in free space. The medium between the plate and the ground plane is basically air or a substrate of very low relative permittivity. A coaxial probe feed is definitely a good option for the SPA because of the large spacing and the very low relative permittivity. Furthermore, to compensate for the large reactance due to the long probe in a broad frequency range, some impedance-matching techniques, such as slotting the plate, using a three-dimensional transition, electromagnetically coupling the plate, L-shape probe, and using the meandering probe, have been developed [10-14]. Up to know, the 2:1 VSWR impedance bandwidth of the SPAs have reached up to 10~40%. A large area for impedance bandwidth techniques will be discussed in details in Section 1.3.

1.2 Microstrip Antennas

A microstrip patch antenna consists of a very thin metallic patch placed at a small fraction of wavelength above a conducting ground-plane[5,15]. The patch and the ground-plane are separated by a dielectric. The patch is generally made of a conducting material such as copper or gold and can take any possible shape square, rectangular, circular, triangular, or some other shapes, but rectangular and circular (elliptic) patches cover all possibilities in terms of pattern, bandwidth and polarization [16]. Even in terms of gain they exhibit a great versatility due to a possible range from 4 to 10 dB. These basic patch configurations also show up with their simple analysis and performance prediction. The dielectric substrate is usually non-magnetic and low loss material. Due to the simple geometry of the MPA, the half-wave rectangular patch is the most commonly used microstrip antenna. It is characterized by its length L, width W and thickness h, as shown in Fig. 1.1(a). MPA can be fed (excited) by a variety of methods. The three most popular feed techniques used are the microstrip line, coaxial probe, and aperture coupling. In the presented work the coaxial feed technique of 50 Ω is used as shown in Fig. 1.1(b). Feeding by a coaxial probe has the advantages of easy to construct and match, reduce spurious feed radiation, and its structure is more suitable for lower frequency band or single patch due to the mechanical drilling and soldering[17,18]. It provides also a good isolation between feed network and radiating elements, and due to the direct contact with the radiator it reduces the dielectric layer misalignment difficulties. A drawback of this configuration it is not capable of producing a wideband due to its inductive reactance coming from the length of the probe [19]. This means that the probe acts like an additional (and of course unwanted) reactance at the feeding point.

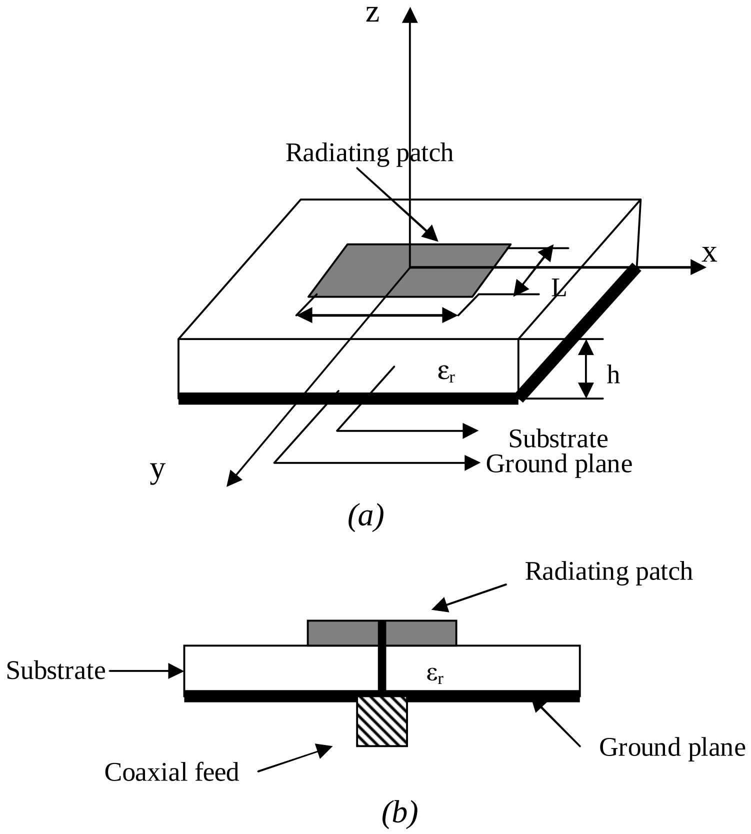

Figure (1.1) (a) Rectangular microstrip patch antenna (b) Side view

1.2.1 Advantages and Drawbacks of MPA

Although there is a tremendous number of an advantage of MPA, only the most important ones have been picked out: [5, 15]

• Light weight, low volume, low profile, and planar configuration which can be made conformal.

Printed circuits are thin and thus require less volume than their waveguide or coaxial counterparts. Due to the fact that printed antennas consist mainly of nonmetallic materials and due to the frequent use of foam materials as substrates, such antennas have an extremely low weight compared to conventional antennas.

• Polarization

With the versatility of patch geometries any polarization can be obtained. You can even realize antennas with multipolarization capability with single or multiple ports. These features can be exploited for dual polarization operation or polarization diversity.

•Dual frequency antenna possible

• Excitation technique

Patches allow a lot of different excitation techniques to be used, compatible with the technology of the active circuitry and beamforming networks.

• Suitable for integration with Microwave Integrated Circuits(MICs).

This is important, since MICs are much easier to handle and less expensive than the alternative methods.

Beside these numerous technological merits, there is also an important economic reason that makes microstrip antennas attractive: Printed antenna technology is suitable for low-cost manufacturing, because photo etching and press machining are the lowest cost technologies for large scale fabrications. The antenna may be easily mounted on missiles, rockets, and satellites without major alterations.

- Of course there are a few drawbacks: First of all there is a limitation in frequency. At low frequencies (~100 MHz), the need of a given thickness (in terms of λ) to achieve a high efficiency and bandwidth leads to bulky (but not heavy) radiators; at high frequencies, once more the (very small) thickness and manufacturing accuracy limit the capability for low-cost production.

- Microstrip antennas are narrowband antennas compared to conventional microwave antennas (typical bandwidth is from less than 1% to several percent for thin substrate). Nevertheless this drawback can be overcome by using many techniques (see Section 1.3) .
- Another fact is that the design engineer has always to keep an eye on losses (mainly dielectric and due to surface wave excitation), since this leads to deform the pattern and a lower gain and a lower efficiency. By selecting low loss-tangent substrates the dielectric losses will not be a serious issue anymore.

Finally, for many practical designs, the advantages of microstrip antennas far outweigh their disadvantages and so lead to many system applications, such as: [5]

• Mobile communications

•Satellite communications

• Remote sensing

• Doppler radar, automotive radar, etc.

1.3 Bandwidth Enhancement Techniques

The fundamental basic principles and their corresponding antenna geometries of broadband design of microstrip antennas can be listed as [9]:

i. Low Q-factor of the magnetic wall cavity under the patch:	Low dielectric constant or larger thickness of the substrate
ii. Multiple resonances:	Parasitic patches in stacked or planar geometry, Reactive loading by shaped slot, notch, cuts, pin or post.
iii. Impedance matching of the feed:	Probe compensation using series capacitor, L-shape probe or any reactive loading
iv. Optimization of patch geometry:	Very irregular and unconventional patch shape optimized using Genetic Algorithm.
v. Suppression of Surface waves in a thick substrate:	Periodic patterns on the ground plane or on any substrate produces Photonic Band Gap(PBG) structure on one face of which microstrip element or arrays are printed.
vi. Frequency dependent substrate or ground plane:	Multiple layers of Frequency Selective Surfaces (FSS) can reflect at respective frequency bands. For closely spaced the FSS combination act over a larger frequency range as pass band.
vii. Various combinations of (ii) and (iii)	

Large areas of bandwidth enhancement techniques will be explained in details as overview to thesis objective:

1.3.1 Thick Substrate and Low Dielectric Constant Technique

A general law for antennas states that the lowest achievable quality factor of an antenna is inversely related to the antenna volume. This implies that the absolute bandwidth increases with increasing patch substrate height (h/λ_o>0.1), since the bandwidth is in inverse proportion to the quality factor. However, this technique introduces various problems. A thicker substrate will support surface waves, which will deteriorate the radiation pattern as well as reduce the radiation efficiency. Also, problems with the feeding technique of the antenna appear. Additionally, depending upon the z-direction, higher order modes may arise, further distortions in the pattern and impedance characteristics [20,21]. The patch width has similar influence on the bandwidth like the substrate thickness. This comes from the fact that by increasing one of these parameters the volume of the antenna is increased.

Another important substrate parameter that influences the bandwidth is the permittivity. The bandwidth of a patch antenna increases with decreasing substrate permittivity. By using low dielectric constant and thick substrate (h/λ_o>0.1), the bandwidth can be reached 10% [22].

1.3.2 Coplanar and Stacked Configuration Technique

Another technique for improving the bandwidth is the parasitic technique. There are two configurations of the parasitic geometry: the coplanar geometry and the stacked geometry. The coplanar geometry consist of many patches incorporate coplanar on the dielectric substrate, and they are coupled to the main patch (only one patch has been excited) as shown in Fig. 1.2(a) [23]. For stacked geometry, the patch radiators are employed one above the other with intervening dielectric layers as shown in Fig. 1.2(b) [24-27].

This allows two or more resonant patches to share a common aperture area. The patches may be fed individually from microstrip lines or coaxial probes, only one or two may be fed directly while the others are coupled parasitically. The stacked dual-patch geometry in which only the lower patch is fed by a coaxial cable and the upper patch is excited electromagnetically from the lower patch has been studied in the presented work. As far as impedance bandwidth goes, Waterhouse [24] reported a 26% bandwidth for VSWR≤2.

The stacked patch configuration has a number of advantages over the coplanar configuration. Since it does not increase the surface area of the element, it can be used in array configurations without the danger of creating grating lobes. Its radiation patterns remain relatively constant over the operating frequency band. The stacked configuration are also possible with aperture coupled feeding, proximity feeding and coaxial feeding. The drawback of stacked patch configuration is that it has a large number of parameters which make the design and optimization process be very complex. Another drawback is that it requires more than one substrate layer to support the patches. Recently, the improved bandwidths of the stacked plate antennas have reached up to the order of 20 to 40 % for VSWR=2:1. There is also an additional methods used with stacked patches in order to increase the bandwidth further, such as slots [25], pin or short [28-30]. The structure in [25] has been proposed recently by P.K.Singhal.et.al where they have presented a novel probe fed stacked square patch slotted wideband microstrip antenna. An input impedance bandwidth of 76.25% for VSWR≤2 has been achieved. This bandwidth is achieved by using five slots in the lower patch and two walls between the patches.

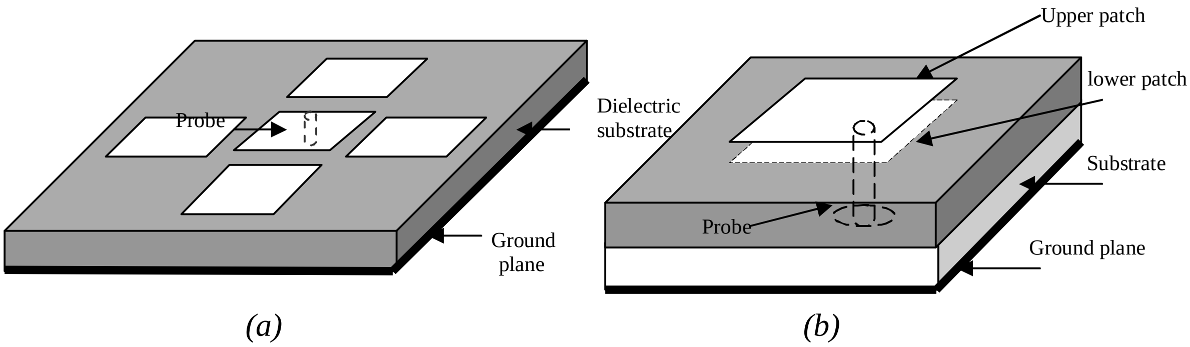

Figure (1.2) Geometry of the multilayer MPA (a) Coplanar geometry (b) Stacked geometry.

1.3.3 Impedance Matching Technique

The essential input impedance of a microstrip antenna can be considered as a parallel resonance R-L-C circuit in addition to the inductive feed effect especially for thick substrate. This introduces inductive reactance connected in series with the parallel resonant circuit of the patch. The object of this technique is to create a series capacitance with the inductive feed probe in order to compensate the inductive reactance caused by the probe, such as using reactive matching network, making slots in the feeding patch, using capacitor in series with the feeding line, using meandering probe, L-shape probe or any reactive loading. Most of them will be discussed below:

1.3.3.1 Impedance matching network

One of the most direct ways to improve the impedance bandwidth of probe fed microstrip antennas, without altering the antenna element itself, is to use a reactive matching network that compensates for the rapid frequency variations of the input impedance. As shown in Fig.1.3, this can typically be implemented in microstrip form below the ground plane of the antenna element.

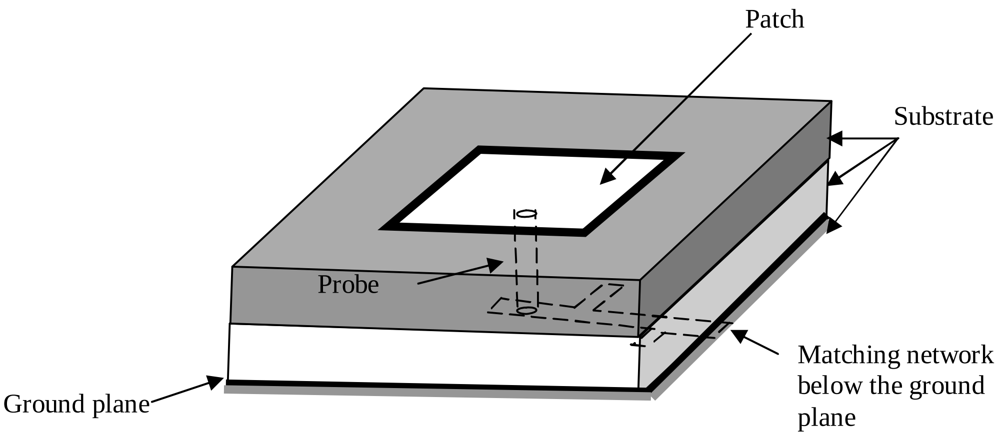

Figure (1.3) Geometry of a probe fed MPA with a wideband impedance matching network.

Pues and Van de Cappele [31] implemented the method by modeling the antenna as a simple resonant circuit. A procedure, similar to the design of a bandpass filter, is then used to synthesize the matching network. With this approach, they have managed to increase the bandwidth from 4.2% to 12% for VSWR of 2:1. Subsequently to that, An et al. [32] used the simplified real frequency technique in order to design the matching network for a probe-fed microstrip patch antenna. They have managed to increase the bandwidth of one antenna element from 5.7% to 11.1% for a VSWR of 1.5:1, and for the second one from 9.4% to 16.8% for a VSWR of 2:1. Recently, De Haaij et al. [33] have shown how parallel resonant circuit can increase the bandwidth from 3.2% to 6.9% for a VSWR of 1.5:1.

1.3.3.2 Shaped probes

A thick substrate can be used to enhance the impedance bandwidth of microstrip patch antenna. However, the input impedance of probe fed microstrip patch antennas become more inductive as the substrate thickness is increased. In order to offset this inductance, some capacitance is needed in the antennas feeding structure. One way to implement such a capacitive feed is to alter the shape of the probe. There are basically two approaches. In the first approach, the probe is connected directly to the patch [34] while in the second approach, the probe is not connected to the patch at all [35-37].

The direct feed can be implemented as shown in the Fig. 1.4 (a), where the feeding structure consists of a stepped probe. The horizontal part of the probe couples capacitively to the patch. Another option is to add a stub to one of the radiating edges of the patch and to feed the stub directly with a probe. For such an approach, Chen and Chia [34] reported an impedance bandwidth of 25%for a VSWR≤2.

The proximity-coupled probe is implemented as shown in the Fig. 1.4 (b), where the probe is bent into L-shape. The horizontal part of the probe runs underneath the patch and also couples capacitively to it. This solution has been implemented for a variety of patch shapes. Make et. al. reported an impedance bandwidth of 36% for rectangular patch [35].

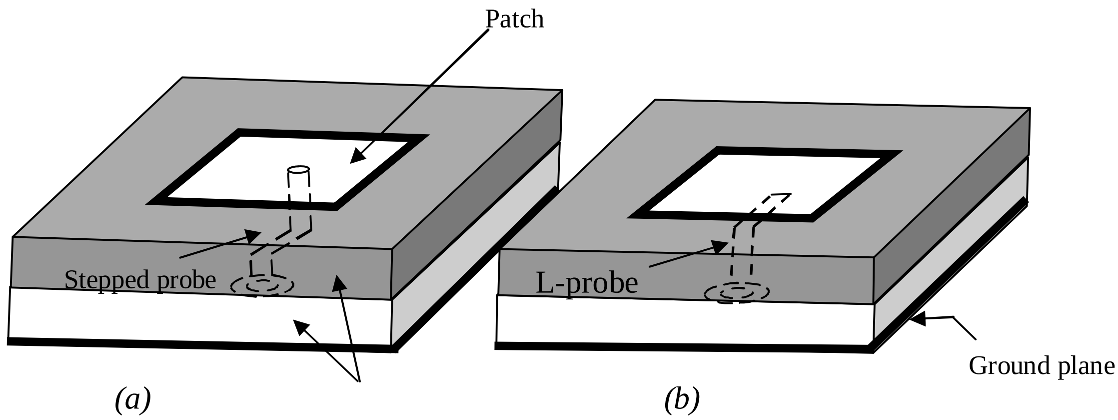

Figure(1.4) Geometries of MPAs with shaped probes (a) Stepped probe (b) L-shaped probe.

1.3.3.3 Capacitive coupling and slotted patches

There are two alternative approaches that can be used to overcome the inductive nature of the input impedance associated with a probe-fed patch on a thick substrate. These are capacitive coupling or the use of slots within the surface of the patch element, examples of such approaches are shown in Fig. 1.5 (a) and (b) respectively. It can be argued that these two approaches are structurally quite similar. The approach in Fig. 1.5 (a) has a small probe fed capacitor patch, which is situated below the resonant patch [38]. The gab between them acts as a series capacitor. Similarly the annular slot in Fig. 1.5 (b) separates the patch into a small probe-fed capacitor patch and a resonant patch [39]. In this case, the slot also acts as a series capacitor. In principle, both of these approaches employs some sort of capacitive coupling and are functionally also, to some degree, equivalent to L-probe as described in Section 1.3.3.2.

For the first approach, Gonzales et al [40] placed a resonant patch, together with a small probe-fed capacitor patch just below it, into a metallic cavity. With this configuration, they managed to obtain an impedance bandwidth of 35.3% for a VSWR of 2:1. A proximity-fed triangular patch in a circular slot is reported in [41] which show more than 90% of VSWR≤ 2 bandwidth.

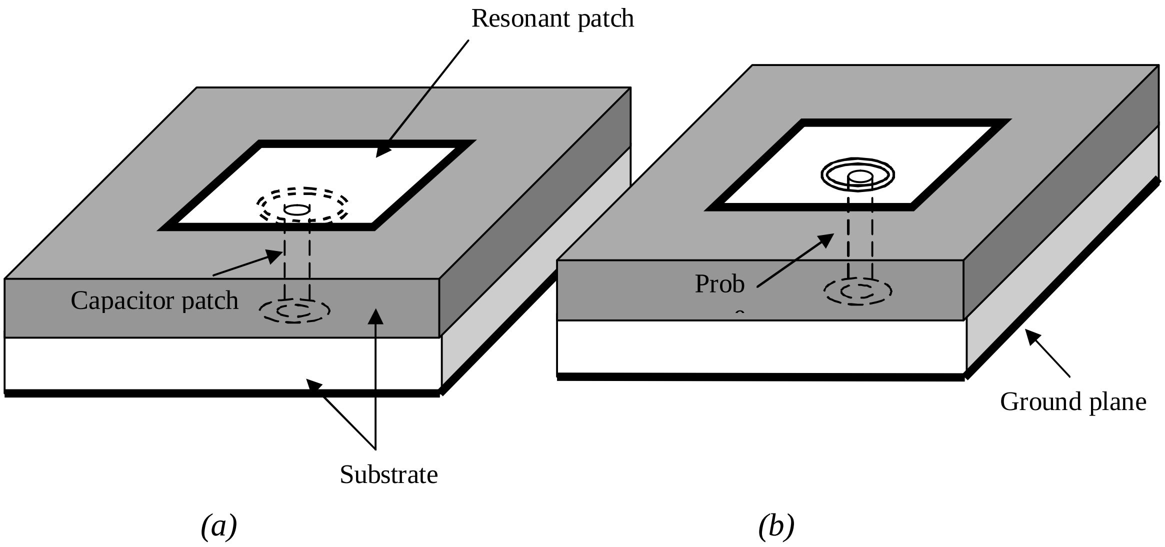

Figure (1.5) Geometries of probe-fed MPAs where capacitive coupling and slots are used. (a) Capacitive coupling (b) Slot in the surface of the patch.

For the second approach, Chen and Chia [39] used a small rectangular probe fed capacitor patch, located within a notch that was cut into the surface of the resonant patch. They managed to obtain an impedance bandwidth of 36% for a VSWR 2:1. Some authors also used a rectangular resonant patch with a U-slot in its surface. Tong et. al. [42] reported an impedance bandwidth of 27% for a VSWR 2:1, also, Guo, et. al. [43] reported an impedance bandwidth of 20% for VSWR 2:1.

The advantage of the approach where the capacitor patch is located below the resonant patch is that the cross-polarization levels in the H-plane are lower than that can be achieved with the approach where the capacitor patch is located within the surface of the resonant patch. However, in order to support the capacitor patch below the resonant patch, an additional substrate layer might be required. In contrast, only one substrate layer is required to support the configuration where the capacitor patch is located inside the surface of the resonant patch. Furthermore, the capacitor patch below the resonant patch can complicate the fabrication process. The advantage of both approaches is that, since they do not increase the surface area of the element, they can be used in array configurations without the danger of creating grating lobes.

1.4 Mathematical Methods of Analysis

The analysis methods that have been followed in Microstrip patch antennas researches can be divided into three categories:

- Experimental measurements method. This way takes long time, expensive, and it needs a wide range of experience.
- Mathematical analysis method.
- Simulating packages method. This method is the easiest one, takes the shortest time, and avoids the experimental errors.

There are a number of mathematical methods that can be used for the analysis of probe-fed patch antennas. Most of these methods fall into one of two broad categories: approximate methods and full-wave methods (also known as the method of moments). The approximate methods are based on simplifying assumptions and therefore they have a number of limitations and are usually less accurate. They are almost always used to analyze single antenna elements as it is very difficult to model coupling between elements with these methods. The solution times are usually small. The full-wave methods include all relevant wave mechanisms. When applied properly, the full-wave methods are very accurate and can be used to model a wide variety of antenna configurations, including antenna arrays. These methods tend to be much more complex than the approximate methods. Very often they also require much computation resources and extensive solution times.

In the reminder of this section an overview of both approximate and full-wave methods will be given.

1.4.1 Approximate Methods

Some of the approximation models include the transmission-line model [3] and cavity model [5044]. Usually they treat the microstrip patch as a transmission line or as a cavity resonator.

The transmission-line model represents the antenna by radiating slots that are separated by a length of low-impedance transmission line [3]. This method is the simplest method for the analysis and design of microstrip patch antennas, but often yields the least accurate results and also lacks versatility. It can be used to calculate the resonance frequency and the input resistance of an antenna element. With this method it is difficult to model the coupling between antenna elements. The method only works reasonably well for antennas with thin substrates and low dielectric constants, while it becomes increasingly less accurate as either the substrate thickness or dielectric constant is increased. The transmission line model has mostly been applied to directly-driven rectangular patches. Some of the drawbacks associated with the transmission-line model can be overcome with the **cavity model**. **The cavity model** is a modal-expansion analysis technique whereby the patch is viewed as a thin cavity with electric conductors above and below it, and with magnetic walls along its perimeter [44, 45]. With this method, the electric field between the patch and the ground plane is expanded in terms of a series of cavity resonant modes or eigenfunctions, along with its eigenvalues or resonant frequencies associated with each mode. Due to the cavity being thin, only transverse magnetic (TM) field configurations, with respect to the height of the cavity, are considered. The field variation along the height of the cavity is also assumed to be constant. Furthermore, due to the fact that a lossless cavity cannot radiate and exhibits a purely reactive input impedance, the radiation effect is modeled by introducing an artificially-increased loss tangent for the substrate. The cavity model can model the resonant frequency and the input impedance more accurate than the transmission-line model. As with the transmission-line model, the cavity model also becomes less accurate as the substrate thickness or dielectric constant is increased. It does not take into account the effect of guided waves in the substrate.

1.4.2 Full-Wave Methods

Three very popular full-wave methods that can be used to model probe-fed microstrip patch antennas, are **the moment method (MM)**, **the finite-element method (FEM)** and **the finite-difference time domain (FDTD)** method. These are the three major paradigms of full-wave electromagnetic modeling techniques. Unlike the approximate methods, these methods include all the relevant wave mechanisms and are potentially very accurate. They all incorporate the idea of discretising some unknown electromagnetic property. For the **MM**, it is the current density, while for the **FEM** and **FDTD**, it is normally the electric field (also the magnetic field for the **FDTD** method). The discretisation process results in the electromagnetic property of interest being approximated by a set of smaller elements, but of which the complex amplitudes are initially known. The amplitudes are determined by applying the full-wave method of choice to the agglomeration of element. Usually the approximation becomes more accurate as the number of elements is increased. Although these methods all share the idea of discretisation, their implementations are very different.

The **MM** is the most widely-used full-wave method for the analysis of microstrip antennas [46], so we taking about this model only. This method is mostly applied in the frequency domain, where only a single frequency is considered at any one time. When using the **MM**, the current density on the antenna is usually the working variable from which all the other antenna parameters are derived. The method is implemented by replacing the antenna with an equivalent surface current density. The surface current density is then discretised into a set of appropriate current-density elements, also known as basis functions, with variable amplitudes. After the surface current density on the surface of the antenna has been solved, the other antenna parameters such as the input impedance, radiation patterns and gain can easily be derived.

A major advantage of the **MM** is its efficient treatment of highly conducting surfaces. With the **MM**, only the surface current density is discretised and not the fields in the surrounding medium. Furthermore, it inherently includes the far field radiation condition, while antennas that are embedded in multilayered media, can be simulated efficiently when using the appropriate Green's function for such a configuration. It is not very well suited for the efficient analysis of problems that include electromagnetically penetrable materials.

In the present work the ways that followed in studying the MPA are:

- The theoretical formulation based on cavity and aperture models have been investigated for studying a single MPA.
- The simulating package (Microwave-Office package) has been used in designing and analyzing all types of antennas presented in this work. This package proved its very high ability to analyze the microstrip patch antenna with a high degree of accuracy. It

helps us to: (1) choose the best feed location (i.e. the location that give good matching between the antenna and the coaxial connector), here the characteristic impedance of the coaxial feed probe is 50Ω , (2) plot the radiation field, input impedance, and VSWR for the designed antennas.

1.5 Work Objective

The aims of this study are listed below

- Understanding the concept and techniques used for achieving broad bandwidth MPA.
- Analyze the single rectangular patch microstrip antenna (for TM_{01}, TM_{02}, and TM_{03} modes) using cavity model beside the aperture model with the aid of Matlab computation.
- Study the ability of producing a narrow main lobe radiation pattern with null side lobes for rectangular MPA operating at TM_{03} mode. Then the bandwidth enhancement for this type of MPA .
- Study the ability of improving the bandwidth of a MPA loaded by a slot in its center with two types of feeding: direct and indirect(capacitive) feed.

1.6 Thesis Outline

Chapter 1 gives thesis introduction about MPA and bandwidth enhancement techniques.

Chapter 2 explains the theory analysis of the single MPA using cavity and aperture models.

Chapter 3 analyses and investigates the single patch microstrip antenna operating at different modes using two methods; theoretical formulations and simulation tool. A bandwidth enhancement of microstrip patch antenna operating at TM_{03} mode using thick substrate with high dielectric substrate material using direct and indirect feed excitation have been investigated.

Chapter 4 studies the performance of the stacked configuration with two types of structure (rectangular and square lower patch configurations). The effect of impedance matching is investigated here.

Chapter 5 procedures bandwidth enhancement based on capacitance generation. A slotted MPA with direct and indirect feed excitation using different techniques have been investigated.

Chapter 6 gives a conclusion for the presented work and also includes some recommendations for future works.

Chapter 2

Theory

2.1 Introduction

The increasing use of microstrip antenna technology requires analysis methods capable of accurately predicting the radiated field pattern, input impedance and mutual coupling. Cavity model beside the aperture model have been some what successful for calculating radiation pattern and input impedance.

In the presented work the cavity model beside the aperture model is used to analyze the single patch microstrip antenna. The theoretical formulations can give a good estimation on rectangular patch performance since the resulted data could be compared with published and MW-Office package results for many modes.

2.2 Theoretical Formulation

A cavity model for the microstrip antennas is based on the following conditions [5], [45]:

(a) The close proximity between the microstrip patch and the ground plane suggests that E has only the z component and the H has only the xy-components in the region bounded by the microstrip and the ground plane

(b) The field in the forementioned region is independent of the z-coordinate for all frequencies of interest.

(c) The electric current in the microstrip must have no component normal to the edge at any point on the edge, which implies that the tangential component of H along the edge is negligible.

Thus the region between the microstrip and the ground plane may be treated as a cavity bounded by a magnetic wall along the edge, and by electric walls from above and below.

2.2.1 Resonance Frequency

The resonance frequency $(f_r)_{mn}$ of the rectangular microstrip patch antenna of (m,n) order mode depends on the patch size, cavity dimension, and the filling dielectric constant ε_r [8, 47]

$$(f_r)_{mn} = \frac{k_{mn} c}{2p \sqrt{e_r}} \tag{2.1}$$

where m,n= 0,1,2…, c is the speed of light

and

$$k_{mn} = \sqrt{(mp/W)^2 + (np/L)^2} \tag{2.2}$$

i.e.

$$(f_r)_{mn} = \sqrt{(mp/W)^2 + (np/L)^2} \cdot \frac{c}{2p \sqrt{e_r}}$$

To obtain the initial value of non-radiating rectangular patch's edge L at a certain resonance frequency and dielectric constant for the lowest order (TM_{01}) mode, we use the following equation [5]

$$L = \frac{c}{2 f_r \sqrt{e_r}} \tag{2.3}$$

In practice the fringing effect causes that the effective distance between the radiating edges of the patch to be slightly greater than *L*. Therefore, the actual value of the resonant frequency is slightly less than f_r. Taking into account the effect of fringing field Δl, *L* can be accurately predicted from [48-50]

$$L_e = \frac{c}{2 f_r \sqrt{e_e}} - 2\Delta l \tag{2.4}$$

where ε_e is the effective dielectric constant and is given by

$$e_e = \frac{e_r + 1}{2} + \frac{e_r - 1}{2}\left(\frac{1}{\sqrt{1 + 10h/W}}\right) \tag{2.5}$$

the expression for the fringing field is given by

$$\Delta l = 0.412h \frac{(e_e + 0.3)(W/h + 0.264)}{(e_e - 0.258)(W/h + 0.813)} \tag{2.6}$$

The effective resonant frequency can be accurately predicted from

$$(f_r)_e = \frac{c}{2(L + 2\Delta l)\sqrt{e_e}} \tag{2.7}$$

The dimension of the radiating edge *W*, patch width, can be chosen according to the selecting distance between the radiating edges. The width *W* is usually chosen such that it lies in the ratio, $L<W<2L$ for good radiation characteristics. If W is too large then higher order modes will move closer to the design frequency. Also the width of the patch affects the resonant resistance of the antenna, with a wider patch giving a lower resistance. The ratio W/L=1.5 is usually chosen to maximize the bandwidth, since the bandwidth is proportional to the width also this ratio gives good performance according to the side lobe appearances [8].

2.2.2 Cavity Field

From the cavity model explained above, the electric field is assumed to act entirely in the z-direction and to be a function only of the x and y coordinates [45]

$$E = \hat{\mathbf{z}} E_z(x, y) \tag{2.8}$$

The z-component of the electric field E_z satisfies the two dimensional form of partial differential equation knowing as wave equation [51]

$$\frac{\partial^2 E_z}{\partial x^2} + \frac{\partial^2 E_z}{\partial y^2} + k^2 E_z = 0 \tag{2.9}$$

Equation (2.9) can be solved by using the separation of variables method (product solution) by letting:

$$E_z(x, y) = X(x)Y(y) \tag{2.10}$$

where $X(x)$ and $Y(y)$ are functions of x and y respectively. Substituting (2.10) in (2.9) and dividing by XY one get:

$$\frac{X^{''}}{X}+\frac{Y^{''}}{Y}=-k^2 \tag{2.11}$$

Since the variables are independent, each term in equation (2.11) must be constant so that the equation can be written as

$$-k_x^2-k_y^2=-k^2 \tag{2.12}$$

where $-k_x^2-k_y^2$ are the separation constants. Thus equation (2.11) is separated as

$$X^{''}+k_x^2X=0 \tag{2.13a}$$

and

$$Y^{''}+k_y^2Y=0 \tag{2.13b}$$

After solving the differential equations (2.13a) and (2.13b) one can get:

$$X(x)=A_1\cos k_x x+A_2\sin k_x x \tag{2.14a}$$

and

$$Y(y)=A_3\cos k_y y+A_4\sin k_y y \tag{2.14b}$$

where A_1,A_2,A_3, and A_4 are constants

Substituting (2.14) into (2.10) gives

$$E_z=(A_1\cos k_x x+A_2\sin k_x x)(A_3\cos k_y y+A_4\sin k_y y) \tag{2.15}$$

Equation (2.15) can not be solved without specifying some boundary conditions for the patch. An obvious requirement is that the outward current flowing on the perimeter of the patch must be zero (since the patch boundary is an open-circuit). It may be shown that this requirement is approximately equivalent to requiring that [5, 51]

$$\frac{\partial E_z}{\partial \mathbf{n}} = 0 \quad \text{for} \quad 0 \le x \le W, \text{ and } 0 \le y \le L \tag{2.16}$$

where **n** is the outward normal vector at the perimeter of the patch, then by applying the following boundary conditions

$$\left.\frac{\partial E_z}{\partial x}\right|_{x=0} = \left.\frac{\partial E_z}{\partial y}\right|_{y=0} = 0 \tag{2.17}$$

One can get

$$E_z = E_o \cos k_x x \cos k_y y \tag{2.18}$$

where $E_o = A_1 A_3$

Now by using the other boundary conditions

$$\left.\frac{\partial E_z}{\partial x}\right|_{x=W} = \left.\frac{\partial E_z}{\partial y}\right|_{y=L} = 0 \tag{3.19}$$

One can get

$$k_x = \frac{m\pi}{W} \tag{2.20}$$

and

$$k_y = \frac{np}{L} \tag{2.21}$$

Finally, substituting (2.20) and (2.21) in (2.18), the electric field of the m and n mode numbers associated with x and y directions in a rectangular resonator (the field inside the cavity) with dimensions *W* and *L* can be written in the form

$$E_z = E_o \cos(mpx/W)\cos(npy/L) \tag{2.22}$$

2.2.3 Far Field

The aperture model is used to calculate the far field. The antenna configuration considered in this work consists of an infinite dielectric substrate coated on one side with a perfect conducting ground plane and on the other side with a perfect conducting overlay S. The contour of S determines the form of the resonator, which in this case is a rectangular, as shown in Fig. 2.1 [52].

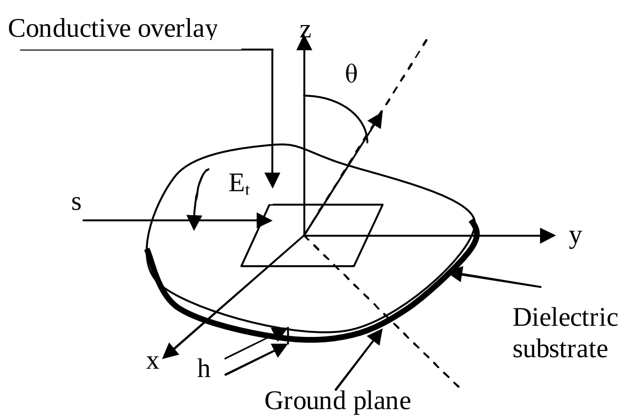

Figure (2.1) Rectangular microstrip resonator antenna: configuration and coordinate systems [52].

The calculation of the radiation field is based on the equivalence principle: the field in the half space $z > 0$ is completely determined by the tangential component E_t of the electric field in the plane z=0.

As the resonator surface S has been supposed to be perfectly conducting, therefore E_t=0 on the surface S.

At large distances from the resonator surface in the plane z=0, E_t decreases to zero. So the most important contribution to the radiation field originates from the region near the surface S. Therefore, one can write [52]

$$\int_0^\infty \left|\overline{E}_t\right| \cdot dl \cong \int_0^L \left|\overline{E}_t\right| \cdot dl \tag{2.23}$$

Since the thickness of the substrate is much smaller than the wavelength λ_o in vacuum, one can assume

$h<<\lambda_o$

As a consequence, the variation of E_t in the plane z=0 along directions perpendicular to the edge of S has no important influence on the radiation field. For this reason one can approximate the field $|E_t|$ in equation (2.24) with a constant E_a over a distance 2a from the edge of the resonator, and outside this area one can suppose E_t=0 as shown in Fig. 2.2 [52]:

$$\int_0^L \left|\overline{E}_t\right| \cdot dl = E_a \cdot 2a \tag{2.24}$$

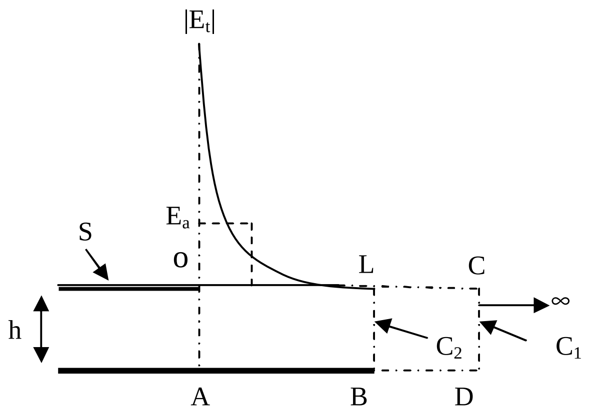

Figure (2.2) Approximation of tangential field component E_t near the edge of the surface S. ——— exact value of $|E_t|$; - - - - approximation of $|E_t|$; contour C_1=OCDAO; contour C_2=OLBAO[52]

The value of E_a should correspond with the *z*-component of the electric field in the dielectric at the edge of the surface S (Fig.2.2).

By comparing $\oint_{c1} \bar{E} \cdot d\bar{l} = 0$ with $\oint_{c2} \bar{E} \cdot d\bar{l} = 0$ (2.25)

and using (2.23), one can conclude that

$$\int_{LB} \bar{E} \cdot d\bar{l} \cong \int_{CD} \bar{E} \cdot d\bar{l} = 0 \tag{2.26}$$

By combining the formula (2.24), (2.25) and (2.26) and supposing E_z constant over the height of the dielectric (cavity model) one can get [52]:

$$E_a \cdot 2a = E_z \cdot h \tag{2.27}$$

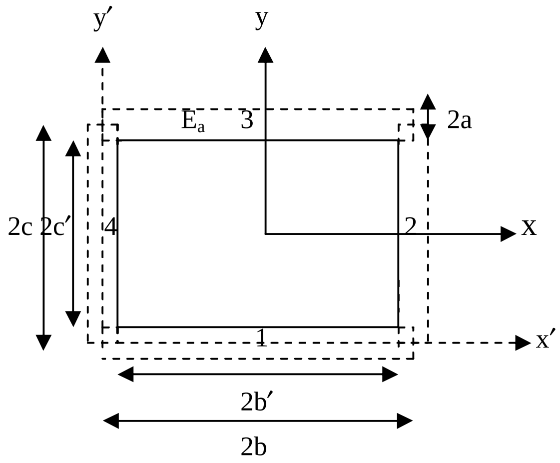

Figure (2.3) Configuration of radiating slots for calculating the far field [52].

The field component E_z of the (m,n) mode in the rectangular resonator with dimensions $2b'$ (W) and $2c'$ (L) as shown in Fig. 2.3 can be written in the form [52]

$$E_z = E_o \cdot \cos\frac{mp}{2b'}x' \cdot \cos\frac{np}{2c'}y' \tag{2.28}$$

with E_o is the maximum amplitude of the E_z field. Equation (2.28) is the same as equation (2.22) but the name of coordinate and the patch dimensions have been change just for the derivative demand.

Finally, we obtain the following "aperture model" for the antenna: "an infinit conducting plane at z=0 with four slots of width $2a$ around the surface S excited by an electric field E_a". This aperture model refers to the theory of aperture antennas which are solved with the spatial Fourier transform of the aperture field.

For the general case of a resonance in the (m,n) mode, one can write expressions for the field in four slots as follows

1- For slot 1, the boundary condition y'=0
then equation (2.28) becomes

$$E_z = E_o \cdot \cos\frac{mp}{2b}x' \text{ with } 0 \le x' \le 2b$$

and by using equation (2.27) one can write the expression for the field in slot 1 as follows

$$E_{a11} = \frac{hE_o}{2a} \cdot \cos\frac{mp}{2b}x' \tag{2.29}$$

note that b' in equation (2.29) is replaced by b as a result of the fact that the slots are placed outside the edge of surface S and also because of the stray field at the angular points of the rectangle [52].The Fourier transformation of the excitation field (2.29)

$$E_{a11} = \int_{-a}^{+a}\int_{0}^{2b} E_{a11} \cdot e^{jVx'} \cdot e^{jhy'} \cdot dx' \cdot dy' \tag{2.30}$$

where

$$V = k\sin q\cos j$$

$$h = k\sin q\sin j$$

$$k = 2p / l_o$$

Substitute (2.29) in (2.30) one get

$$E_{a11} = \frac{hE_o}{2a}\int_0^{2b}\cos\frac{mp}{2b}x' \cdot e^{jVx'}dx'\int_{-a}^{a}e^{jhy'} \cdot dy' \tag{2.31}$$

$$E_{a11} = \frac{hE_o}{2a}\frac{e^{jha} - e^{-jha}}{jh} \cdot \frac{1}{2} \cdot \int_0^{2b}\left(e^{j\frac{mp}{2b}x'} + e^{-j\frac{mp}{2b}x'}\right) \cdot e^{jVx'} \cdot dx' \tag{2.32}$$

$$E_{a11} = hE_o \cdot \frac{\sin ha}{ha} \cdot \frac{1}{2}\int_0^{2b}\left(e^{j(V+\frac{mp}{2b})x'} + e^{j(V-\frac{mp}{2b})x'}\right) \cdot dx' \tag{2.33}$$

$$E_{a11} = \frac{hE_o}{2} \cdot \sin c(ha) \cdot \left[\frac{e^{j(V+\frac{mp}{2b})2b} - e^0}{j(V+\frac{mp}{2b})} + \frac{e^{j(V-\frac{mp}{2b})2b} - e^0}{j(V-\frac{mp}{2b})}\right] \tag{2.34}$$

$$E_{a11} = \frac{hE_o}{2} \cdot \sin c(ha) \cdot \begin{bmatrix} 2 \cdot e^{j(V+\frac{mp}{2b})b} \cdot \left(\dfrac{\sin(V+\frac{mp}{2b})b}{(V+\frac{mp}{2b})} \right) + \\ 2 \cdot e^{j(V-\frac{mp}{2b})b} \cdot \left(\dfrac{\sin(V-\frac{mp}{2b})b}{(V-\frac{mp}{2b})} \right) \end{bmatrix} \tag{2.35}$$

$$E_{a11} = hE_o \cdot \sin c(ha) \cdot b \cdot e^{jVb} \begin{bmatrix} e^{j\frac{mp}{2}} \cdot \left(\dfrac{\sin(V+\frac{mp}{2b})b}{(V+\frac{mp}{2b})b} \right) + \\ e^{-j\frac{mp}{2}} \cdot \left(\dfrac{\sin(V-\frac{mp}{2b})b}{(V-\frac{mp}{2b})b} \right) \end{bmatrix} \tag{2.36}$$

$$E_{a11} = hE_o \cdot \sin c(ha) \cdot b \cdot e^{jVb} \left[(j)^m \cdot \sin c(Vb + \frac{mp}{2}) + (-j)^m \cdot \sin c(Vb - \frac{mp}{2}) \right] \tag{2.37}$$

with $\sin c(x) = \dfrac{\sin(x)}{x}$

2- For slot 3, the boundary condition $y' = 2c$

$$E_z = E_o \cdot \cos\frac{mp}{2b} x' \cdot \cos np$$

$$E_{a12} = \frac{hE_o}{2a} \cdot \cos\frac{mp}{2b} x' \cdot \cos np$$

By following the same procedure used for finding the field in slot 1one can get

$$E_{a12} = hE_o \cdot \cos np \cdot \sin c(ha) \cdot b \cdot e^{jVb}$$
$$\left[(j)^m \cdot \sin c(Vb + \frac{mp}{2}) + (-j)^m \cdot \sin c(Vb - \frac{mp}{2}) \right] \tag{2.38}$$

3- For slot 2, the boundary condition $x'=0$ then

$$E_z = E_o \cdot \cos\frac{np}{2c} y' \quad \text{with} \quad 0 \le y' \le 2c$$

$$E_{a21} = \frac{hE_o}{2a} \cdot \cos\frac{np}{2c} y'$$

By following the same procedure used for finding the field in slot 1one can get

$$E_{a21} = hE_o \cdot \sin c(Va) \cdot c \cdot e^{jhc}\left[(j)^n \cdot \sin c(hc+\frac{np}{2}) + (-j)^n \cdot \sin c(hc-\frac{np}{2})\right] \tag{2.39}$$

4- For slot 4, the boundary condition $x'=2b$ then

$$E_z = E_o \cdot \cos\frac{np}{2c} y' \cdot \cos mp$$

$$E_{a22} = \frac{hE_o}{2a} \cdot \cos\frac{np}{2c} y' \cdot \cos mp$$

$$E_{a22} = hE_o \cdot \cos mp \cdot \sin c(Va) \cdot c \cdot e^{jhc} \cdot \left[(j)^n \cdot \sin c(hc+\frac{np}{2}) + (-j)^n \cdot \sin c(hc-\frac{np}{2})\right] \tag{2.40}$$

The Fourier transformation of the complete excitation field is

$$E_a = \bar{i}_x \left[1-\cos(mp) \cdot e^{j2bV})\right] \cdot E_{a21} + \bar{i}_y \cdot \left[1-\cos(np) \cdot e^{j2ch})\right] \cdot E_{a11} \tag{2.41}$$

After a translation of the coordinates (x',y') to the system (x,y) (Fig. 2.3), one finds the expression

$$E_a = \bar{i}_x \cdot E_x + \bar{i}_y \cdot E_y \tag{2.42}$$

with

$$E_x = \left[(-1-(-1)^m)\cdot j\cdot \sin(Vb) + (1-(-1)^m)\cdot \cos(Vb)\right]$$
$$\cdot h\cdot E_o \cdot c\cdot \sin c(Va)\cdot j^n \cdot \left[\sin c(hc+\frac{n\pi}{2}) + (-1)^n \cdot \sin c(hc-\frac{n\pi}{2})\right] \quad (2.43)$$

and

$$E_y = \left[(-1-(-1)^n)\cdot j\cdot \sin(hc) + (1-(-1)^n)\cdot \cos(hc)\right]$$
$$\cdot h\cdot E_o \cdot b\cdot \sin c(ha)\cdot j^m \cdot \left[\sin c(Vb+\frac{m\pi}{2}) + (-1)^m \sin c(Vb-\frac{m\pi}{2})\right] \quad (2.44)$$

The far field can be written as [52]

$$E(r) = \frac{jke^{-jkr}}{2\pi r}\left\{\begin{array}{l}\bar{i}_\theta\left[E_x\cdot\cos\varphi + E_y\cdot\sin\varphi\right] + \\ \bar{i}_\varphi\left[-E_x\cdot\sin\varphi\cdot\cos\theta + E_y\cdot\cos\varphi\cdot\cos\theta\right]\end{array}\right\} \quad (2.45)$$

the far field components E_θ and E_φ are

$$E_\theta = \frac{jke^{-jkr}}{2\pi r}\left(E_x\cos\varphi + E_y\sin\varphi\right) \quad (2.46)$$

and

$$E_\varphi = \frac{jke^{-jkr}}{2\pi r}\left(-E_x\sin\varphi\cos\theta + E_y\cos\varphi\cos\theta\right) \quad (2.47)$$

Equation (2.45) enables to plot the radiation pattern for every mode of the rectangular microstrip patch antenna.

2.2.4 Input Impedance

The input impedance Z_{in} of an antenna is the impedance presented by the antenna at its terminal; it should be accurately known so as to provide a good match between the element and the feed. The input impedance of the microstrip antenna may be represented by a parallel *RLC* circuit. The equivalent circuit of the antenna is shown in Fig. 2.4 The input impedance is composed of real and imaginary parts [53]

$$Z_{in} = R_{in} + jX_{in} \tag{2.48}$$

The input resistance, R_{in} , represennts dissipation of power. Power can be dissipated in two ways (radiation resistance and a ohmic loss resistance). On many antennas ohmic losses are small compared to radiation losses. The input reactance,X_{in}, represents power stored in the near field of the antenna.

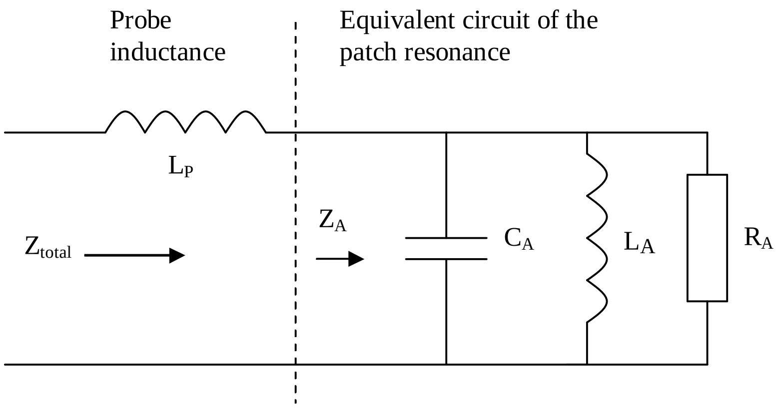

Figure (2.4) Equivalent circuit of the antenna divided to the probe inductance part and patch resonator. L_p is the probe inductance, R_A is the radiation resistance, L_A and C_A are the inductive and capacitive parts of the antenna resonant circuit. Z_A is the impedance of the patch only and Z_{Total} is the total impedance of the antenna.

The input impedance of the MPA can be represented in other form

$$Z_{in} = \frac{A}{\frac{1}{R} + jwC + \frac{1}{jwL_{ind}}} \tag{2.49}$$

where A is a constant and equals 1.5 and R, C, and L_{ind} are the resistance, the capacitance, and the inductance of the patch respectively, and ω is the angular frequency.

The resistance R of the patch can be written as [5]

$$R = \frac{V^2}{2P_T} \tag{2.50}$$

where V is the terminal voltage and P_T is the total power dissipated by the antenna and it is equal to :

$$P_T = P_r + P_c + P_d$$

where P_r represent the radiated power outside the antenna surface (radiation losses) and it is given by [5]:

$$P_r = \frac{1}{h_o} \int_{j=0}^{2p} \int_{q=0}^{p/2} \left|E_q\right|^2 + \left|E_j\right|^2 r^2 \sin q \, dq \, dj \tag{2.51}$$

where η_o is the intrinsic impedance of free space. E_θ and E_φ and far field components given by equations (3.46) and (3.47) respectively.

The power losses inside the dielectric P_d (part of ohmic losses) is given by [5]:

$$P_d = \frac{we_o e_r \tan d}{2} \iiint_v E_z . E_z^* dv \tag{2.52}$$

where *tand* is the loss tangent of the dielectric. E_z represents the field inside the cavity given by equation (2.22).

The power losses inside the conductor surface of radiator and the ground plane P_c (another part of ohmic losses) is given by [5]

$$P_c = 2\frac{R_s}{2}\iint_s \left(H_x^2 + H_y^2\right) dx\, dy \qquad (2.53)$$

where R_s is the surface resistance and is given by:

$$R_s = \sqrt{\frac{wm_o m_r}{2s}} \qquad (2.54)$$

where μ_o , μ_r , and σ are the permeability of free space, relative permeability, and the conductivity respectively.

The magnetic field components inside the microstrip antenna are given by [5]:

$$H_x = \frac{j}{wm}\frac{\partial E_z}{\partial y}\text{, and} \qquad (2.55)$$

$$H_y = \frac{-j}{wm}\frac{\partial E_z}{\partial x} \qquad (2.56)$$

The inductance L_{ind} and the capacitance C of the patch are given as follows

$$L_{ind} = \frac{R}{2pf_r Q_T}$$

(2.57)

and

$$C = \frac{Q_T}{2p\ f_r R} \qquad (2.58)$$

The total antenna quality factor Q_T has been expressed in the form [51]:

$$Q_T = R\sqrt{\frac{C}{L_{ind}}} \tag{2.59}$$

i.e.

$$Q_T = \frac{wW_T}{P_T} \tag{2.60}$$

where W_T is the total energy stored in the antenna element and is given by [5]:

$$W_T = \frac{e_o e_r}{2} \iiint_v |E_z|^2 dv \tag{2.61}$$

where v is the volume occupied by the cavity.

Knowing the far field expression (2.45), one can determine, by numerical integration (using Matlab computation), the input impedance of the patch as a function of the feed position as follows [52]:

Normalizing the input voltage at the feed point ($x_o' y_o'$) to 1V, one can write

$$h.E_z(x_o' y_o') = 1 \tag{2.62}$$

Applying this condition in equation (2.28), one finds the maximum amplitude of the E_z field as

$$E_o = \left[h.\cos\left(\frac{mpx'_o}{2b'}\right)\cos\left(\frac{npy'_o}{2c'}\right)\right]^{-1} \tag{2.63}$$

when E_o is known, the radiated power outside the antenna surface given in equation (2.51) can also be known, note that only the radiated power is a function of feed location, P_d and P_c are independent on the feed location, so when P_r, P_d, and P_c are known that means R is known, knowing also L_{ind} and C from equations (2.57) and (2.58) respectively, then Z_{in} can be calculated with the aid of Matlab computation.

2.2.5 Reflection Coefficient and VSWR

To have maximum source power delivered to the antenna, the transmitting source must be matched to the antenna. If the match is not ideal, then the degree of mismatch can be measured using the voltage standing wave ratio (VSWR), or by the reflection coefficient, Γ, defined by [53]

$$\Gamma = \frac{Z_{in} - Z_o}{Z_{in} + Z_o} \tag{2.64}$$

where

Z_{in}=antenna input impedance (Ω)

Z_o=characteristic impedance of the transmission line (Ω)

$$VSWR = \frac{1+\Gamma}{1-\Gamma} \tag{2.65}$$

A particular antenna design should have a standard input impedance of either 50 Ω or 75 Ω and a very low reflection coefficient and VSWR.

2.2.6 Power Gain

The power gain of an antenna is defined as a ratio of its radiation intensity to that of an isotropic antenna radiating the same total power as accepted by the real antenna [53].

To compute the gain of a radiation pattern that has a single main lobe and considerably small minor lobes, an empirical formula can be used [53]:

$$Gain(dB) = 10\log\left(\frac{41000}{HPBW_E^o \cdot HPBW_H^o}\right) \qquad (2.66)$$

where

$HPBW_E^{o}$ = half-power beam width in one E-plane

$HPBW_H^{o}$ = half-power beam width in H-plane at a right angle to the other

2.2.7 Bandwidth

The bandwidth (BW) of an antenna can be defined in terms of frequencies as its ability to operate over a wide frequency range on either side of the center frequency [8]

$$BW = \frac{f_2 - f_1}{f_c} \times 100\,\% \qquad (2.67)$$

where, f_c is the center frequency, f_1 and f_2 are the frequencies between which the magnitude of the reflection coefficient of the antenna is less than or equal to 1/3 or VSWR$\leq$ 2. It is usually given as a percentage of the nominal operating frequency. Furthermore, the impedance bandwidth is inversely proportional to the quality factor (Q) of an antenna as given by [8, 54]

$$BW = \frac{100\times(SWR-1)}{Q\times\sqrt{SWR}}\% \qquad (2.68)$$

2.3 Investigation of Resonance Frequency for Multilayer

For multilayer microstrip patch antenna (stacked configuration) as shown in Fig.2.5, the resonance frequency of the top patch is [55]

$$(f_r)_t = \frac{c}{2(L_t + 2\Delta L_t)\sqrt{e_{et}}} \qquad (2.69)$$

where L_t and e_{et} are length and the effective dielectric constant of the top patch respectively, e_{et} is expressed as

$$e_{et} = \frac{e_{ri}+1}{2} + \frac{e_{ri}-1}{2}\left[1+\frac{10.0\sum_{i=1}^{n} h_i}{L_t}\right]^{-1/2} \qquad (2.70)$$

where

$$e_{ri} = \frac{\sum_{i=1}^{n} h_i}{\sum_{i=1}^{n} \frac{h_i}{e_{ri}}} \qquad (2.71)$$

ε_{ri} and h_i represent the dielectric constant and the dielectric thickness between the plates respectively. The line extension of the upper patch, Dl_t, is given by

$$\Delta l_t = 0.412\sum_{i=1}^{n} h_i \left[\frac{e_{et}+0.3}{e_{et}-0.258}\right]\cdot\left[\frac{\dfrac{L_t}{\sum_{i=1}^{n} h_i}+0.264}{\dfrac{L_t}{\sum_{i=1}^{n} h_i}+0.8}\right] \tag{2.72}$$

where i represent the number of antenna dielectric layers

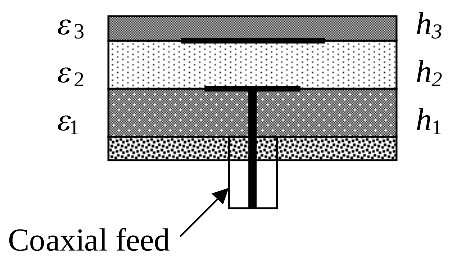

Figure (2.5) Geometry of multilayer (stacked) MPA

CHAPTER 3

Investigation of Single Patch Microstrip Antenna

3.1 Introduction

The goal of this chapter is to investigate and analyze the single microstrip patch antenna for three different modes TM_{01},TM_{02}, and TM_{03} using the theoretical formulation presented in chapter 3 with the aid of Matlab computation. This analysis includes the radiating field pattern and the input impedance. A deep study on the characteristics of TM_{03} mode is established in this chapter. This study was focused on: (a) producing a good radiation pattern (narrow main lobe without side lobes), (b) the effect of feed location on the input impedance, and (c) bandwidth enhancement using thick substrate with two types of feeding, direct and indirect feed excitation. This work has been assisted by using computer simulator package (MOP). In order to be in confidence with the accuracy of our cavity formulations and the performance of the MOP, a previously published results that have been obtained by different approaches have been re-calculated using the cavity formulations and the MOP.

3.2 Magnetic Current and Electric Field Distribution

The electric field (perimeter arrows) and magnetic surface current distributions on the side walls for TM_{01}, TM_{02}, and TM_{03} modes are illustrated in Fig. 3.1. For TM_{01} and TM_{03} , the magnetic currents are constant and in phase along x-direction (assocaited with dimension *W*) because there is no field variation and are out of phase and vary sinusoidally along y-direction (assocaited with dimension *L*) because the field varies as a cos (πy/L). For this reason, the W edge is known as the radiating edge since it contributes predominantly to the radiation. The L edge is known as the non-radiating edge since it contributes very little in the far field because its net effect cancels itself.

The vertical perimeter arrows for TM_{01} and TM_{03} modes, radiating edge, indicate the co-polar edge field, and indicate the cross-polar edge field in the TM_{02} mode. Notice that the cross-polar arrows in Fig. 3.1(b) are pointed in opposite directions. This is why that the cross-polar field of a rectangular or square patch of MPA operating at TM_{02} mode always yields a null at the broadside direction [56].

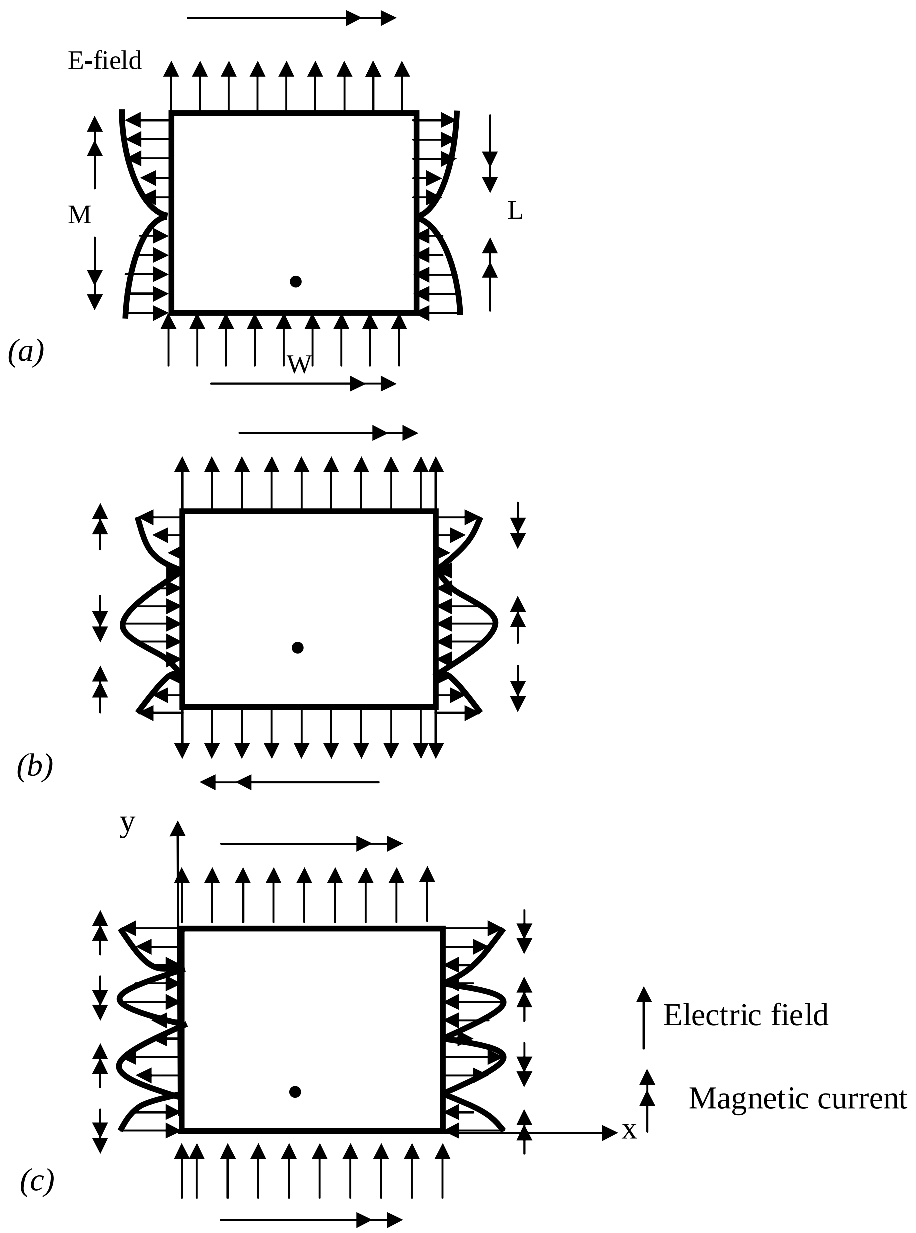

Figure (3.1) Electric field and magnetic surface current distribution in walls for different modes of a rectangular MPA; (a)TM_{01} mode, (b)TM_{02} mode, and (c) TM_{03} mode.

3.3 Simulation Results for Published Rectangular MPA

The far field radiation pattern in two principal planes; E(x-z)-plane($\varphi=0^o$) and H(x-y)-plane($\varphi=90^o$) have been calculated for very famous published work by Lo [45] in order to check the accuracy and the performance of our cavity formulations and the simulation tool(MOP). For H-plane E_q is the co-polar component, and for E-plane E_j is the co-polar component. The cross-polar component is zero for the two planes. E_q and E_j components are calculated for the two planes using equations (2.46) and (2.47) respectively with the aid of Matlab computation (see appendix A). Also they are re-simulated using the MOP. The computed patterns are very close to the published results. This published work consist of a single rectangular patch of dimensions 11.43 cm x 7.62 cm operating at resonance frequency f_r= 1.19 GHz with dielectric constant ε_r= 2.62 of thickness h= 0.159 cm. Fig. 3.2(a), (b), and (c) show the agreement between published pattern, that computed using cavity formulations, and that simulated using MOP respectively. The agreement between them is excellent [57].

The cavity formulations and the MOP are also applied to further published work in [8]. There is a good agreement between the published and the calculated results.

3.4 Design of Rectangular MPA

Rectangular microstrip patch antennas for three different modes TM_{01}, TM_{02}, and TM_{03} are designed at resonance frequency 2.15 GHz. The patches are printed on a dielectric substrate of e_r=4.45 with thickness h=0.16cm . This value of dielectric constant is chosen because this type is available and easy to manufacture. The antenna design parameters are calculated using equations (2.1-2.7), and the dimensions are calculated at aspect ratio (W/L)=1.5. Table (3.1) shows the geometrical parameters of the microstrip patch antennas for these different modes. The antenna design parameters for TM_{03} mode printed on a different dielectric substrate materials with the same thickness, h=0.16cm, and aspect ratio, W/L=1.5, operating at the same frequency 2.15GHz have been tabulated in this table in order to study the effect of the dielectric substrate material on the radiation pattern.

Table (3.1) Antenna design parameters of MPAs operating at TM_{01},TM_{02},and TM_{03} modes with parameters: f_r= 2.15 GHz, W/L=1.5,and h= 0.16 cm.

Mode	ε_r	$\tan\delta$	L (cm)	W(cm) (cm)	L_e (cm)	W_e (cm)	ε_e (cm)	$(f_r)_e$ (GHz)
TM_{01}	4.45	0.0005	3.3	4.95	3.25	4.87	4.224	2.117
TM_{02}	4.45	0.0005	6.61	9.92	6.56	9.84	4.325	2.134
TM_{03}	4.45	0.0005	9.92	14.88	9.815	14.722	4.364	2.139
TM_{03}	2.62	0.001	12.93	19.39	12.836	19.25	2.588	2.136
TM_{03}	9.8	0.0004	6.68	10.02	6.657	9.985	9.486	2.142

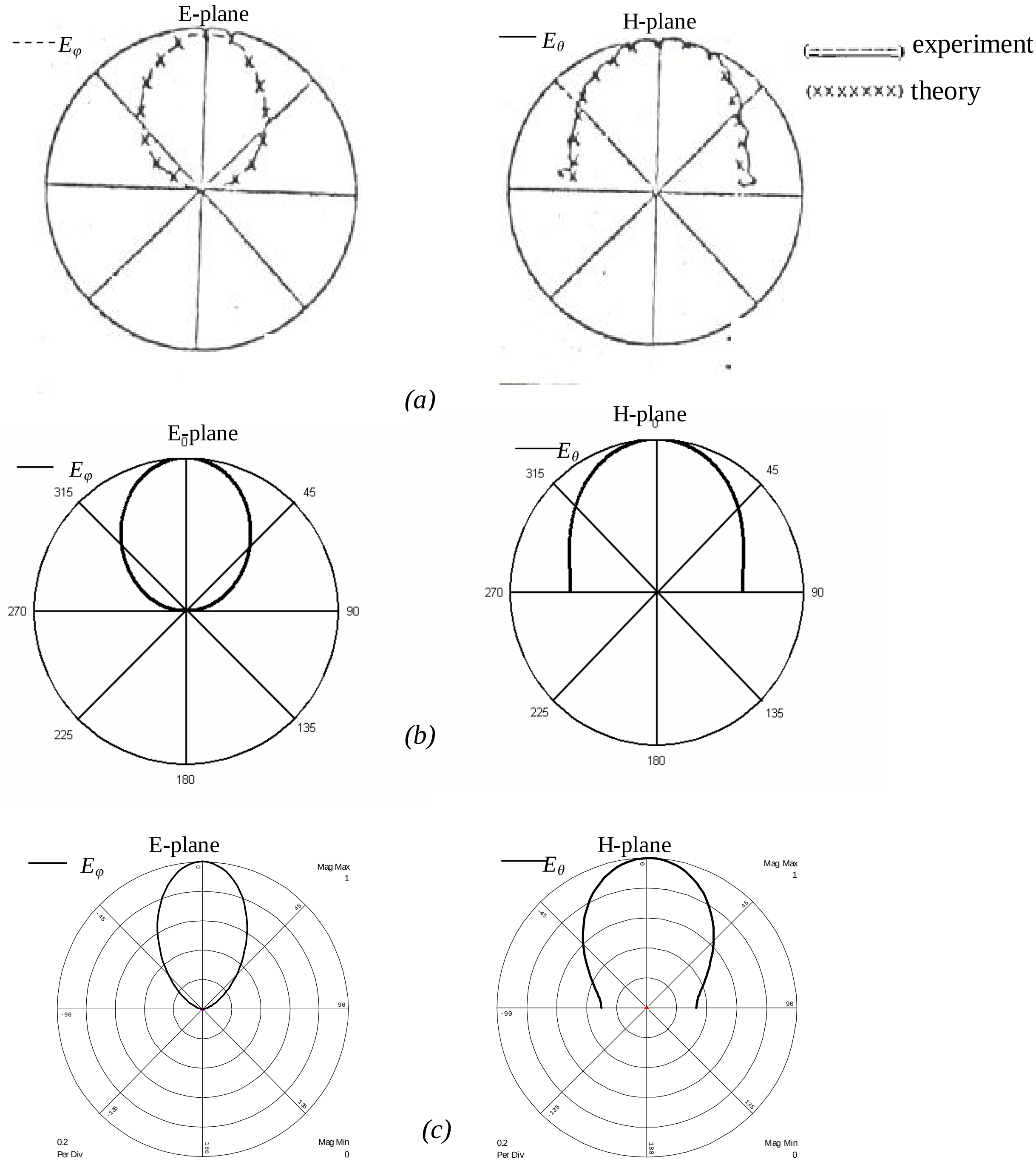

Figure (3.2) E-plane (j $=0^o$) and H-plane (j $=90^o$) for TM_{01} mode of a MPA with WxL=11.43cm x 7.62cm operating at resonance frequency 1.19GHz. (a) Published work[45], (b) Calculated by using cavity formulations, and (c) Calculated by using MOP.

3.5 Simulation and Results of Rectangular MPA

The characteristics of the single patch (radiation field and the input impedance) for three modes TM_{01}, TM_{02}, and TM_{03} using the cavity formulations and MOP are investigated.

3.5.1 Radiation Field

The far field components E_j and E_q for the two principal planes, E -and H –planes respectively, of MPAs operating at TM_{01}, TM_{02}, and TM_{03} modes have been calculated using equations (2.46) and (2.47) respectively. The patch dimensions for all modes are shown in table (3.1). The radiation field patterns for these modes are shown in Fig. 3.3. It can be noticed that TM_{01} and TM_{03} have broadside radiation pattern, whereas TM_{02} has E_q component in the H-plane (with null radiation with respect to the zenith ($\theta=0^o$)), and there is no radiation in the E-plane.

Also, the far field components in the two principal plans for each mode are computed by the MOP as shown in Fig. 3.4, the agreement between the results obtained by the cavity formulations and by the MOP are very good. The radiation field components obtained by MOP appeared narrower than that produced by the cavity formulations.

The MOP simulation conditions for MPAs operating at these three modes are:

- TM_{01} mode: (1) the number of divisions=64, (2) the division cell size (x=0.309cm, y=0.206cm).
- TM_{02} mode: (1) the number of divisions=64 , (2) the division cell size (x=0.62cm, y=0.413cm).

- TM_{03} mod: (1) the number of divisions=128, (2) the division cell size=(x=0.46cm, y=0.31cm). For all modes the top dielectric layer of the enclosure is set to have the properties of air with thickness=1cm.

It can be noticed from Fig. 3.3 that TM_{03} mode has higher gain(dB) than the two other modes but with small side lobes in the E_q component, so we focus our study on TM_{03} mode in order to get maximum gain with side lobes reduction by studying the effect of the dielectric substrate material and the aspect ratio on the radiation pattern using cavity formulations with the aid of Matlab computation as follows:

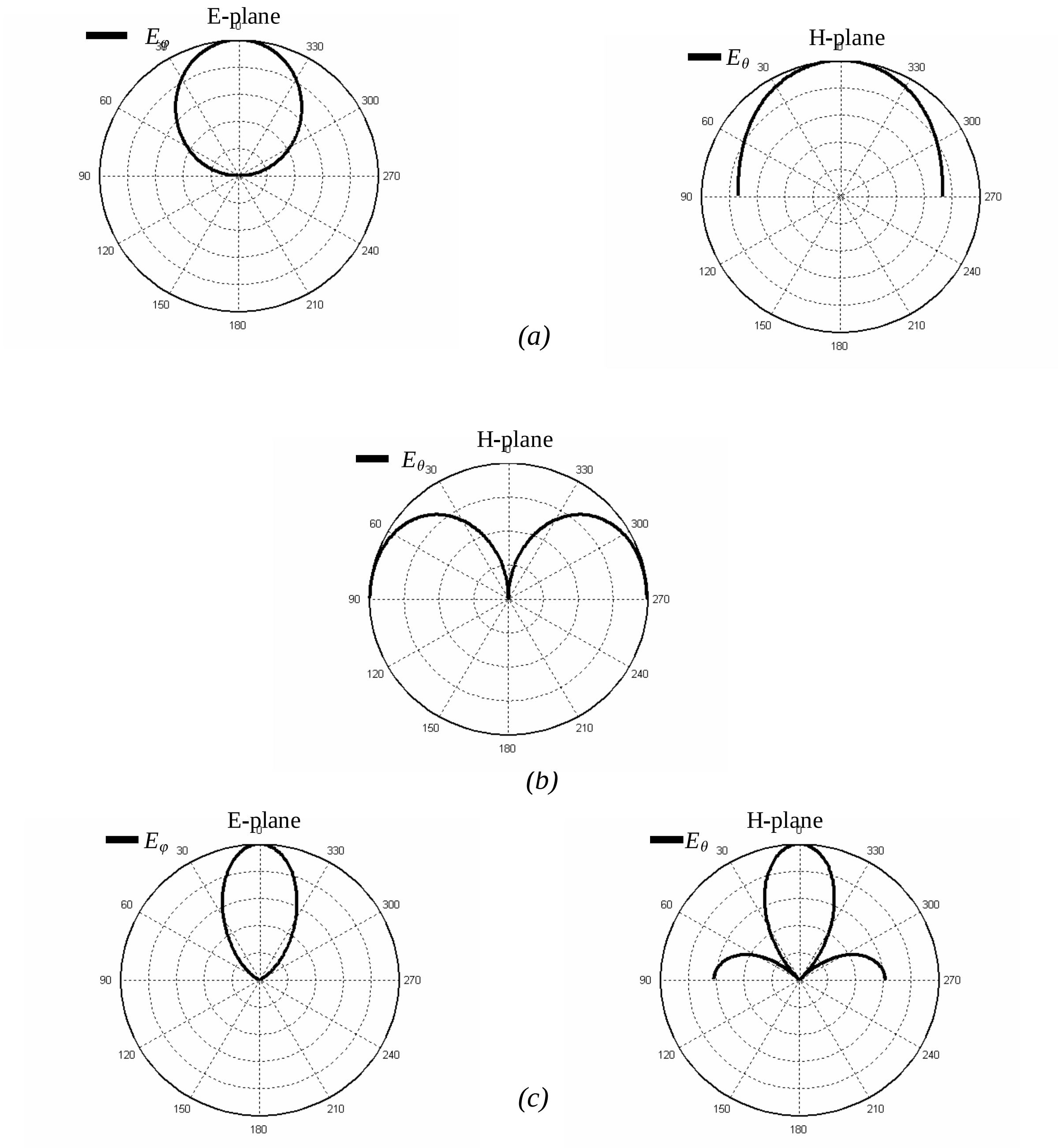

Figure (3.3) E-plane and H-plane of a MPA with parameters: f_r= 2.15 GHz, h=0.16cm, and e_r=4.45 for three different modes (a) TM_{01} mode , (b) TM_{02} mode ,and (c) TM_{03} mode calculated by using cavity formulations.

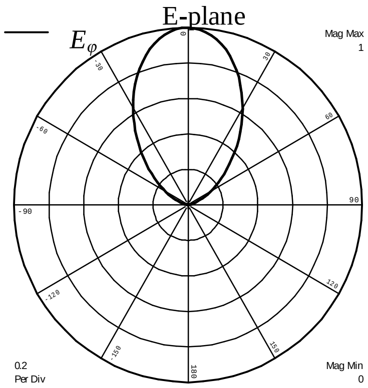

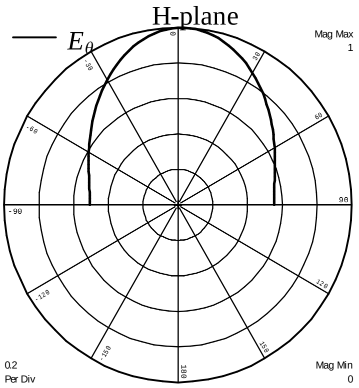

(a)

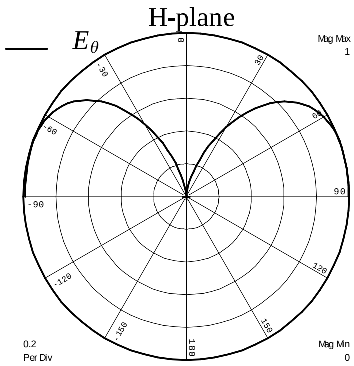

(b)

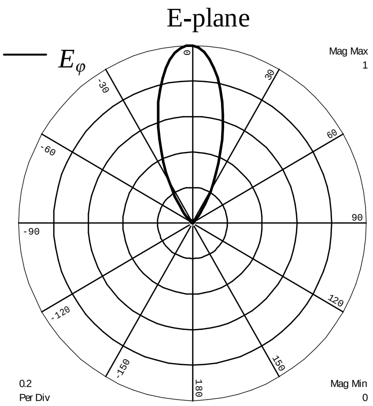

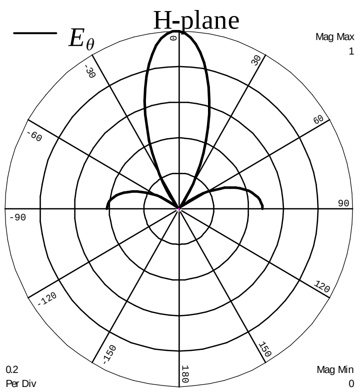

(c)

Figure (3.4) E-plane and H-plane of a MPA with parameters: f_r= 2.15 GHz, h=0.16cm, ande$_r$=4.45 for three different mode (a) TM_{01} mode , (b) TM_{02} mod , and (c) TM_{03} mode calculated by using MOP.

3.5.1.1 Effect of dielectric constant on radiation pattern

Three different values of e_r (e_r=2.62, 4.45, and 9.8) have been used in order to study their effect on the radiation pattern. This means that there are three sets of patch dimensions are produced according to equations 2.1-2.7. The calculated dimensions are taken at aspect ratio W/L=1.5. These values of the geometrical dimensions are shown in table (3.1). All these kinds of dielectric substrate have thickness of 0.16cm. Fig. 3.5 shows the effect of e_r on the radiation pattern. It is seen that, the radiation pattern changes appreciably with e_r, the E_q component contain side lobes which disappear in E_j component. This figure illustrate a very important case; it shows that the side lobes decrease with increasing e_r. Fig. 3.5(e) shows E_q without any side lobes; this form of radiation pattern is obtained at e_r=9.8. This pattern is quit important because there are no side lobes and gives rather high gain with respect to other types of dielectric substrate.

3.5.1.2 Effect of aspect ratio on radiation pattern

In order to increase the gain further the effect of aspect ratio on radiation pattern is studied. Three values of aspect ratios, W/L=1,1.5, and 2, have been studied. So that three sets of patch dimensions have been produced as shown in table (3.2). The resonance frequency, the substrate and its thickness are fixed at 2.15GHz, 9.8, and 0.16cm respectively. The effect of aspect ratio on the radiation pattern is shown in Fig. 3.6. It can be noticed that E_q does not appear to be sensitive with increasing W/L as shown in Fig. 3.6, whereas the $HPBW_E^o$ will improve(become narrower) for E-plane and the best value of $HPBW_E^o$ is found at W/L=2. Taking into account the best value of e_r(e_r=9.8) and W/L(W/L=2), the gain of the MPA is 9.74 dB according to equation 2.66. For the same parameters of MPA operating at TM_{03} mode, the radiation pattern obtained by using the MOP is shown in Fig. 3.7. It can be noticed from the figure that the radiation pattern using the package gives narrower main lobe than the cavity formulations. The gain produced using the package is 12.6 dB.

Table (3.2) Antenna dimensions of a MPA operating at TM_{03} mode for different aspect ratios (W/L) with parameters: f_r= 2.15 GHz ,ε_r= 9.8,and h= 0.16 cm.

W/L	*L(cm)*	*W(cm)*
1	6.68	6.68
1.5	6.68	10.02
2	6.68	13.36

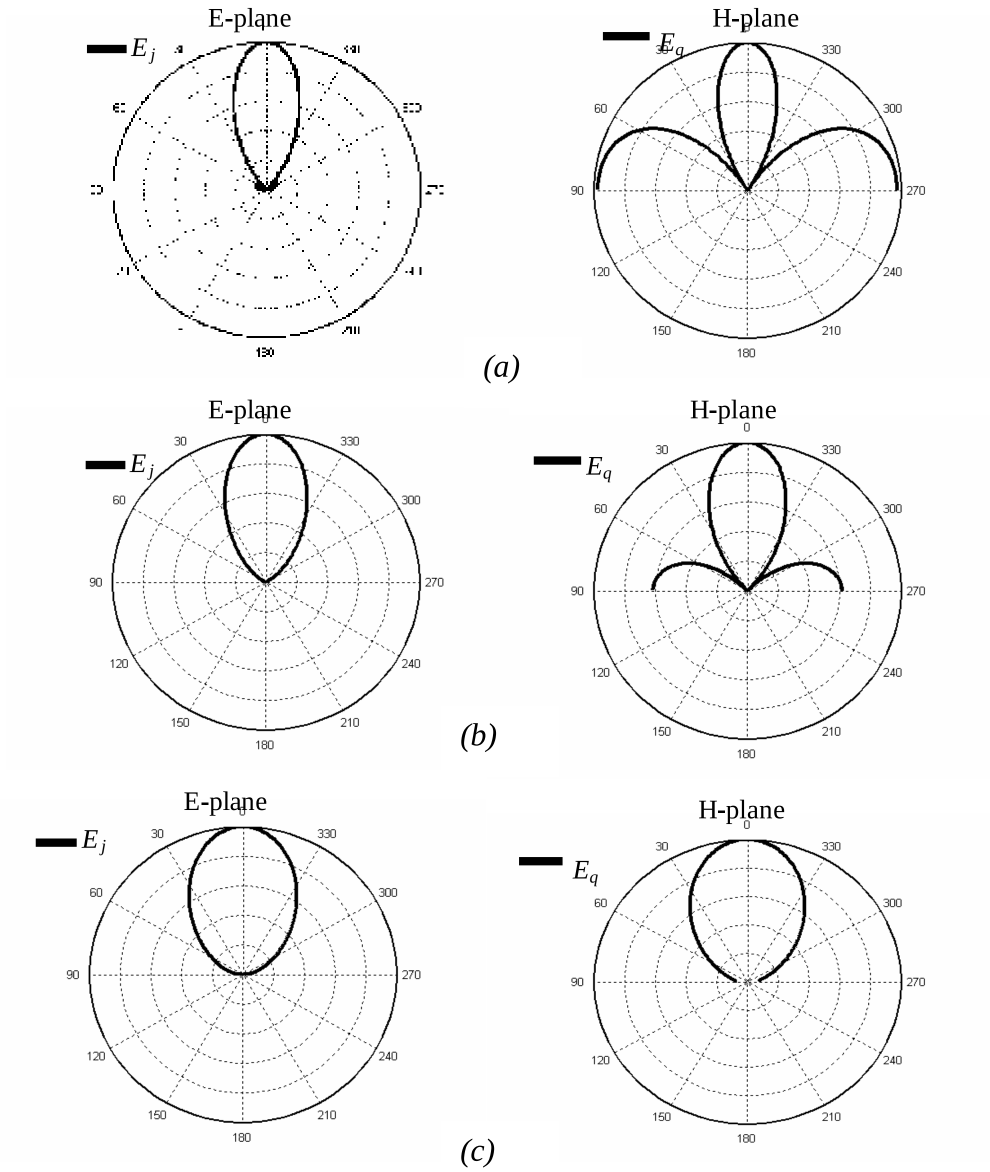

Figure (3.5) E-plane and H-plane of a MPA operating at TM_{03} mode with parameters: WxL=10.02x6.68cm^2 (W/L=1.5), f_r=2.15GHz, h=0.16cm , for different dielectric constants : (a)e_r=2.62, (b) e_r=4.45, and (c) e_r=9.8 calculated by using cavity formulations.

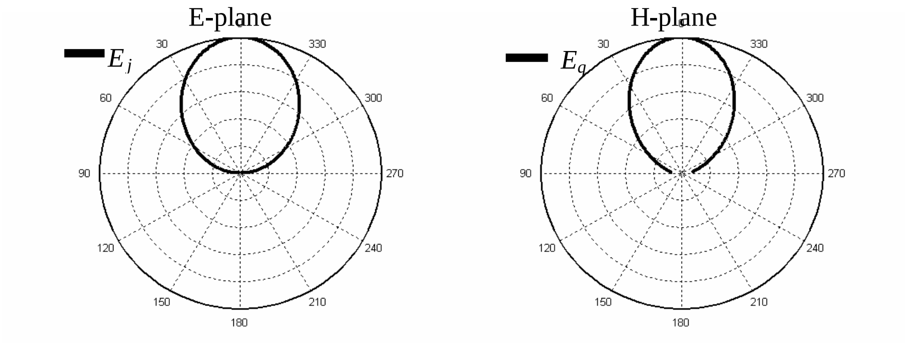

(a)

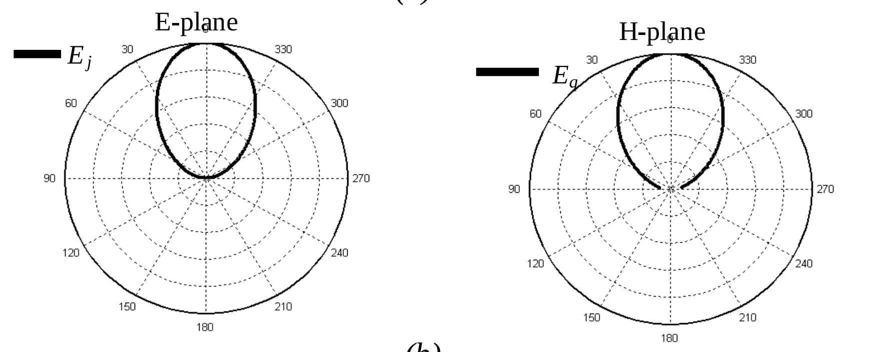

(b)

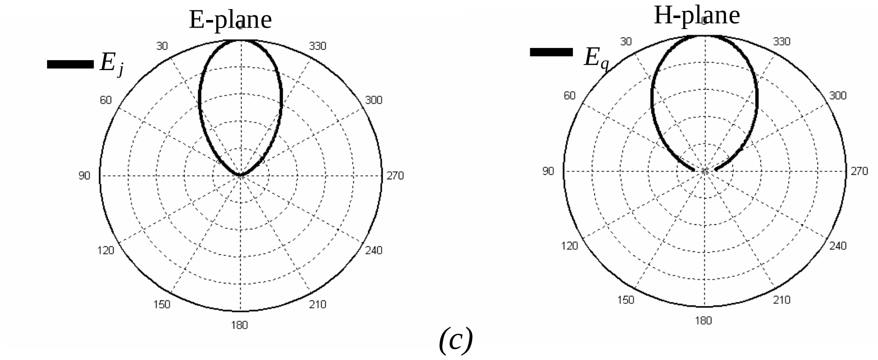

(c)

Figure (3.6) E-plane and H-plane of a MPA operating at TM_{03} mode with parameters: f_r=2.15GHz, h=0.16cm, and ε_r=9.8 for different aspect ratios:
(a)W/L=1, (b)W/L=1.5,and(c)W/L=2 calculated by using cavity formulations.

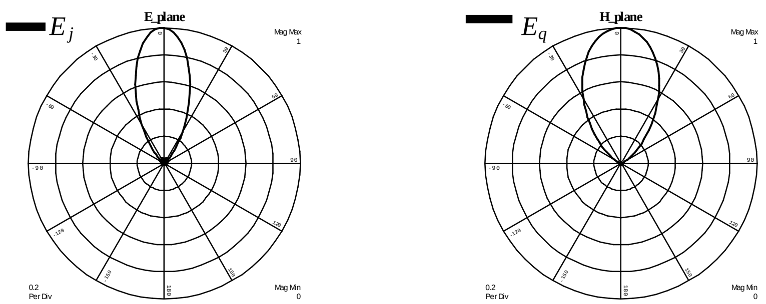

Figure (3.7) E-plane and H-plane of a MPA operating at TM_{03} mode with parameters:W x L=13.36cm x 6.68cm(W/L=2), f_r=2.15GHz, h=0.16cm, ande_r=9.8 calculated by using MOP.

3.5.2 Current Distribution

In order to understand the symmetry in the radiation, the aperture fields for plane parallel to the patch surface has been calculated by MOP. Fig.3.8 depicts the field distribution for these interested three modes. The aperture field's picture gives good correlation with the contribution excited mode number. The good symmetry in the high dense region appears in one of feed locations. This optimum location is selected by this easy method. The phenomena of symmetry illustrate the existing of the dominant modes whereas the asymmetry cases are due to absence of the dominant modes. This means that the proper optimum location gives high impedance matching with the dominant mode and with other excited modes.

3.5.3 Input Impedance Calculations

The input impedance depends on the position of the feed. Therefore the antenna is matched by choosing the proper feed position [58]. For a feed point at the radiating edge, the input impedance is maximum, and for a feed point at the center of the patch the input impedance is minimum. Thus, the input impedance can be controlled by adjusting the position of the feed point according to the following approximated equation [59]:

$$R(x) = R_o \cos^2(p\ x / L) \tag{3.1}$$

where R_o is the resistance at the edge of the patch and x is the distance from the edge. Also, the position of the feed point determines which mode is excited.

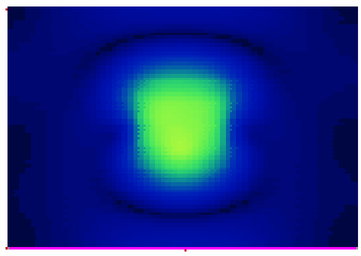

(a)

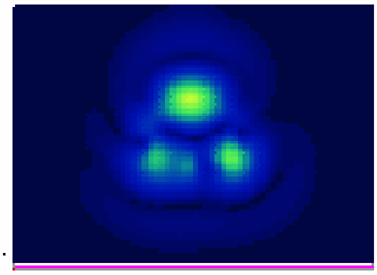

(b)

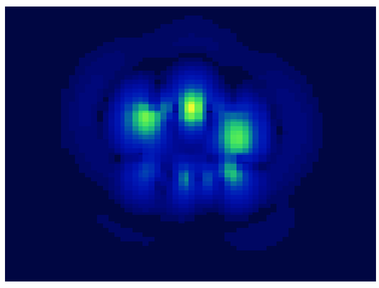

(c)

Figure (3.8) Current distribution of a rectangular MPA with e_r =4.45 and h=0.16 cm operating at (a) TM_{01},(b) TM_{02}, and (c) TM_{03} modes.

The input impedance calculations using the cavity formulations presented in Section 2.2.4 and the MOP are studied here. At *A*=1.5 in equation (2.49) the results for calculating the input impedance give good agreement with the published and the simulated (using the MOP) results. In order to be in confidence with our cavity formulations and the MOP in calculating the input impedance, it is re-calculated for a published work [44] by using these two methods. This published work consists of rectangular patch of dimensions (11.43 x 7.62) cm^2 operating at resonance frequency 1.19 GHz with three different feed locations (x_f,y_f)= (5.33,0.76),(5.33,2.29), and (5.33,3.05). Fig.3.9 shows the published and the calculated (using cavity formulations) input impedance (real and imaginary parts) results for these feed locations with the aid of Matlab computation (see appendix B). It can be seen that there is a small shift between the published and the calculated results. So depending on these results, the cavity formulations can be applied to any other examples. Fig.3.10 shows the published [44] and the calculated (using MOP) input impedance (Smith chart) results. It can be observed from this figure that there is a high degree of agreement between the published and computed results.

Now the input impedance calculations for TM_{01}, TM_{02} and TM_{03} modes are done by the cavity formulations and MOP. The patches for the three modes are printed on the same dielectric substrate of e_r=4.45, with thickness h=0.16cm and their dimensions are presented in table (3.1).

The MOP and the cavity formulations are used to get the best feed location for antennas operating at these different modes i.e. give good matching between the antenna and probe feeding, nearly at 50Ω. The results are tabulated in table (3.3). This table shows the antenna characteristics (maximum resistance, feed location, and resonance frequency) for three modes by using MOP and cavity formulations, it is shown from this table that there is an excellent agreement between these two methods so this give good indication about our theoretical formulations.

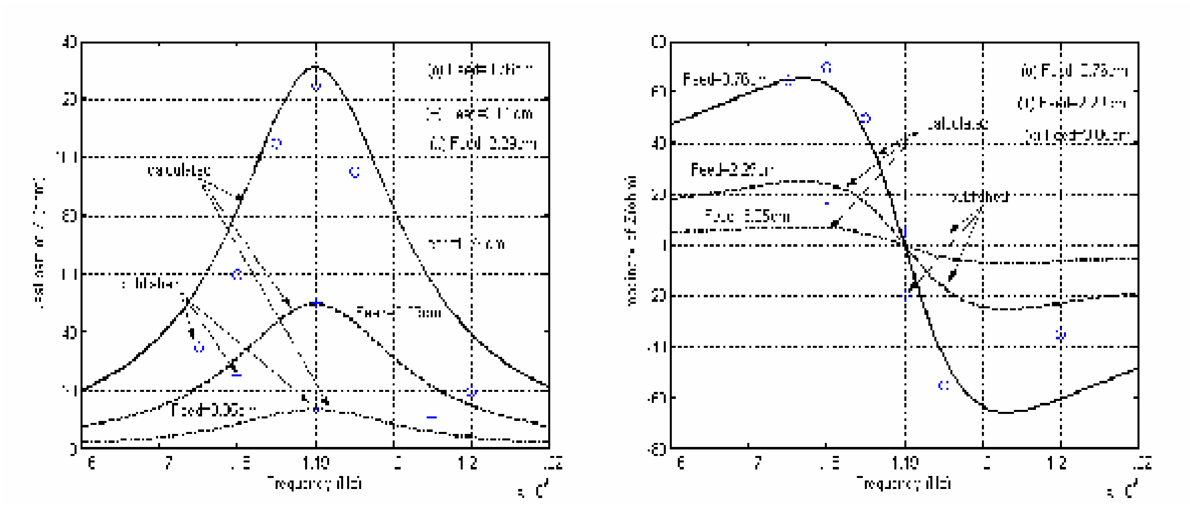

Figure (3.9) Input impedance (real and imaginary parts) comparison between the cavity formulations and the published results[44] for rectangular MPA of dimensions=(11.43 x 7.62) cm^2 operating at f_r= 1.19 GHz.

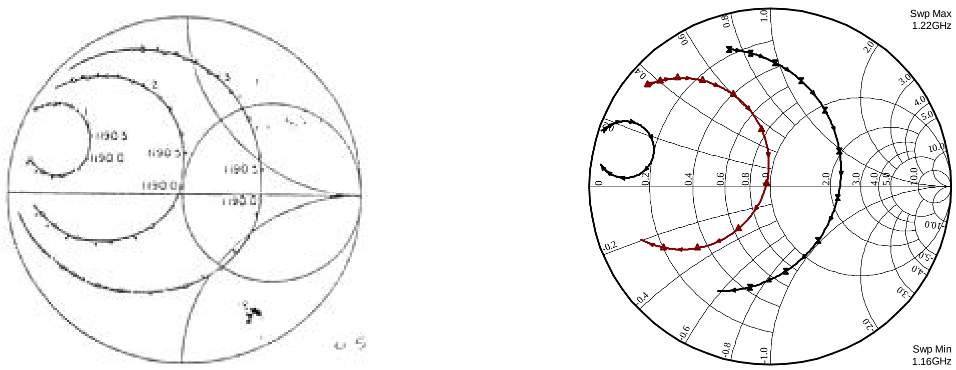

(a) *(b)*

Figure (3.10) Input impedance results of a rectangular MPA with dimensions =(11.43 x 7.62) cm^2 operating at f_r 1.19GHz (a) Published results[44] (b) Calculated by using MOP.

Table (3.3) Antenna design characteristics (maximum resistance, feed position, and resonance frequency) of MPAs operating at TM_{01}, TM_{02}, and TM_{03} modes with parameters: f_r=2.15 GHz, e_r=4.45, and h=0.16 cm computed by using MOP and cavity formulations.

Mode	MOP package			Cavity formulations		
	Max. R(W)	Feed position (x_f,y_f)(cm)	f_r(GHz)	Max. R(W)	Feed position (x_f,y_f)(cm)	f_r(GHz)
TM_{01}	56	(2.47,1.03)	2.09	51	(2.47,1.046)	2.117
TM_{02}	49	(4.96,0.83)	2.11	49.6	(4.96,0.707)	2.13
TM_{03}	41	(7.44,2.48)	2.06	51	(7.44 ,2.9)	2.139

By using the cavity formulations with the aid of Matlab computation, the best feed location can be obtained easily taking short computation time. By using the package it is also easy to do that but it takes longer time (simulation time), but both of them are considered very easy methods for obtaining matching condition when they are compared with the experimental method.

3.5.3.1 Effect of feed position on input impedance

Input impedance (real and imaginary parts) for different feed locations is studied for microstrip patch antenna (MPA) operating at TM_{03} mode using cavity formulations and MOP. The parameters of the (MPA) are: patch dimensions=10.02 cm x 6.68 cm, e_r=9.8, and h=0.16 cm. The MPA operating at this mode with this type of e_r is chosen due to its good advantage of producing broad side radiation pattern without side lobes with narrow main lobe. The package is used to simulate the antenna with proper mish divisions, (the number of divisions =128 divisions, x cell size= 0.313cm, y cell size=

0.208cm, and the top dielectric layer of the enclosure is set to have the properties of air with thickness=1cm).

The cavity formulations and the MOP results for different feed locations are shown in Fig.3.11 and Fig. 3.12 respectively. It can be seen that there is a little difference between them. Cavity formulations results are shown only one resonance peak appear at f_r=2.14GHz while for MOP (Fig. 3.12), the result shows that there are two resonance peaks one at f_r=2.07 GHz and the second at 2.13 GHz for the same feed locations This is because the cavity formulations omit the feed effect and the presence of other modes while the MOP results include that. A comparison between the input impedance results from MOP and cavity formulations are summarized in table (3.4). The first resonance is appearing according to presence of other modes beside the dominant one. It can be noticed from the MOP results that when the feed location increases from the radiating edge toward the center of the patch, the first resonance peak decrease until it reaches minimum values at the center of the patch, while the second resonance varies randomly. Also it can be seen that the resonance frequency does not effected by the feed location. It can be observed that the resonance frequency produced from the cavity formulations is very close to the second resonance obtained from the MOP results. Changing the location of the feed point leads to change the impedance matching for dominant and non dominant modes. This leads to the possibility of choosing the position that gives a pure TM_{03} mode in a certain value of Z_{in}. In other words matching circuit between the coaxial feed and input impedance must be done. The location 2.9cm gives nearly pure TM_{03} mode. Fig. 3.13 shows the comparison of input impedance calculated by cavity formulations and the MOP for TM_{03} mode at feed position = (5.01cm, 2.9cm).

Table (3.4) Impedance characteristic of a MPA operating at TM_{03} mode with parameters: patch dimensions (10.02 x 6.68) cm^2, f_r= 2.15 GHz ,ε_r= 9.8,and h= 0.16 cm computed by using the MOP and the cavity formulations.

	MOP				Cavity formulations	
Feed location (y_f) (cm) x_f=5.01cm	First resonance (f_{r1})(GHz)	Second resonance (f_{r2})(GHz)	Max. R for f_{r1}(W)	Max.R for f_{r2} (W)	Resonance frequency f_r(GHz)	Max. R (W)
0	2.07	2.13	180	80	2.142	118
1.25	2.07	2.13	150	---	2.142	4.3
1.67	2.07	2.13	118	40	2.142	60
2	2.07	2.13	80	90	2.142	106
2.9	2.07	2.13	10	40	2.142	38
3.34	2.07	2.13	---	---	2.142	---

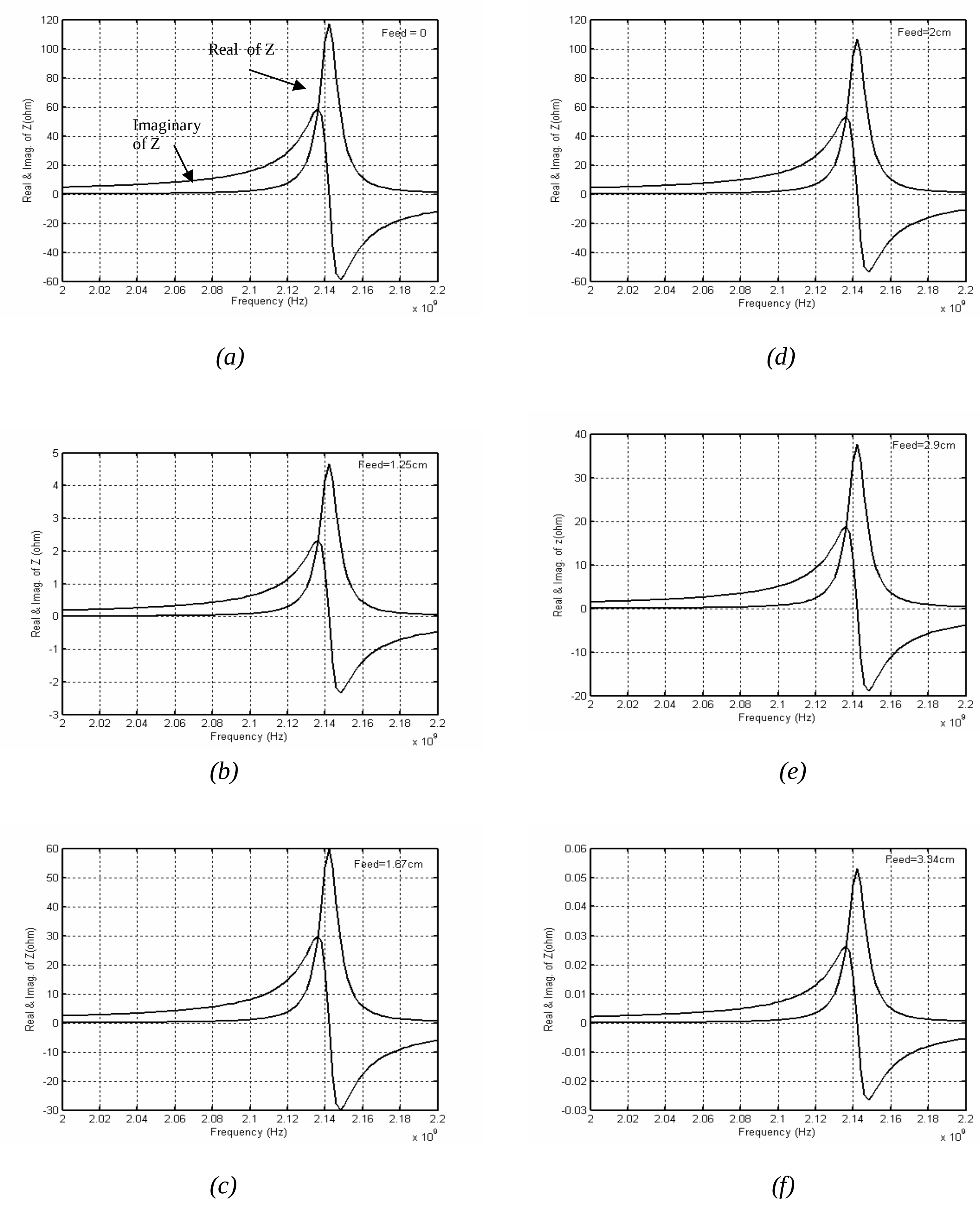

Figure (3.11) Input impedance(real and imaginary parts) of a MPA operating at TM_{03} mode with parameters : patch dimensions=(10.02x6.68) cm^2 (W/L=1.5), e_r= 9.8 and h =0.16cm at the middle of the x-dimension of the patch and different y- axis locations(y_f): (a)0,(b) 1.25 cm, (c)1.67cm , (d)2 cm, (e)2.9 cm,and (f) 3.34cm calculated by using cavity formulations.

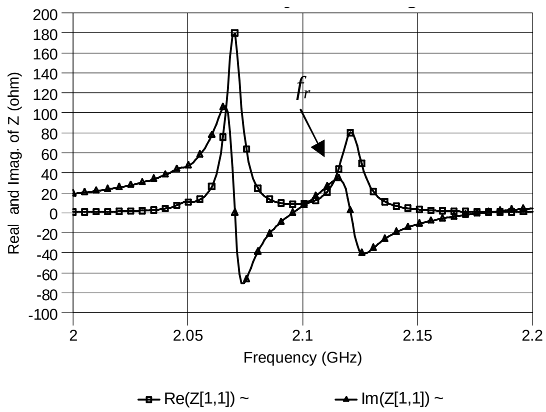

(a)

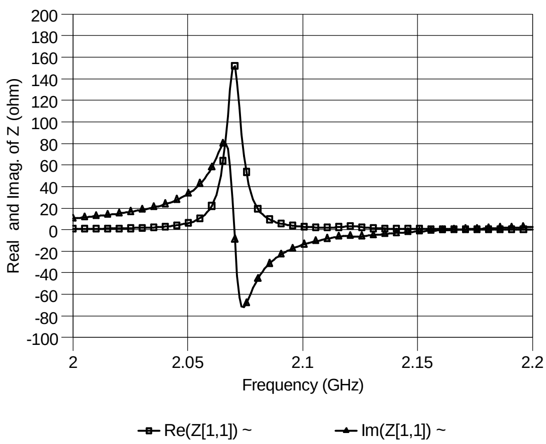

(b)

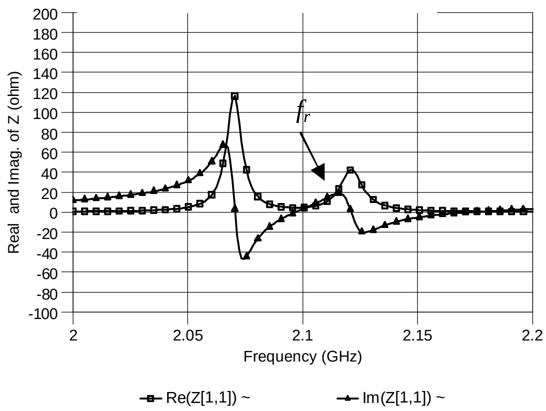

(c)

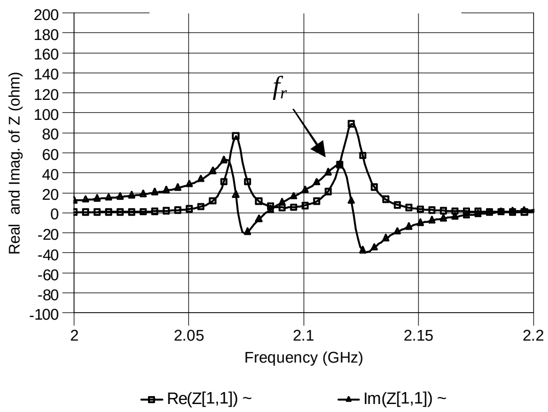

(d)

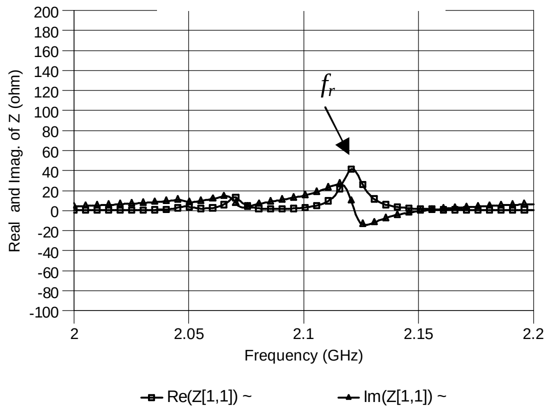

(e)

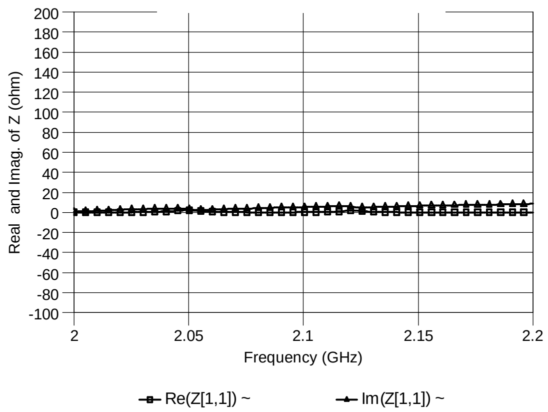

(f)

Figure (3.12) Input impedance (real and imaginary parts) of a MPA operating at TM_{03} mode with parameters : patch dimensions=(10.02 x 6.68) cm^2 (W/L=1.5), e_r= 9.8 and h =0.16cm at the middle of the x-dimension of the patch and different y-axis locations(y_f): (a) 0,(b) 1.25 cm, (c)1.67cm , (d) 2 cm, (e)2.9 cm, and(f)3.34 calculated by using MOP.

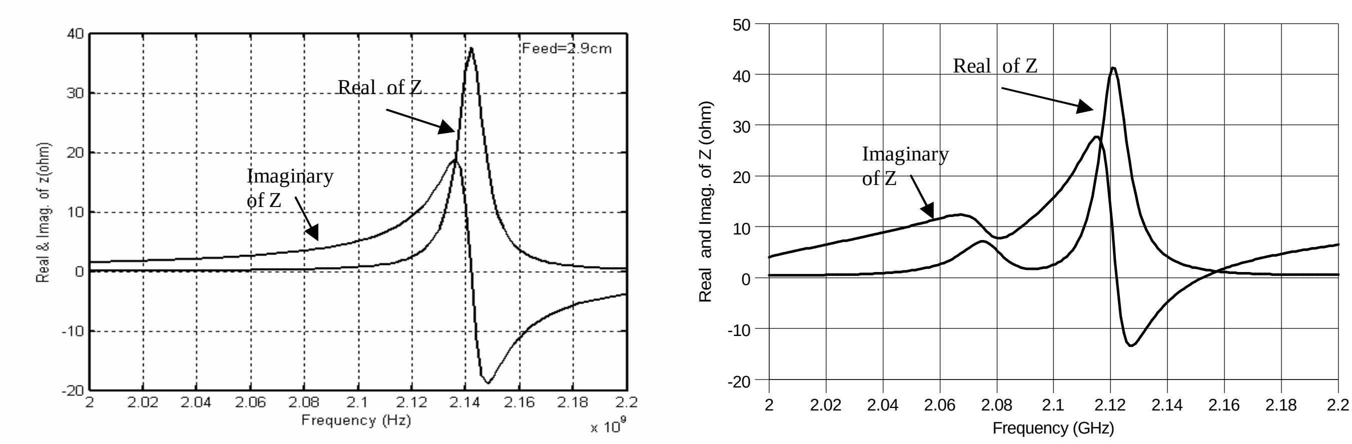

(a) *(b)*

Figure (3.13) Input impedance results of a MPA operating at TM_{03} mode with parameters : patch dimensions(10.02 x 6.68) cm^2 (W/L=1.5), e_r= 9.8 and h =0.16cm at feed location(5.01cm,2.9cm)calculated by using:
(a) Cavity formulations (b) MOP

3.6 Bandwidth Enhancement of MPA Operating at TM_{03} Mode

The MPA operates at TM_{03} mode (Section 3.5.1.2) with parameters; WxL=(13.36 x 6.68)cm^2 (W/L=2), h=0.16cm(thin substrate) , feed position (x_f=6.68cm,y_f=1.67cm), and ε_r=9.8, has the advantage of producing radiation pattern with narrow main lobe without side lobes and with rather high gain(12.6dB). The feed point is selected such that a good matching between the antenna and the coaxial cable (nearly 50Ω)can be produced. This is clearly shown in Fig.3.14(a) and (b). This thin MPA has disadvantage of very small bandwidth (8MHz) as shown in Fig. 3.14(c). Therefore; the TM_{03} mode will be examined in order to produce large bandwidth in addition to the high gain by using the MOP. Two techniques were followed to get this purpose: The first one is to use thick substrate with coaxial feed excitation (direct feed). The second one (in order to increase the bandwidth further) is to feed the first structure capacitively (indirect feed). The configuration for both kinds of antennas (probe-feed and capacitive-feed thick substrate MPA) are shown in Fig. 3.15

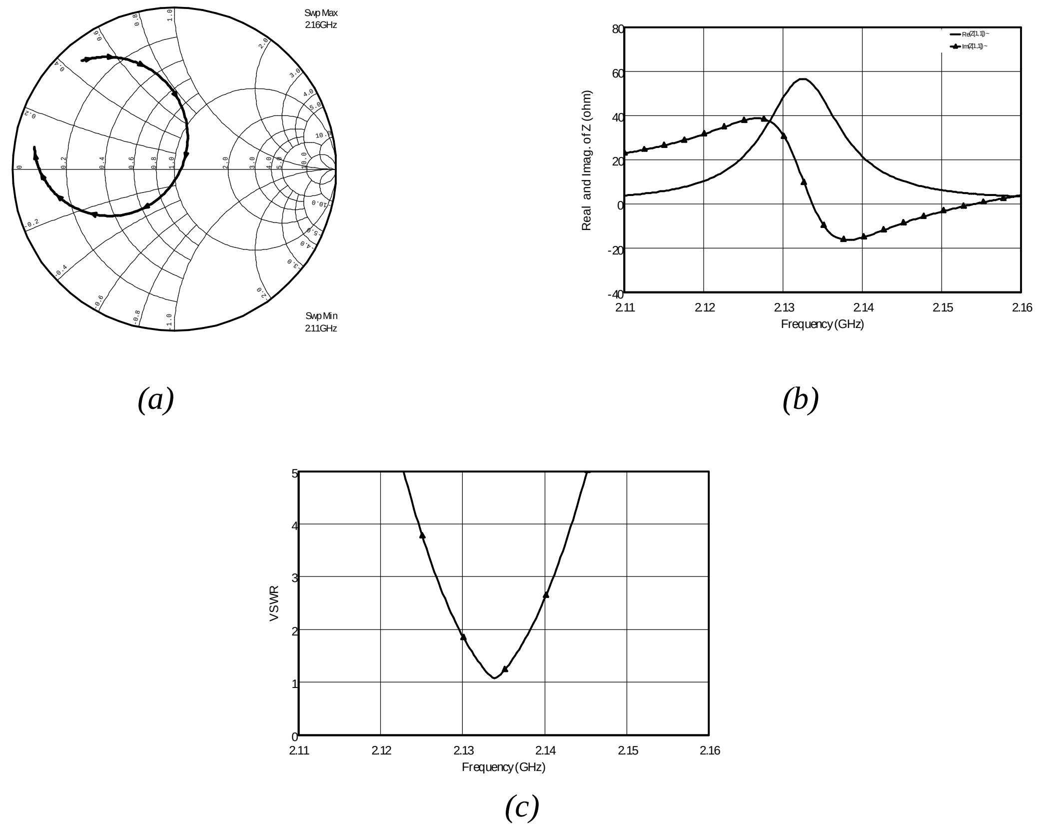

Figure (3.14) (a) Smith chart , (b)Real and imaginary parts of input impedance, and (c) VSWR curves of a probe-fed thin substrate MPA operating at TM_{03} mode with parameters: patch dimensions = 13.36cmx 6.68cm, e_r= 9.8, and h=0.16cm.

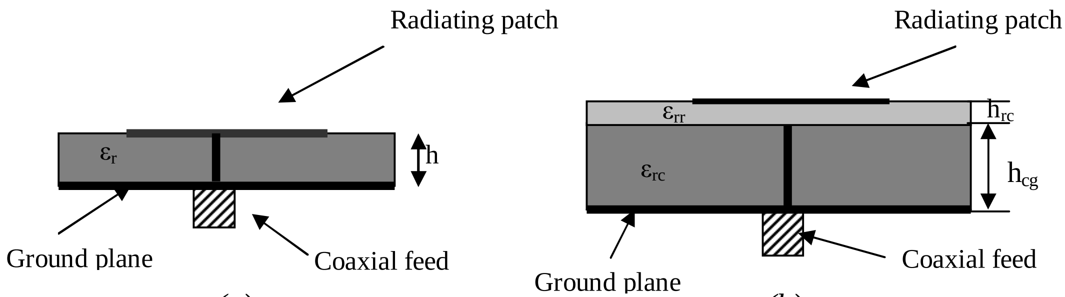

(a) *(b)*

Figure 3.15 The configuration of the MPA operating at TM_{03} mode, patch dimensions =13.36cmx6.68cm (W/L=2), (a) Probe-fed with parameters; e_r=9.8, h=0.96cm (b) Capacitivly-fed with parameters; $e_{rr}=e_{rc}$=9.8,h_{rc}=0.1cm and h_{cg}=0.96cm.

3.6.1 Thick Substrate of Rectangular MPA Operating at TM_{03} Mode

First the thick substrate with direct feed is applied in order to enhance the bandwidth, Fig. 3.15(a). This design consists of a rectangular patch with dimensions 13.36cm x 6.68cm printed on dielectric substrate with e_r= 9.8 of thickness h=0.8cm(0.12 λ_d) where λ_d is the wavelength inside the dielectric at f_r 2.15GHz. The radiating patch is excited by coaxial feed probe at feed position (x_f=6.68cm, y_f=1.67cm).

The maximum impedance bandwidth produced (with keeping the same form of the radiation field pattern) is 2.6%. This value produced by choosing the proper feed location and dielectric substrate thickness. The input impedance and the VSWR of this antenna are shown in Fig.3.16. It can be observed that the frequency range was positioned near the center of Smith chart but in the inductive region due to the probe length. The radiation field pattern for three values of frequency within the band is shown in Fig. 3.17. It can be noticed that in the H-plane E_θ component has symmetrical shape with respect to the zenith($\theta=0^o$). In the E-plane there is a small shift from the zenith (asymmetric shape) for E_φ component which increase when the frequency increases. The gain produced from this design at operating frequency 1.92GHz is 13.94dB. Also it can be seen that there is no cross-pol components will appear in both planes. The bandwidth can be improved by this technique to nearly 8 times larger. Further increase in the thickness will deteriorate the pattern.

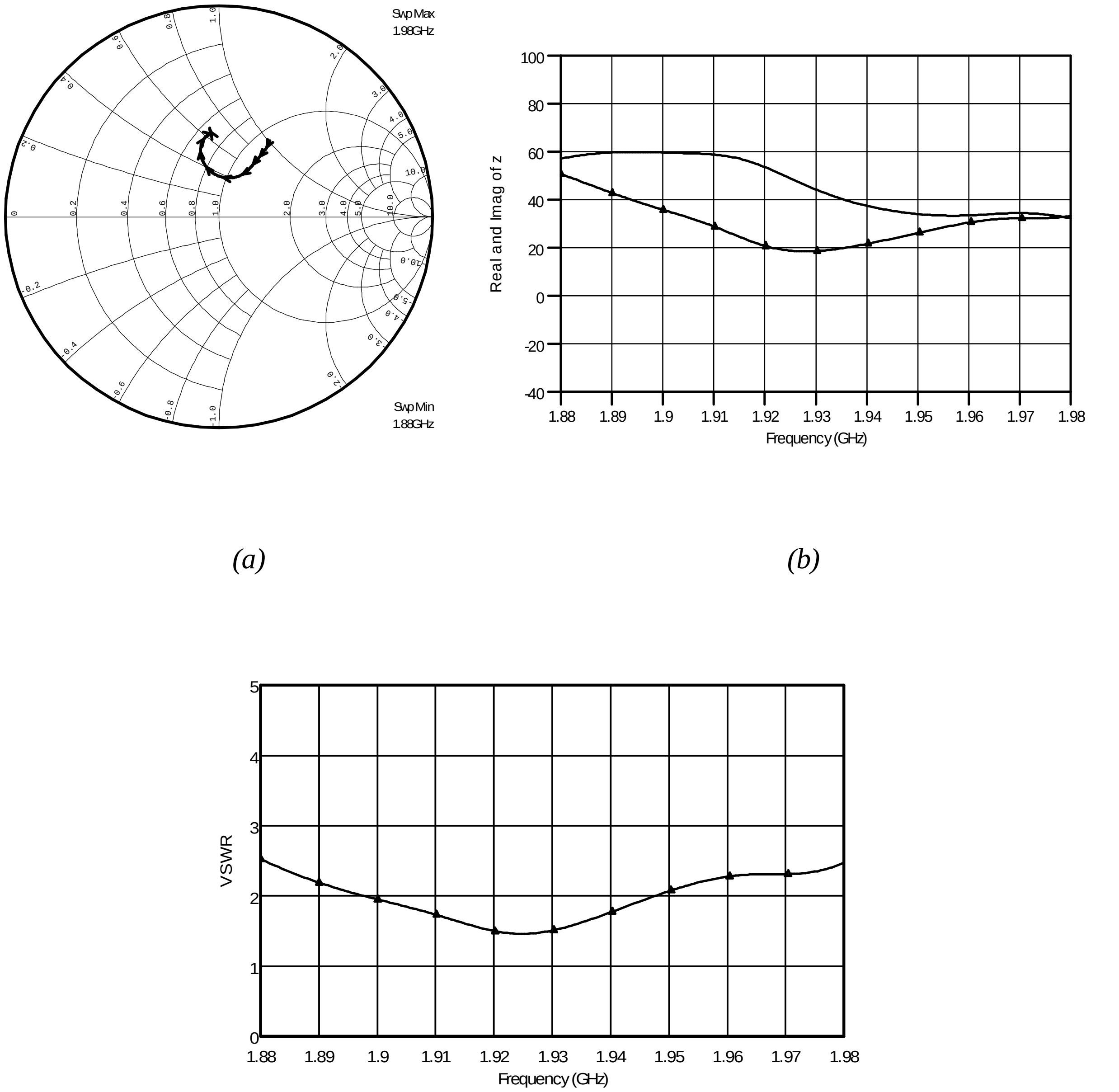

(a) *(b)*

(c)

Figure (3.16) (a) Smith chart , (b)Real and imaginary parts of input impedance, and (c) VSWR curves of a probe-fed thick substrate MPA operating at TM_{03} mode with parameters: patch dimensions =(13.36 x6.68)cm^2, e_r= 9.8, and h=0.96cm.

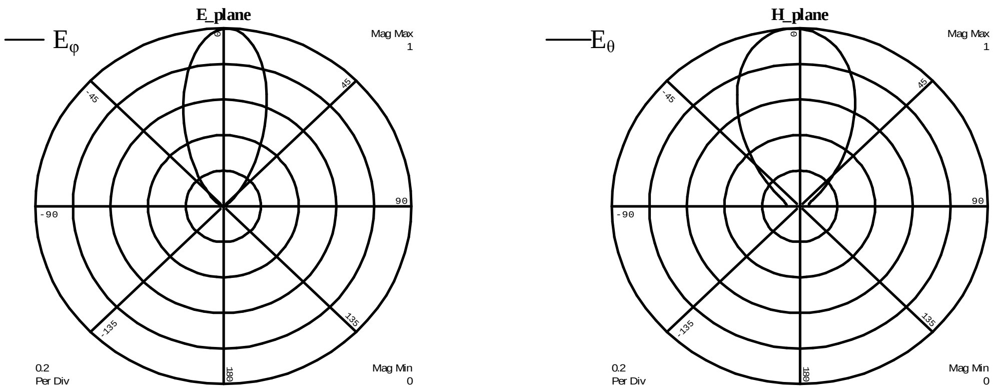

(a)

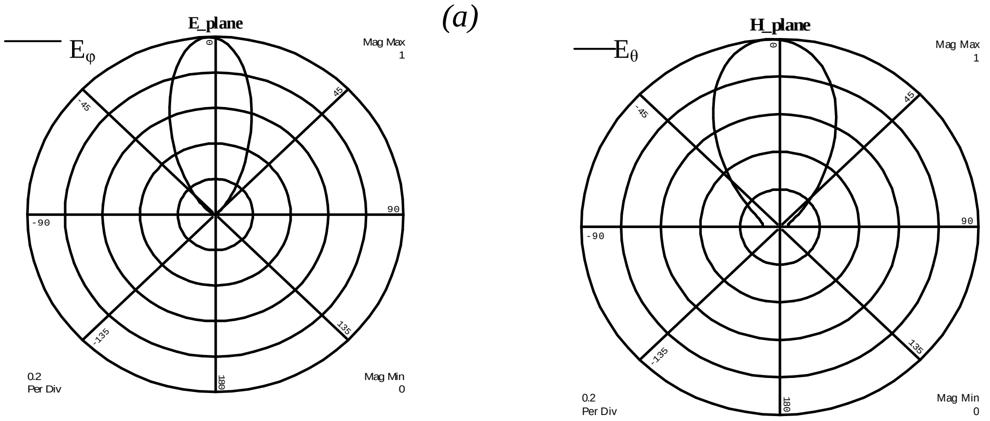

(b)

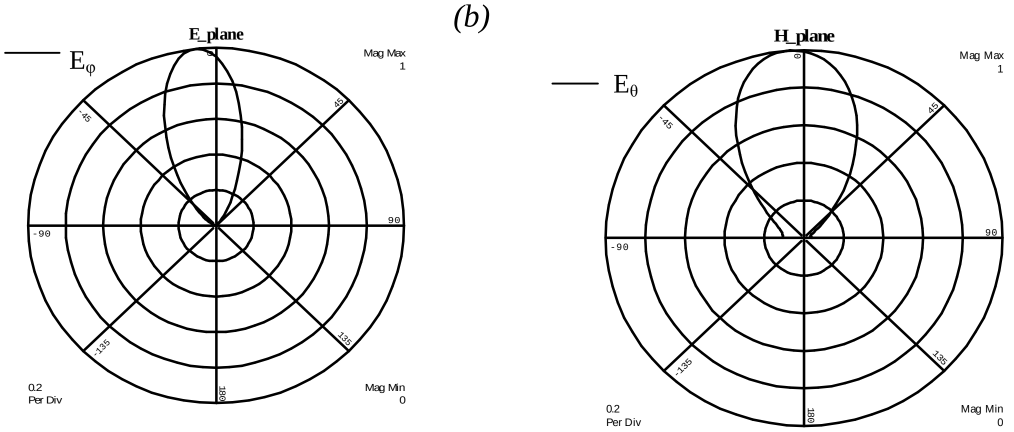

(c)

Figure (3.17) E-plane (j =0^o) and H-plane (j =90^o) of a probe-fed thick substrate MPA operating at TM_{03} mode with parameters: patch dimensions = 13.36cm x6.68cm, e_r= 9.8, and h=0.96cm for different frequencies; (a) f= 1.9, (b) f= 1.92, and (c) f= 1.94GHz.

3.6.2 Capacitively-Fed of Rectangular MPA Operating at TM_{03} Mode

In order to increase the bandwidth further a second technique, using the capacitive feeding technique is examined, see Fig.3.15 (b). In this design the MPA consists of a radiating patch, a ground plane, and a small patch located between the ground plane and radiating patch. The small patch is fed by a coaxial feed probe. The radiating patch (13.36cm x 6.68cm) is printed on a dielectric substrate of e_{rr}=9.8 with thickness h_{rc}(the spacing between the radiating and the capacitor patches)=0.1cm. A small rectangular (capacitor) patch with dimensions 0.83cm x 0.41cm (the same dimensions of the coaxial probe feed) is printed on a dielectric substrate of e_{rc}=9.8 with thickness h_{cg}(the spacing between the capacitor patch and the ground plane)=0.96cm. The radiating patch is fed by electromagnetic coupling from the capacitor patch. Fig. 3.18 shows the input impedance and VSWR of the antenna for this design. It can be noticed that all the frequency range located in the region near the center of Smith chart with capacitive and inductive values as shown in Fig.3.18(a). This means good matching condition is achieved. This is due to the capacitive part generated between the capacitor and radiating patches making the total input impedance of the MPA less inductive. The impedance bandwidth produce from this design is 22.6% for VSWR $\leq$2 as shown in Fig. 3.18(c). Fig. 3.19 shows the radiation pattern for different values of frequency within the band. The gain produce from this design at 1.9 GHz is 13.5 dB. It can be noticed that by using this technique, the radiation field patterns and the gain will nearly remain unchanged having main lobe with symmetric shape with respect to the zenith pattern for both E- and H-planes. Also it can be noticed that E_φ component in the E-plane and E_θ component H-plane, will shifted from the zenith by small angle when the frequency increases.

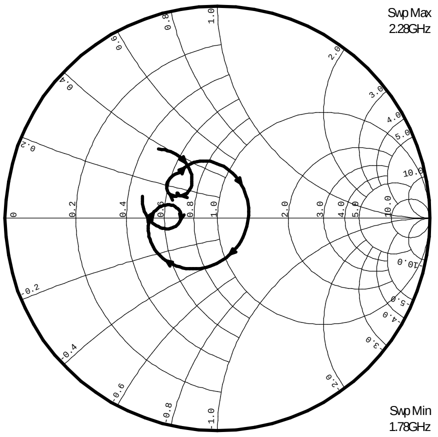

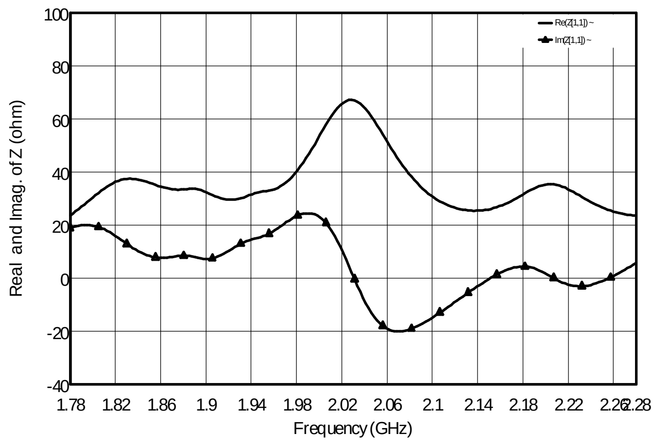

(a) *(b)*

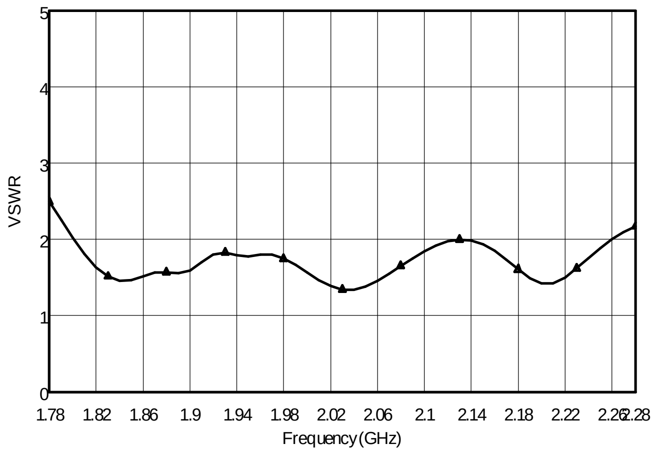

(c)

Figure (3.18) (a) Smith chart ,(b) Real and imaginary parts of input impedance, and (c) VSWR curves of a capacitively-fed thick substrate MPA operating at TM_{03} mode with parameters: patch dimensions =13.39cmx6.68cm, $e_{rr}=e_{rc}=9.8$, $h_{rc}=0.1cm$, and $h_{cg}=0.96cm$.

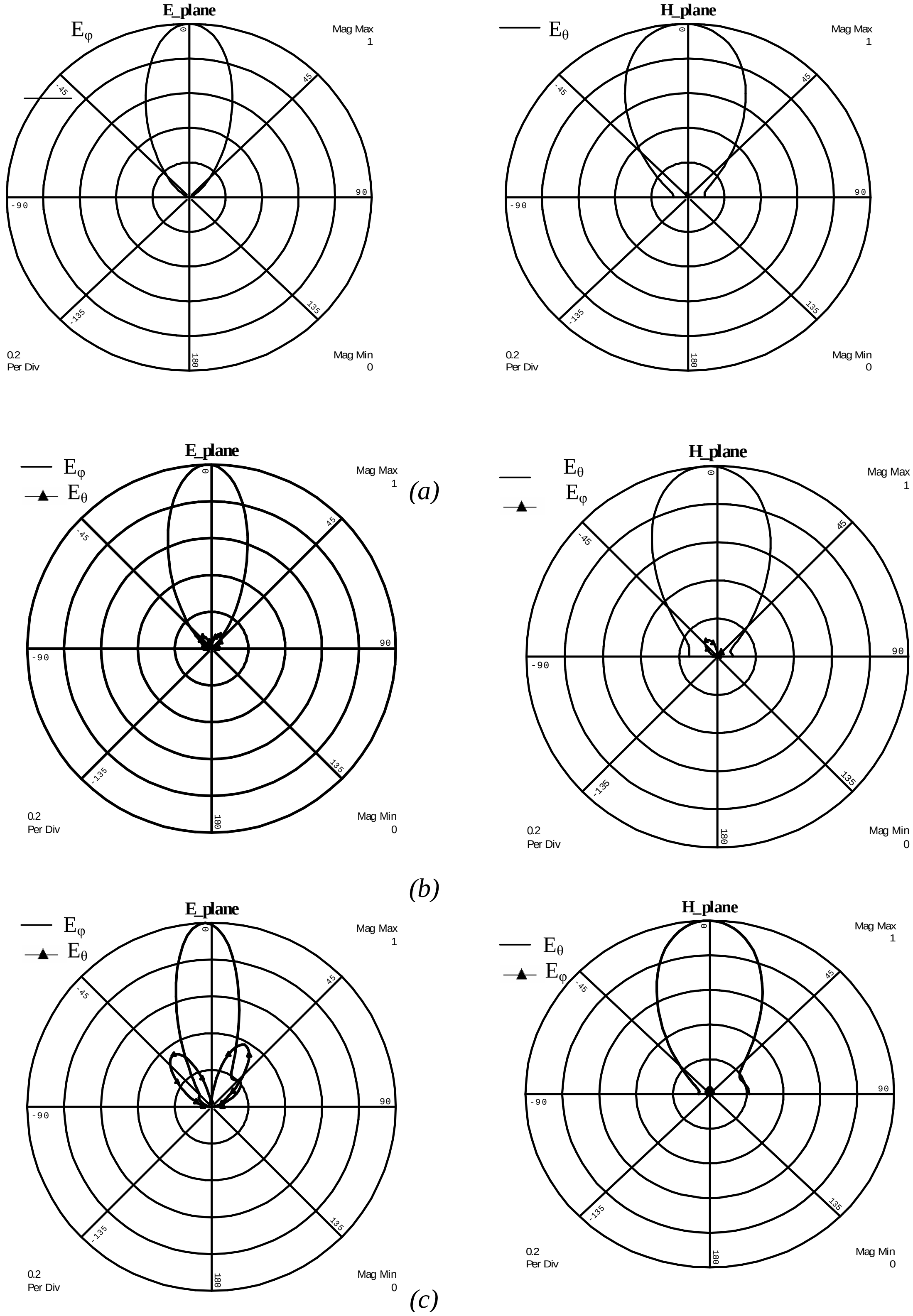

Figure (3.19) E-plane and H-plane of a capacitively-fed thick substrate MPA operating at TM_{03} mode with parameters: patch dimensions =13.36cm x6.68cm,e_{rr}=e_{rc}=9.8, h_{rc}=0.1cm, and h_{cg}=0.96cm for different frequencies; (a)f=1.82, (b)f= 1.9, and (d)f=1.98GHz

Chapter 4

Simulation of Stacked Patch Microstrip Antenna

4.1 Introduction

This chapter deals with stacked dual-patches configuration. A stacked dual-patch configuration is one of the solutions that have been used to improve the bandwidth. The basic geometry of the stacked dual-patch configuration consists of two layers stacked parasitically above each other, (see Fig. 1.2(b)). The upper patch is excited via electromagnetic coupling from the lower patch, which is connected directly to the feed line. The top and bottom patches are referred to as the radiating and the feeding patches, respectively. The spacing between them is filled with a dielectric substrate material.

Electromagnetic coupling technique applied for microstrip patches was first proposed by Saban [8], who has reported experimental results in the frequency range of 2-4 GHz on circular, annular ring and rectangular electromagnetic coupled patches.

In this chapter two designs of stacked dual-patch electromagnetic-coupled microstrip antenna have been analyzed:

In the first design a published work [45] which consists of a single rectangular microstrip patch has been considered as a lower feeding patch. Another rectangular patch (radiating patch) is suspended above the feeding patch. The spacing between the two patches is filled with air. The effects of this spacing and the upper patch dimensions have been studied extensively.

Then with the optimum design parameters a thicker substrate has been taken to produce a wider bandwidth. In the second design the lower patch is a square patch of length equals to $\lambda_o/2$ where λ_o is the free space wavelength while the upper patch is a square patch with larger dimensions than the lower one.

MOP is used to analyze the stacked configurations. The impedance locus and the radiation pattern are computed by the package.

In order to demonstrate the performance of the package for the analysis of this type of MPAs, a previously published work is re-simulated by the MOP.

4.2 Simulation Results for Published Stacked MPA

A stacked rectangular patch antenna, of published work for R.B.Waterhouse [60] is investigated using MOP. The antenna structure consists of a first patch on top of a second patch on top of a ground plane with one dielectric layer between the first (radiating) and the second (feeding) patches (e_{rr}=1.07) and one dielectric layer between the second patch and the ground plane((e_{rf}=2.2), the dimensions of the upper patch are 15mm x 16mm and the dimensions of the lower patch are 13.5mmx12.5mm.

The MOP conditions are: (1) the number of divisions=128, (2) the division cell size=(x=0.42mm, y=0.39mm), (3) the top dielectric layer of the enclosure is set to have the properties of air with thickness=10mm.

The impedance locus of this antenna with probe fed excitation measured between 6 and 9 GHz with a set of 0.5 GHz are computed. The agreement between these two values was shown in Fig. 4.1.

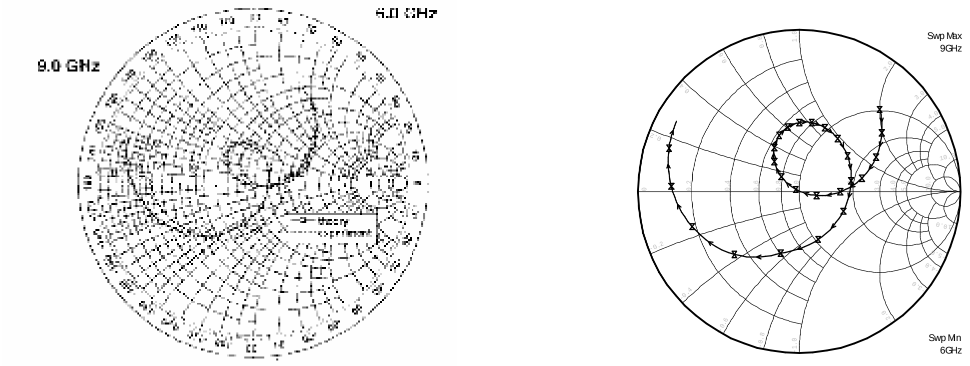

Figure (4.1) Input impedance(Smith chart) of a stacked dual-patch microstrip antenna
a) Published experimental and computed results [60].
(b)Computed results using MOP.

4.3 The Configuration of the Rectangular Stacked MPA

The geometry of the proposed (first design) stacked dual-patch electromagnetic coupled microstrip antenna is shown in Fig. 4.2. A rectangular patch (feeding patch) of dimensions L_f=11.43cm and W_f= 7.62cm operating at resonance frequency (f_r =1.19 GHz) is printed on ground plane with dielectric material of e_{rf} =2.62 and thickness h_{fg}(the spacing between the feeding patch and the ground plane) =0.16 cm ($0.01\lambda_d$) where λ_d (15.5cm) is the wavelength inside the dielectric substrate at f_r=1.19GHz. These values were kept constant for all sets of variation. Another thin rectangular parasitic conducting plate(radiating patch) of dimensions L_r x W_r is placed above the lower patch and separated by a region of air (e_{rr}=1) of width Δ. The top element is excited via electromagnetic coupling from the lower element, which is located closer to the ground plane and is connected directly to a coaxial feed line.

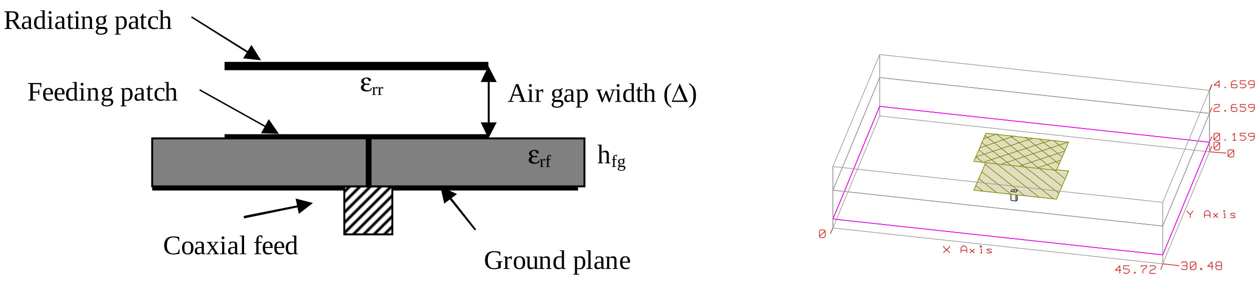

(a) *(b)*

Figure (4.2) The configuration of the stacked suspended MPA (a) Side view (b) MOP view.

4.3.1 Simulation and Results of Rectangular Stacked MPA

An extensive study on the parameters that affected the impedance bandwidth is given below

4.3.1.1 Effect of the air gap width

This section was pointed to study the effect of the air gap width Δ on input impedance and VSWR behaviors. The dimensions of feeding and radiating plates are 11.43cm x 7.62cm. The analytical computations is taken to study the effect of Δ on antenna parameters by keeping the feed position in a location that gives real input impedance (nearly at 50 Ω) before inserting parasitic conducting plate (single MPA). The feed location is (x_f =5.35cm, y_f=2.14cm). The impedance curve for a single element is located at the center of the Smith chart. This means good impedance matching between the antenna and the feed probe. When adding a stacked patch with different air gaps the impedance locus was changed as well as VSWR as shown in Fig. 4.3

The MOP conditions were: (a) the number of divisions=64, (b) the division cell size was x=0.714cm, y=0.476cm, and (c) the top dielectric layer of the enclosure was set to have the properties of air with 2 cm in thickness; the antenna was fed with excitation port of 50 Ω.

The results are tabulated in table (4.1). The bandwidth values for VSWR≤2 are calculated for different Δ ($0.01\lambda_o$ to $0.5\lambda_o$) where λ_o (25cm) is the free space wavelength at f=1.19GHz. It is seen that the resonance frequency, will change slightly when Δ was changed, and the maximum bandwidth lies between ($0.025\lambda_o$ to $0.25\lambda_o$). These important results give us good indication for stable resonance frequency. Also it is noticed from the table that the bandwidth at $\Delta=0.1\lambda_o$ and $0.5\lambda_o$ has no values, this is because the VSWR curves are above 2, results from the mismatch.

The important point here, is trying to cancel the mismatch, in other word, keeping the input impedance to nearly 50 Ω for each Δ , this is done by changing the location of the feed probe for each case so that the impedance curves position is constrain in small area near the center of the Smith chart as shown in Fig. 4.4(a). This is done after many simulation trials for each Δ. So the impedance bandwidth has been changed as shown in Fig. 4.4(b).

Experimentally, it is difficult to satisfy this point, i.e. for each case changing the feed location many times until the proper location was reached, there is a lost of time in addition it needs high cost. But with the aid of our method the time and the cost are reduced and give us an experience about the knowledgment on the superposition of parameters interfere.

The simulated results for the bandwidth after matching is demonstrated in table (4.2). It is seen that, the resonance frequency was not effected by the feed location and the best bandwidth (2.76%) for VSWR≤2 achieved when $\Delta = 0.1\lambda_o$ (2.5cm).

Table (4.1) Effect of the air gap width on impedance characteristics (before matching)of a stacked MPA with parameters:L_rxW_r=L_fxW_f=11.43x7.62 cm^2, h_{fg}=0.16cm, e_{rf} =2.62, (x_f,y_f)=(5.35,2.14)and e_{rr}=1.

Before matching				
Air gap width D in l_o (cm)	*f_r (MHz)*	*f_{r2}-f_{r1} (MHz)*	*BW (2:1) %*	*Maximum resistance (W)*
Single patch	1195	14	1.17	48
0.01	1190	14	1.17	43
0.025	1187	10	0.84	36
0.05	1186	10	0.84	28
0.1	1189	----	----	23
0.25	1206	14	1.1	49
0.3	1204	7	0.58	77
0.5	1195	----	----	120

Table (4.2) Effect of air gap width on impedance characteristics (after matching)of a stacked MPA with parameters:L_rxW_r=L_fxW_f=11.43x7.62 cm^2, h_{fg}=0.16cm, e_{rf} =2.62, and e_{rr}=1.

After matching					
Air gap width D in l_o(cm)	*f_r (MHz)*	*f_{r2}-f_{r1} (MHz)*	*BW (2:1) %*	*Maximum resistance (W)*	*Feed position (x_f,y_f) cm*
Single patch	1195	14	1.17	48	(5.35,2.14)
0.01	1190	14	1.17	43	(5.35,2.14)
0.025	1187	18	1.51	55	(5.35,1.78)
0.05	1186	21	1.77	44	(5.35,1.71)
0.1	1195	32	2. 76	48	(5.35,0.95)
0.25	1206	12	0.99	49	(5.35,2.14)
0.3	1204	7	0.58	43	(5.35,2.64)
0.5	1193	5	0.41	43	(5.35,0.85)

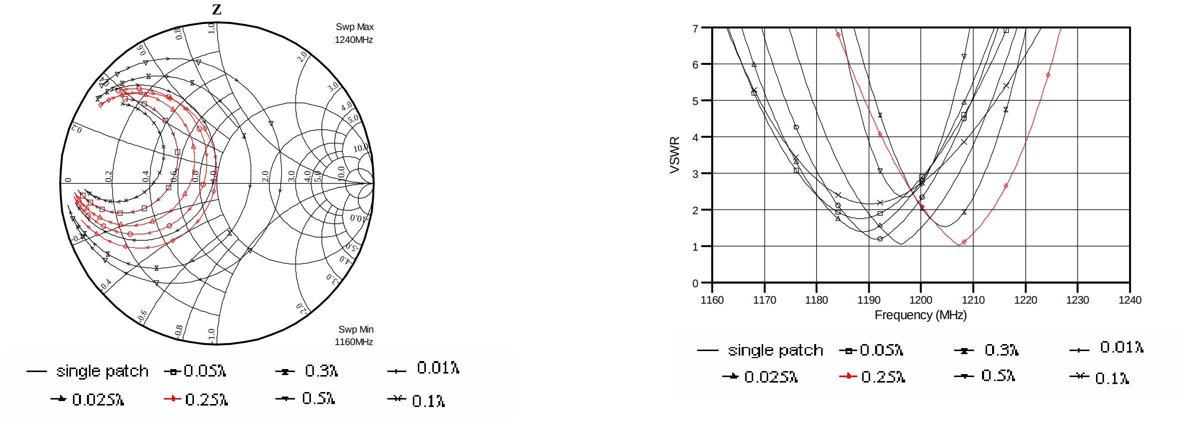

(a) *(b)*

Figure (4.3) (a) Smith chart and (b) VSWR results of a thin substrate stacked MPA (before matching) with parameters: L_f x W_f = L_r x W_r *=11.43cmx7.62cm,* h_{fg}*=0.16cm(0.01* l_d*),* e_{rf} *=2.62 ,* e_{rr} *=1, for different D.*

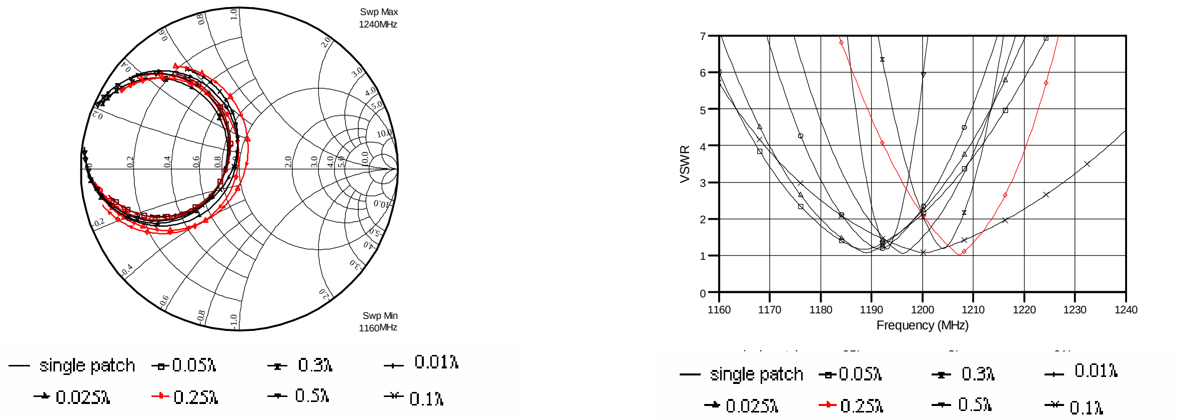

(a) *(b)*

Figure (4.4) (a) Smith chart and (b) VSWR results of a thin substrate stacked MPA(after matching) with parameters: L_f x W_f = L_r x W_r *=11.43cmx7.62cm,* h_{fg}*=0.16cm(0.01* l_d*),* e_{rf} *=2.62 ,* e_{rr} *=1 and for different D.*

4.3.1.2 Effect of the parasitic patch size

After selecting the best spacing (the air gap width $\Delta=0.1\lambda_o$), the effect of the parasitic patch size on the bandwidth was studied. Results show that there is no effect on bandwidth by varying the parasitic length L_r. But the width variation gives sensitive effect. Table (4.3) demonstrates the effect of W_r variation on the bandwidth of the stacked patch antenna by keeping L_r constant. The impedance curve locus was changed with W_r variation. For each W_r a proper feed location is distinguished for maximum bandwidth. It is seen that the best size is W_r=8.57 cm which gives BW=3.5%, this is shown in Fig. 4.5. It can be observed that the frequency range (1.16-1.26 GHz) is shifted small distance from the center of Smith chart with inductive and capacitive values. The radiation pattern for this design are calculated in two principal E(x-z)- and H(y-z)-planes at resonance frequency 1.195GHz as shown in Fig. 4.5(c) and (d) respectively. It can be seen that E_φ will be the co-pol radiation pattern in the E-plane with $HPBW_E^o$ of 41.5°, while in the H-plane, E_θ will be the co-pol radiation pattern with $HPBW_H^o$ 38.1°. The gain produced at this value of frequency is 14.13dB . Both have symmetrical shape with respect to the zenith. The cross-pol radiation patterns for two planes are zero. It has been found that better bandwidth can be obtained when the radiating patch has larger size than the lower patch. This is because; a larger upper patch effectively couples to the fringing fields of the bottom patch but there is a limit for this increasing because when the patch dimensions increase further another modes will appeared beside the dominant one causing a drop in VSWR and a deterioration in the radiation field.

As a result from the above work, the bandwidth is improved from 1.6% for a single patch antenna to 3.5% for a stacked patch antenna. This result is considered too small.

As a conclusion from the above results is that whatever the distance between the two patches increased or the size of the radiating patch increased with keeping the matching condition in consideration, the bandwidth does not succeed 4%. This is due to thin dielectric substrate.

Simulating steps shows that the bandwidth can be increased further by using thicker substrate. After many simulation trials, the bandwidth can reach 11% with the following optimum parameters: h_{fg} =1cm (0.064λ_d), e_{rf} =2.62 , e_{rr} =1, Δ=0.3cm, WxL=11.43cmx7.62cm, L_rxW_r =11.34cm x8.57cm, and x_f =5.35cm , y_f=0. This result is shown in Fig. 4.6. It can be noticed that the frequency range (0.95-1.21GHz) is positioned in the inductive part near the center of the Smith chart , this is due to the probe length. The radiation field pattern for both E- and H-planes have been computed as shown in Fig. 4.6 (c and d) respectively. It can be noticed that the pattern in both planes have uniform shape(symmetric with respect to the zenith). In the H-plane the $HPBW_H^o$ at resonance frequency f_r=1.01GHz is equal 63.8^o while in the E-plane the $HPBW_E^o$ is 48.1^o, so that the gain that can be produced from this design by applying equation 2.66 is 11.25dB.

Table (4.3) Effect of size W_r on impedance characteristic of a stacked MPA with parameters: L_fxW_f=11.43x7.62 cm^2, D=2.5cm,L_r=11.43cm, h_{fg}=0.16cm, e_{rf} =2.62, and e_{rr}=1.

Stacked patch width (cm)	*f_r (MHz)*	*f_{r2}-f_{r1} (MHz)*	*BW (2:1) %*	*Maximum resistance (W)*	*Feed position (x_f,y_f) cm*
6.66	1193	14	1.67	50	(5.35,1.66)
7.62	1195	32	2.67	48	(5.35,0.95)
8.57	1198	42	3.5	39	(5.35,0)
9.5	1220	39	3.19	42	(5.35,0)
10.47	1225	25	2	53	(5.35,1.19)

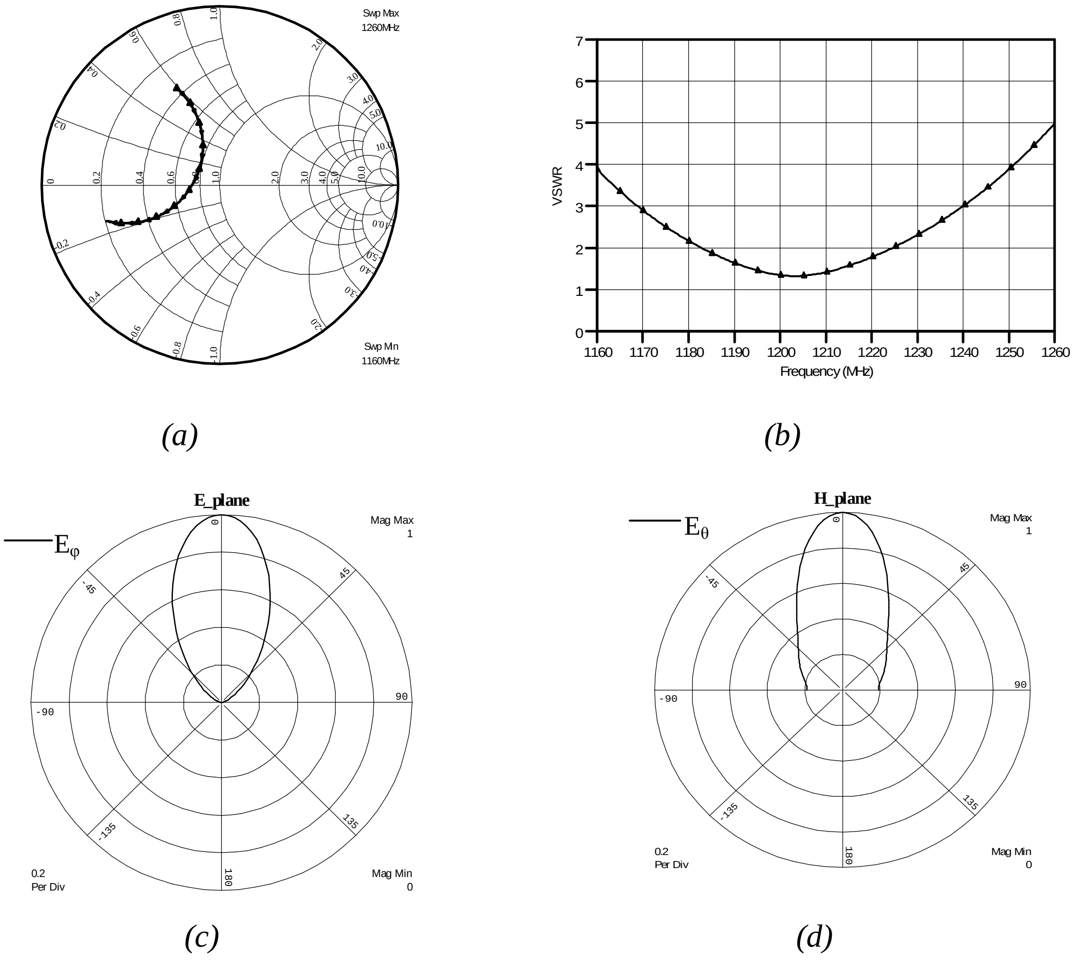

Figure (4.5) The characteristics of a thin substrate stacked MPA with parameters:
L_f x W_f =11.43cmx7.62cm, h_{fg}=0.16cm($0.01\lambda_d$), D=2.5cm ($0.1\lambda_o$), L_r x W_r =11.43cm x 8.57cm, and (x_f=5.35 , y_f=0 cm) for:

(a) Smith chart (b) VSWR, (c) E-plane and(d) H-plane radiation patterns at f_r= 1.195GHz.

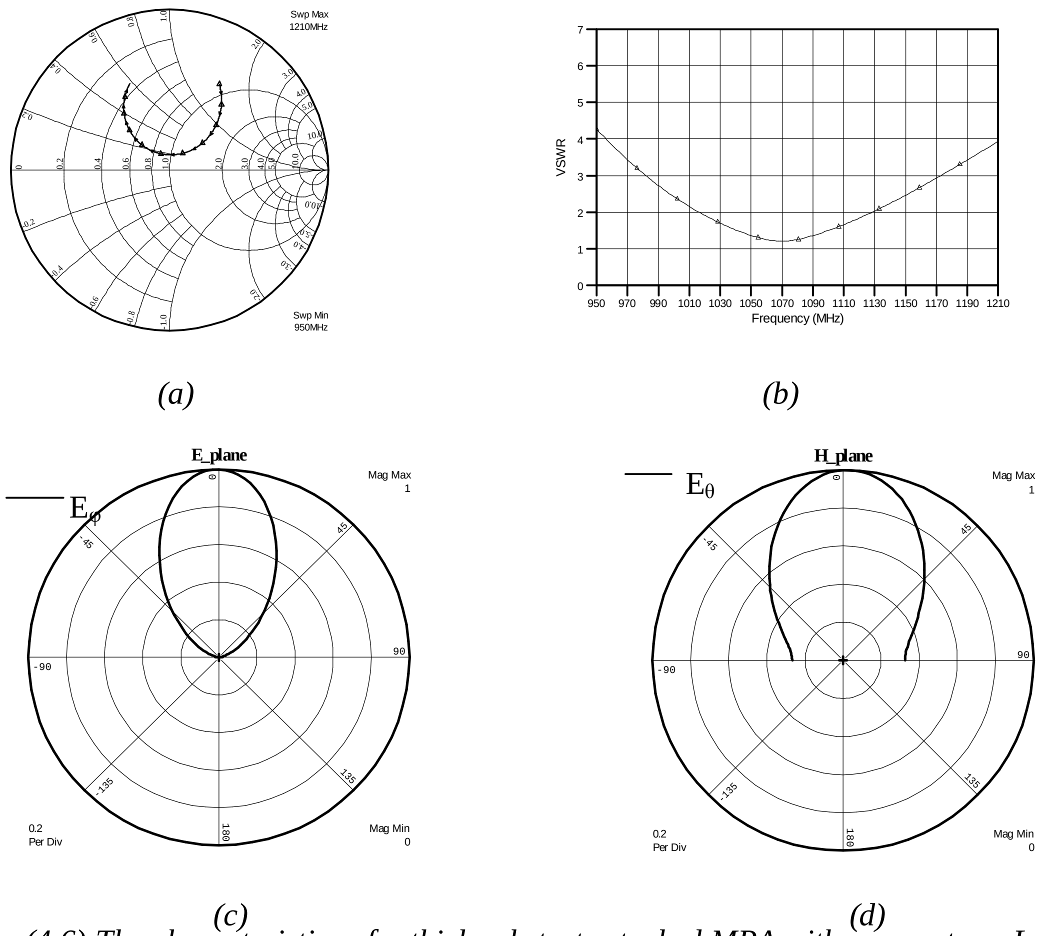

Figure (4.6) The characteristics of a thick substrate stacked MPA with parameters: L_f x W_f =11.43cm x7.62cm,h_{fg}=1cm(0.064λ_d),D=0.3cm(0.012l_o), and L_r x W_r =11.43cmx8.57cm for: (a)Smith chart, (b) VSWR, (c) E-plane and (d)H-plane radiation patterns at f_r= 1.01GHz.

4.4 The Configuration of the Square Stacked MPA

Another design example of dual-patch stacked configuration has been studied here. The configuration of this design is shown in Fig.4.7. The dimensions of the feeding patch is 7.03cm x 7.03cm which is taken equals to $\lambda_o/2$ where λ_o is the wavelength of free space taken at resonance frequency 2.15GHz printed on a dielectric substrate with ε_{rf}=4.45 and thickness h_{fg}=0.96cm (0.145λ_d). The feeding patch is fed by a coaxial feed probe at the center of its one edge, i.e (x_f=0,y_f=3.5).The stacked radiating patch is taken with dimensions 8.9cmx8.9 cm printed on a dielectric substrate with ε_{rr}=4.45 and thickness h_{rf} (the spacing between the radiating and the feeding patches). The radiating patch is shifted in the x-direction a distance of 1.4cm from one edge of the feeding patch, and the shift in the y-direction is 0.93cm from the other edge of the feeding patch. The feeding patch is fed at the center of one edge by coaxial probe feed as shown in Fig.4.7.

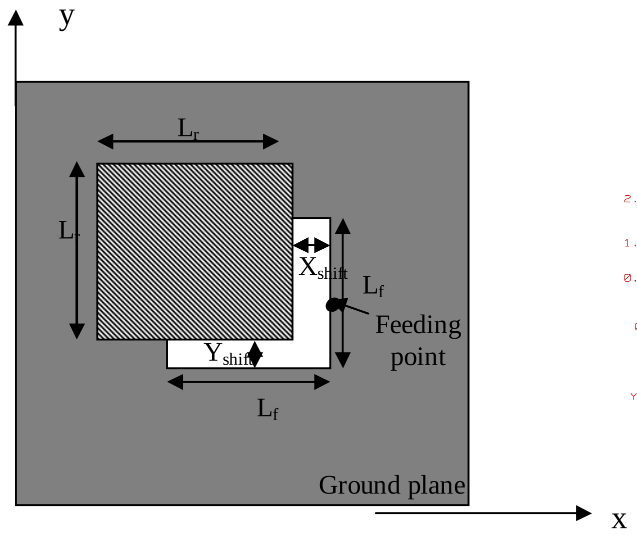

(a)

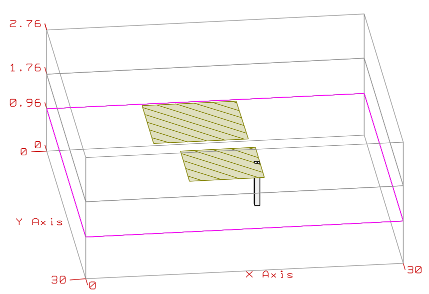

(b)

Figure (4.7) The configuration of the probe-fed square stacked MPA (a)Top view (b) MOP view.

4.4.1 Simulation and Results of Square Stacked MPA

The stacked structure has to be considered as two coupled cavities. The lower cavity is probe coupled and the upper one is coupled only through the fringing fields (proximity coupled). So the effect of coupling between the upper and lower cavities is to be included in the analysis of the structure. This coupling produces a loop in the impedance locus when plotted on a Smith chart.

To optimize the impedance behavior, we must be able to control the coupling (size of the coupling loop) between the feeding and the radiating patches. The spacing between the radiating and the feeding patch, h_{rf}, is very much dependent on that of the spacing between the feeding patch and the ground plane, h_{fg}: the greater h_{fg} , the less freedom available for the selection of h_{rf}. Typically, if h_{fg} is too electrically thick, h_{rf} must be electrically thick as well and, therefore the overall bandwidth is not improved. Four sets of spacing between the radiating and the feeding patches, h_{rf}, have been taken in order to study their effect on impedance bandwidth. Fig. 4.8 shows the VSWR and Smith chart for these four sets. It is noticed that h_{rf} controls the tightness of the resonant loop or the interaction between the two patches: the further the second patch is away from the lower patch (Fig 4.8(d)), the tighter the loop and less impedance bandwidth. For all sets, as shown in Fig. 4.8, the small loop in the impedance curve is seen near the center of the Smith chart, which indicates very good matching for the input impedance was obtained. The best value of the bandwidth obtained from this design (nearly 16%) when h_{rf}=0.32cm as shown in Fig. 4.8(a). The radiation patterns for both E- and H-planes (for the best value of impedance bandwidth) at different frequencies within the band are shown in Fig. 4.9. It can be seen that in each plane there is E_θ and E_φ components with nonuniform shapes. This is may be due to the use of high dielectric substrate material which produced a surface waves that deteriorate the radiation pattern or due to the size of the radiating patch (λ_o/2) which may introduce many modes beside the dominant one resulting pattern deterioration.

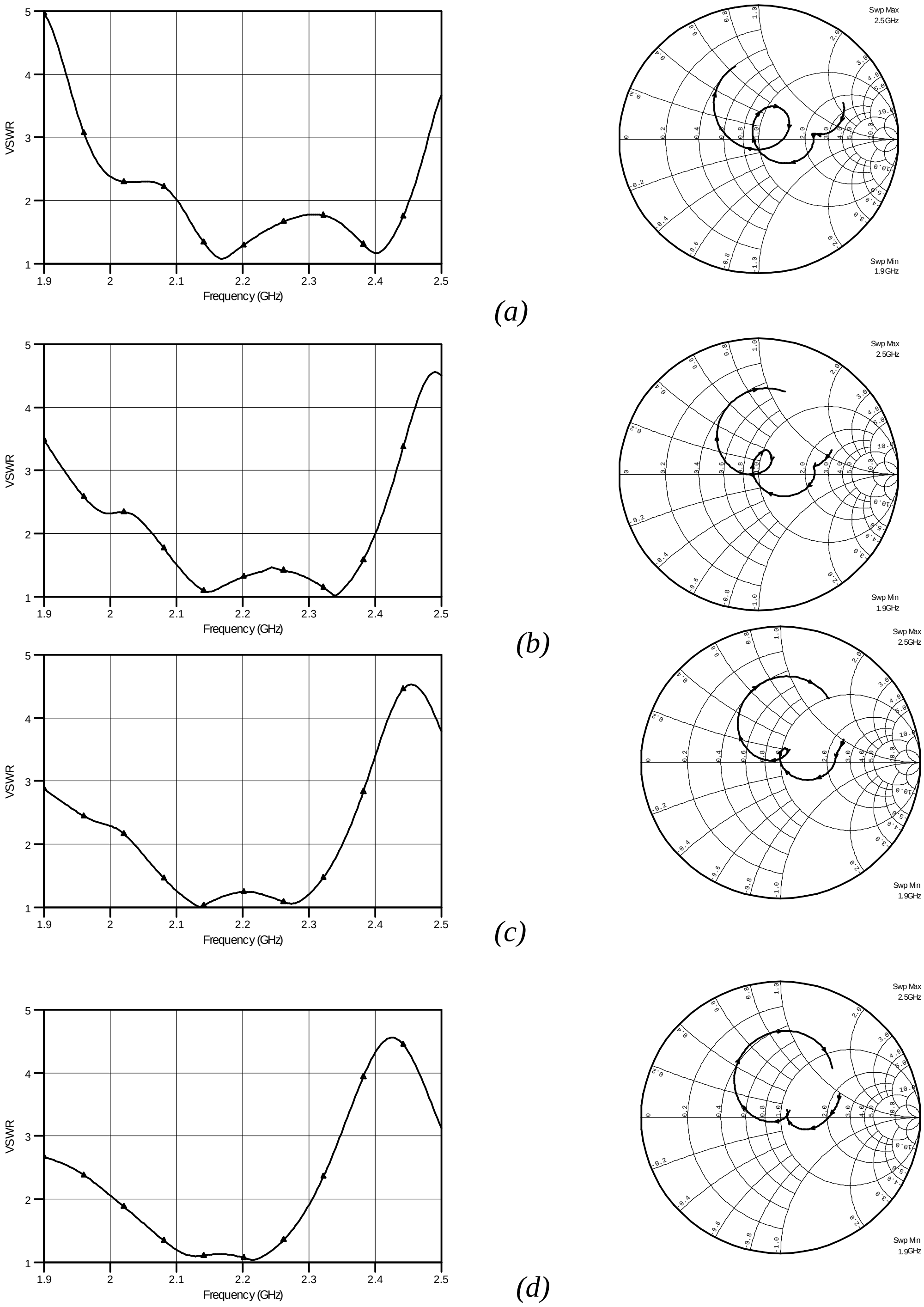

Figure (4.8) VSWR and input impedance (Smith chart) of a probe-fed square stacked MPA with parameters: L_f xW_f=7.03cm x 7.03cm, L_rxW_r=8.9cmx8.9cm, $\varepsilon_{rr}=\varepsilon_{rf}$= 4.45, h_{fg}=0.96cm, and (x_f =0 , y_f=3.5cm) for different h_{rf}: (a) h_{rf}=0.32cm (b) h_{rf} =0.48cm ,(c) h_{rf} =0.64cm, and (d) h_{rf} =0.8cm.

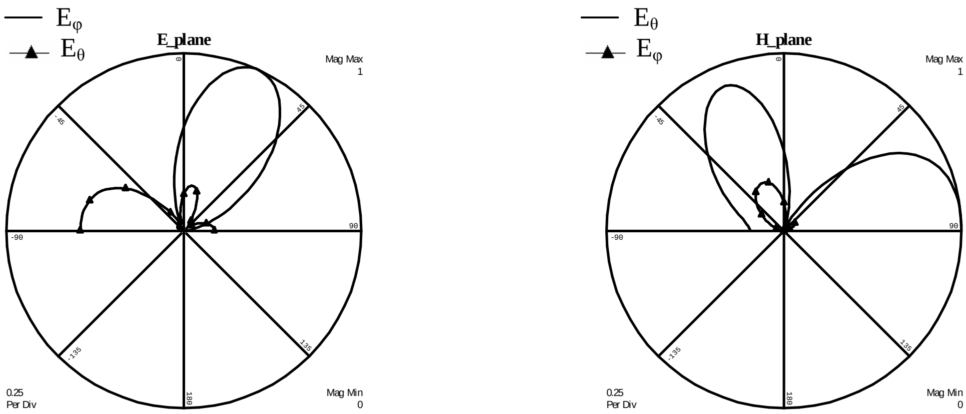

(a)

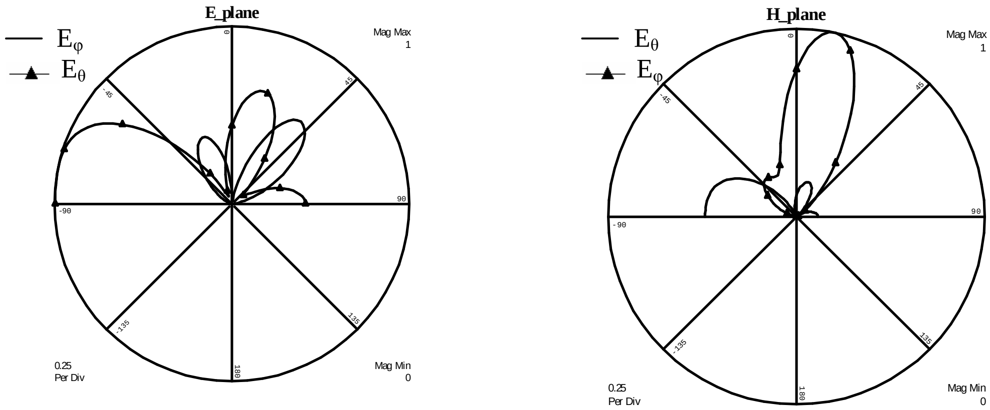

(b)

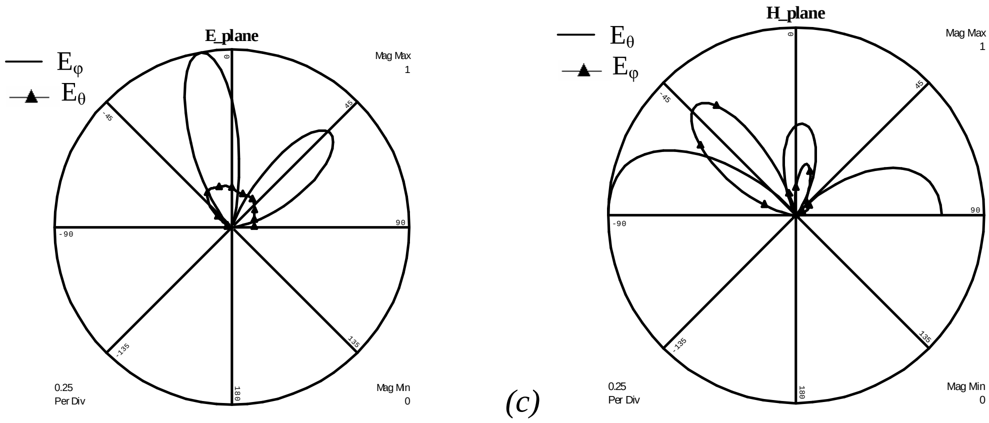

(c)

Figure(4.9) E-plane and H-plane radiation patterns for a probe-fed square stacked MPA with parameters: L_f xW_f=7.03cm x 7.03cm, L_r xW_r=8.9cmx8.9cm, h_{rf}=0.32cm, h_{fg}=0.96cm, and (x_f=0 , y_f=3.5cm) for different frequencies; (a) f=2.1GHz, (b) f=2.3GHz, and (c) f=2.45GHz.

Chapter 5

Rectangular-Slot Microstrip Patch Antenna

5.1 Introduction

The thick substrate is one of the solutions to overcome the inherently narrow bandwidth of a coaxially fed microstrip patch antenna but also it is limited the achievable bandwidth to less than 10% due to the increased inductance introduced by the longer probe required [26]. One way to compensate the probe inductance is the capacitive feeding technique [38,61]. Small capacitor patch, connected to the coaxial feed, excites the radiating patch through capacitive coupling.

Recently, a feeding approach employing an L-shape probe/strip has been proposed. The L-shape probe/strip incorporated with the radiating patch introduces a capacitance suppressing some of the inductance introduced by the probe/ strip itself. The bandwidth using this technique can reach 36% [62]. It is found that by etching a U-slot [63], the bandwidth can be substantially increased, typically to larger than 30%. A theoretical study is presented in [64], where a rectangular slot is proposed to be cut in the center of the rectangular patch, a dual-frequency has been achieved. In this chapter a single slotted patch printed on thick substrate with coaxial feed probe is selected as microstrip element for bandwidth enhancement. An extensive study oriented on the parameters that effects the performance of this kind of MPA. In order to broaden the bandwidth further, a capacitive feed instead of coaxial feed has been designed.

Then a stacking configuration (with the slotted patch is used as a feeding patch) is another class of antennas proposed in this chapter for bandwidth enhancement. This kind of MPA with two types of feeding; a probe-fed and a capacitively-fed have been analyzed. The effect of a short wall on impedance bandwidth of the stacked configuration is also examined here with two types of feeding; the probe-fed, and the capacitively-fed.

For all designs the effects of there geometrical parameters were discussed on the basis of the simulated results by MOP. The information derived from the studies is helpful for antenna designer.

5.2 Probe-Fed Rectangular-Slot MPA

In this Section, a single-patch wide-band microstrip antenna fed by coaxial feed probe has been proposed as a wideband microstrip antenna. This single patch is printed on thick substrate in order to enhance the bandwidth. The inductive reactance produced from the probe length can be compensated by adding a capacitance to the total input impedance of the MPA. This capacitance is achieved by etching a rectangular slot in the radiating patch.

5.2.1 Simulation Results for Published U-Slot MPA

A published work presented in [42] has been re-investigated using MOP in order to check the package performance in analyzing this kind of MPAs. This work consists of a U- shaped slot etched in the center of a rectangular patch. The published experimental data of this work including the impedance locus and radiation pattern were in good agreement with the theory.

The antenna is simulated by the MOP. The package conditions are: (a) the number of divisions=128, (b) the division cell size was x=0.56mm, y=0.406mm, and (c) the top dielectric layer of the enclosure was set to have the properties of air with 10mm in thickness, the antenna was fed with excitation port of 50 Ω . With these conditions the computed impedance loci of this antenna gives good agreement with the computed and experimental published results as shown in Fig. 5.1. The impedance bandwidth of antenna B from the published result is 25.3% while that from the package is 27%. Accordingly the slot loading effect on microstrip patch can be analyzed by such software.

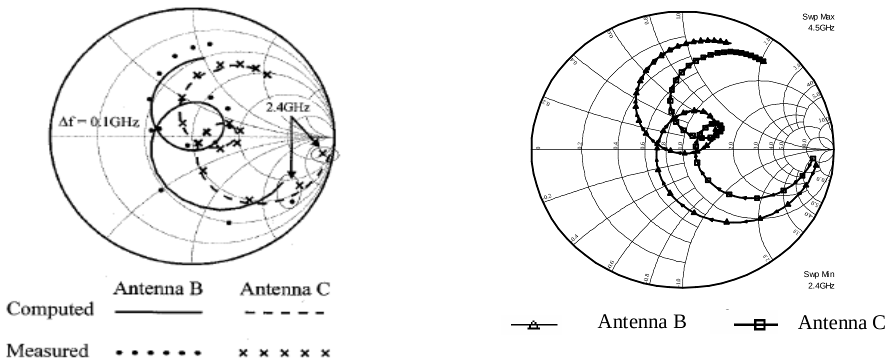

(a) *(b)*

Figure (5.1) Input impedance of a U-slot rectangular microstrip antenna
(a) Published experimental and computed results[42]
(b) Computed result using MOP.

5.2.2 The Configuration of the Probe-Fed Rectangular-Slot MPA

The geometry of the proposed antenna is shown in Fig. 5.2. The antenna has a square radiating patch on one side of a dielectric substrate of thickness *h* with a ground plane on the opposite side. The length of the square patch, L, is equal to nearly $\lambda_o/2$ where λ_o is the wavelength of the free space at operating frequency 2.15 GHz which is equal to 7.03 cm. The patch is excited by 50 Ω coaxial cable at feed position (x_f=0.46 cm, y_f=3.5 cm) which gives the best matching results in this work. To expand the antenna bandwidth, a single rectangular slot with length L_s and width W_s is etched at the center of the patch. A dielectric substrate of ε_r =4.45 with loss tangent 0.0005 has been used.

5.2.3 Simulation and Results of Probe-Fed Rectangular-Slot MPA

The MOP is used to analyze our proposed antenna. The package conditions are: (1) the number of divisions=64, (2) the division cell size=(x=0.46cm, y=0.46cm), (3) the top dielectric layer of the enclosure is set to have the properties of air with thickness=1cm, frequency simulation step= 0.05GHz.

The geometric parameters (L_s,W_s,h), play an important rule to control the wide-band behavior of the proposed antenna. The effect of these parameters on the VSWR and input impedance of the square slotted microstrip patch antenna is discussed on the basis of the simulated results by MOP. When varying one of the geometric parameters, the two other parameters are fixed. In the simulation, the frequency band ranged from f_{start}=1.8GHz to f_{final}=3.1GHz, which gives central frequency, f_c = 2.45GHz.

For all the following example designs, the length of the patch was set at 7.03cm and the coaxial feed location was set at (x_f=0.46 cm, y_f=3.5cm). Fig. 5.3(a) shows the effect of the slot width on the antenna performance (VSWR and input impedance) with the other parameters are fixed at; (L_s and h) =(4.2cm, and

0.96 cm($0.145\lambda_d$ where λ_d is the wavelength inside the dielectric substrate at operating frequency 2.15GHz) respectively.

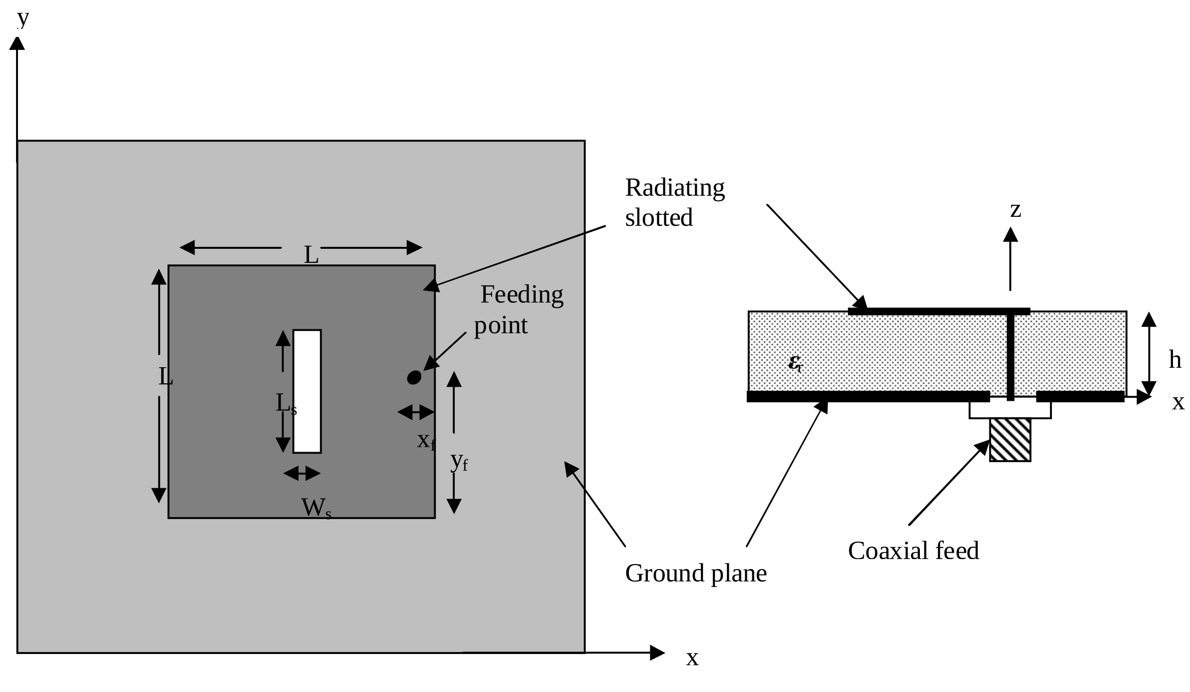

Top view *Side view*

(a)

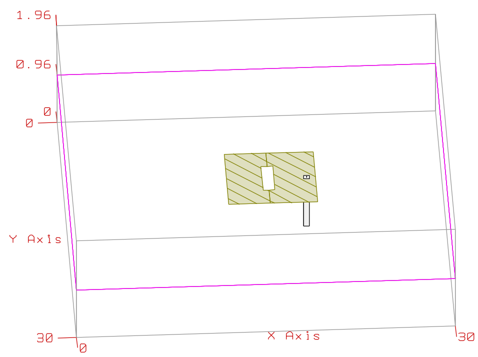

(b)

Figure (5.2) The geometry of the probe-fed rectangular-slot MPA (a) Top and side view (b) MOP view

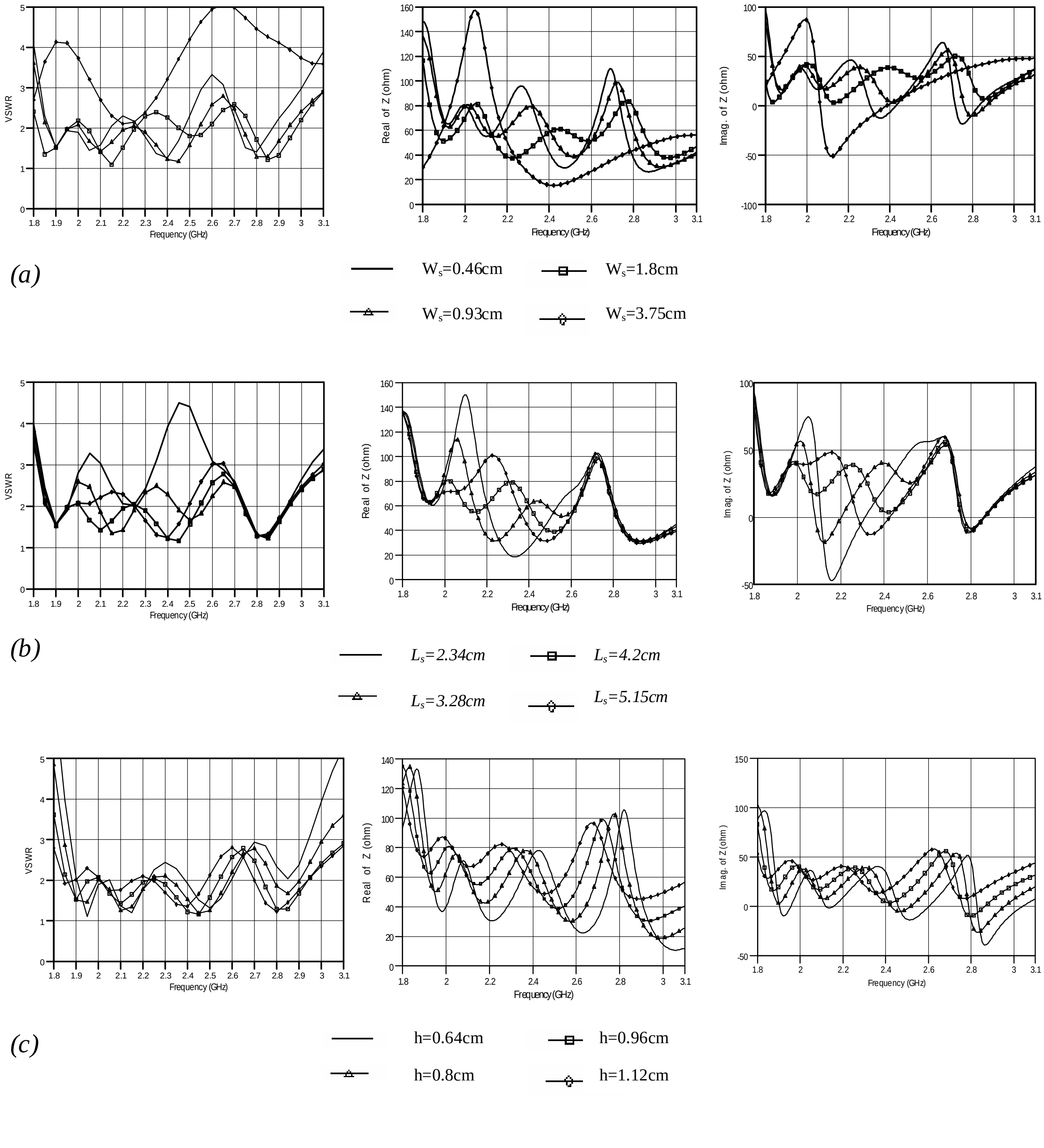

Figure (5.3) VSWR and input impedance (real and imaginary parts) variations versus frequency of a probe-fed rectangular-slot MPA with parameters: L=7.03cm,ε_r=4.45 and (x_f,y_f)= (0.46cm,3.5cm) for:
(a)Different slot width; W_s=0.46, 0.93,1.8,and 3.75 cm at L_s =4.2cm and h=0.96cm
(b)Different slot length ; L_s=2.34, 3.28, 4.2, and 5.15 cm at W_s=0.93cm and h=0.96cm
(c)Different dielectric substrate thickness; h=0. 64, 0.8,0.96, and 1.12 cm at L_s=4.2cm and W_s=0.93cm.

In this Fig. a series of four values of patch slot width were taken (W_s=0.46,0.93,1.8,and 3.75cm). It can be seen from the impedance curves that around the center of the band (f_c=2.45GHz), the real part of the input impedance decrease when W_s become wider while the imaginary part become more inductive. The best value of impedance bandwidth was achieved when the slot width is set to 0.93cm.

Then, with the slot width fixed at 0.93cm, and *h* at 0.96cm , the slot length, L_s, is varied to further optimized the bandwidth of the slotted MPA , a series of four values of slot length were taken (L_s=2.34,3.28, 4.2,and 5.15cm). The VSWR and input impedance variations due to the change in the slot length are shown in Fig. 5.3(b). It is observed from the impedance curves that around the center of the band, the real part of the input impedance increase when L_s become longer and the imaginary part become less inductive. The best value of impedance bandwidth was achieved when the slot length is 4.2cm.

Last, the effect on the antenna performance caused by the change in the dielectric thickness ,*h*, has been investigated. The dielectric thickness was varied while retaining the slot width and length at 0.93 and 4.2cm respectively. Fig. 5.3(c) shows the VSWR and input impedance obtained with respect to different four patch thicknesses (*h*=0.64,0.8,0.96,and 1.12 cm). Results illustrate that there is four resonance peaks in the resistance curve and similarly there are four transition regions in the reactance curve. This means that the antenna becomes as four sequential cavity resonators of low Q factor. As seen in Fig 5.3(c) the thickness increment plays an important role to reduce the Q factor and the resonance frequency of each cavity, also *h* is the main control parameter to make the input resistance near the characteristic impedance of the coaxial feed line. From the reactance curve in Fig. 5.3(c) it can be noticed that the input inductance increases when *h* become larger, this is due to increase the length of the coaxial probe-feed as h increased. It is seen that the best value of impedance bandwidth was achieved when the patch height is 0.96cm. An overview of the above designs are shown in table (5.1).

By observing the influence of various parameters (L_s,W_s,and h) on resonance frequency it is found that around the center of the band the resonant frequency decrease when h and L_s increase, and increase when W_s increase.

The radiation patterns for the three classes of variations (W_s,L_s, and h) are computed in three principal cuts; E(x-z)($\varphi=0^o$)-, H(y-z)($\varphi=90^o$)-,and E(x-y)($\theta=90^o$)-planes at operating frequency 2.15GHz as shown in Fig. 5.4(a),(b), and (c) respectively. It can be seen that E_θ will be the co-polarization (co-pol.) radiation patterns in the E-plane, while in the H-plane, E_φ will be the co-pol radiation and E_θ is the cross-pol radiation. Each of co-pol and cross-pol radiation patterns was normalized by the maximum of co-pol radiation. In general it can be seen that in the E-plane there is no cross-pol component while in the H-plane the cross-pol component is rather high, and it is shown to break into two lobes, these lobes may be due to excitation of higher order modes. Also it can be noticed that both the E-plane and H-plane radiation patterns show little variation, with W_s,L_s and h variations.

Figure 5.4(a) shows the effect of W_s on radiation patterns. It can be seen that in the E- plane the co-pol patterns are very slightly broadened when W_s increased (have symmetrical shape with respect to the zenith) except for W_s=3.75cm which is appear narrowed with an asymmetrical shape with respect to the zenith. In the H-plane the co-pol patterns are narrowed as W_s become wider. The cross-pol in the H-plane increasing (with respect to the endside ($\theta=90^o$)) as W_s become wider.

Figure 5.4(b) shows the effect of L_s on radiation patterns. It can be seen that in the E- and H-planes the co-pol patterns are slightly broadened when L_s

increased. The cross-pol in the H-plane decrease slightly (with respect to the endside) as L_s becomes longer.

It is observed from Fig. 5.4(c) that the co-pol pattern in the E-and H-planes are almost unchanged for the different *h*, having symmetrical shapes with respect to the zenith. The cross-pol level in the H-plane is slightly high with respect to endside.

From the above results one can conclude that the best result for obtaining the best antenna characteristic is that when: L_s=4.2 cm, W_s=0.93cm, and *h*=0.96cm (0.145λ_d) as shown in Fig. 5.5 and table 5.1 (set 2). Dual-band 27.75% and 8.5% for VSWR≤2, covering the frequency range 1.86 to 2.54GHz, and 2.74 to 2.95GHz respectively have been achieved. Also it can be noticed from this Figure that good matching was produced for antenna with these geometrical parameters which appear clearly in the Smith chart in which most of the frequencies ranged from 1.8 to 3.1 GHz were concentrated near the center of Smith chart, but with inductive nature. Table (5.2) gives the geometrical parameters and the antenna characteristics for this final optimum design (set 2).

Table(5.1) The effect of L_s , W_s , and h on the frequency band of the probe-fed rectangular-slot MPA.

set	*L_s (cm)*	*W_s (cm)*	*h (cm)*	*Frequency band (GHz)*
1	4.2	0.46	0.96	(1.86-2.15)(2.27-2.47)(2.72-2.86)
2	4.2	0.93	0.96	(1.86-2.54) (2.74- 2.95)
3	4.2	1.8	0.96	(1.82-1.96)(2.04-2.26)(2.78-2.98)
4	4.2	3.75	0.96	------
5	2.34	0.93	0.96	(1.87-1.96) (2.75-2.94)
6	3.28	0.93	0.96	(1.86-1.95)(2.09-2.26)(2.44-2.57) (2.74-2.95)
7	5.15	0.93	0.96	(1.85-1.96) (2.25-2.5) (2.74-2.94)
8	4.2	0.93	0.64	(1.9-2.23)(2.39-2.6)
9	4.2	0.93	0.8	(1.88-2.24)(2.32-2.58)(2.79-2.91)
10	4.2	0.93	1.12	(2 -2.15)(2.25-2.49) (2.7-2.95)

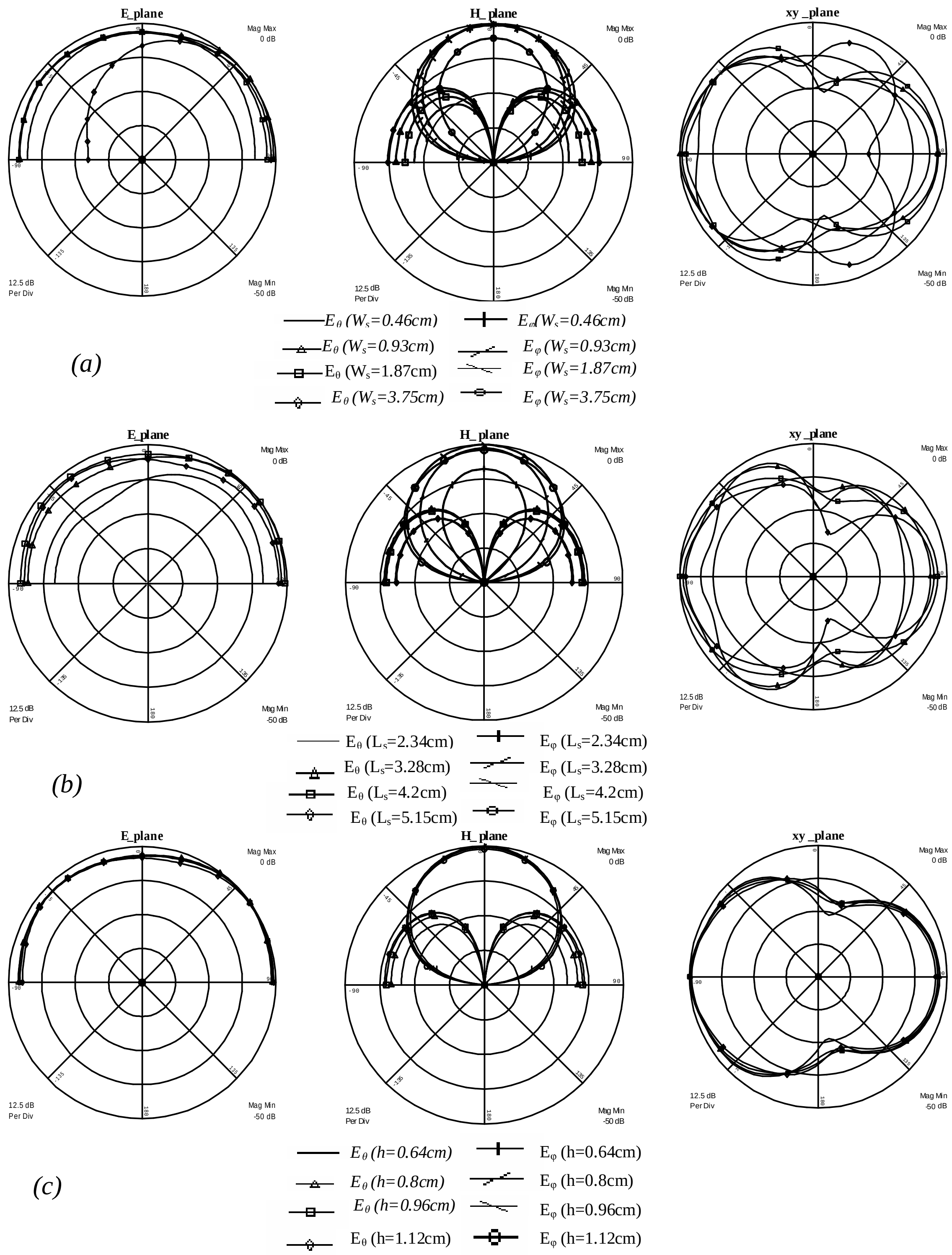

Figure (5.4) E-_plane , H-plane, and xy-plane radiation patterns at operating frequency 2.15 GHz of a probe-fed rectangular-slot MPA with parameters: $L=7.03cm, \varepsilon_r=4.45$ and $(x_f,y_f)=(0.46cm,3.5cm)$ for:
(a)Different slot width; W_s=0.46, 0.93,1.8,and 3.75 cm at L_s =4.2cm and h=0.96cm
(b)Different slot length ; L_s=2.34 , 3.28, 4.2, and 5.15 cm at W_s=0.93cm and h=0.96cm
(c)Different dielectric substrate thickness; h=0. 64, 0.8,0.96, and 1.12 cm at L_s=4.2cm and W_s=0.93cm.

Table (5.2) The geometrical parameters and characteristics of the optimum probe-fed rectangular-slot MPA(set 2)

L(cm)	7.03
L_s(cm)	4.2
W_s(cm)	0.93
ε_r	4.45
h(cm)	0.96
(x_f cm, y_f cm)	(0.46,3.5)
f_c GHz	2.45
Δf GHz	0.68 and 0.21
BW($VSWR \leq 2$)	27.75% and 8%
Gain dB	14.01

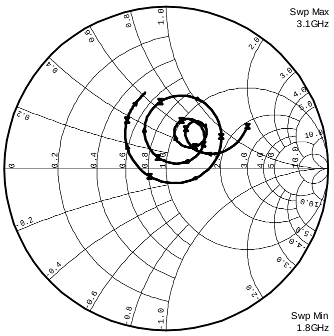

(a)

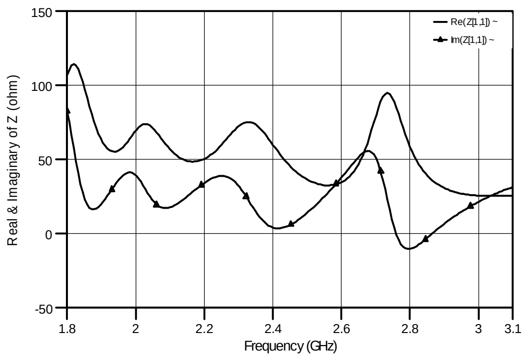

(b)

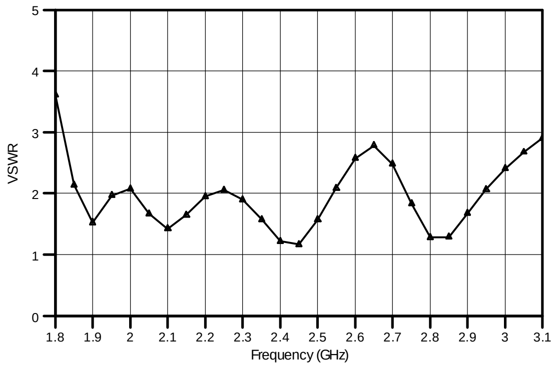

(c)

Figure (5.5) (a) Smith chart, (b) Real and imaginary parts of the input impedance,and (c) VSWR variations versus frequency of the optimum probe-fed rectangular-slot MPA (set 2) with parameters: L=7.03cm, (L_sxW_s)=(4.2x0.93)cm^2, ε_r=4.45,h=0.96cm, and (x_f,y_f)= (0.46cm,3.5cm) simulated by MOP and gives BW of 27.75% and 8%.

The radiation patterns for this optimum design (set 2) are calculated for both E(x-z)- and H(y-z)-planes at specific frequencies within the bandwidth(VSWR≤2) as shown in Fig. 5.6. It can be observed that in the E-plane the co-pol patterns were changed as the frequency increased. The half-power beamwidth in the E-plane ($HPBW_E{}^o$) at 2.15GHz ranging from 24.4 to -11^o. There is no cross-pol patterns in the E-plane. Also it can be noticed that in the H-plane the co-pol radiation patterns are quit stable (having symmetrical shape) with increasing frequency while the cross-pol pattern decrease with the frequency increment. The half power beamwidth in the H-plane ($HPBW_H{}^o$) ranging from 22.6 to -22.6^o. So that the gain that can produce from the optimum slotted MPA at 2.15GHz by applying equation 2.66 is 14.08 dB.

From the above results one can conclude that a wide-band with relative high gain can produce from single- layer single-patch microstrip antenna. The wideband behavior is probably due to the fact that the currents along the edges of the slot introduce an additional resonance, which, in conjunction with the resonance of the main patch, produce an overall broadband frequency response characteristic. The slot also appears to introduce a capacitive reactance which counteracts the inductive reactance of the probe.

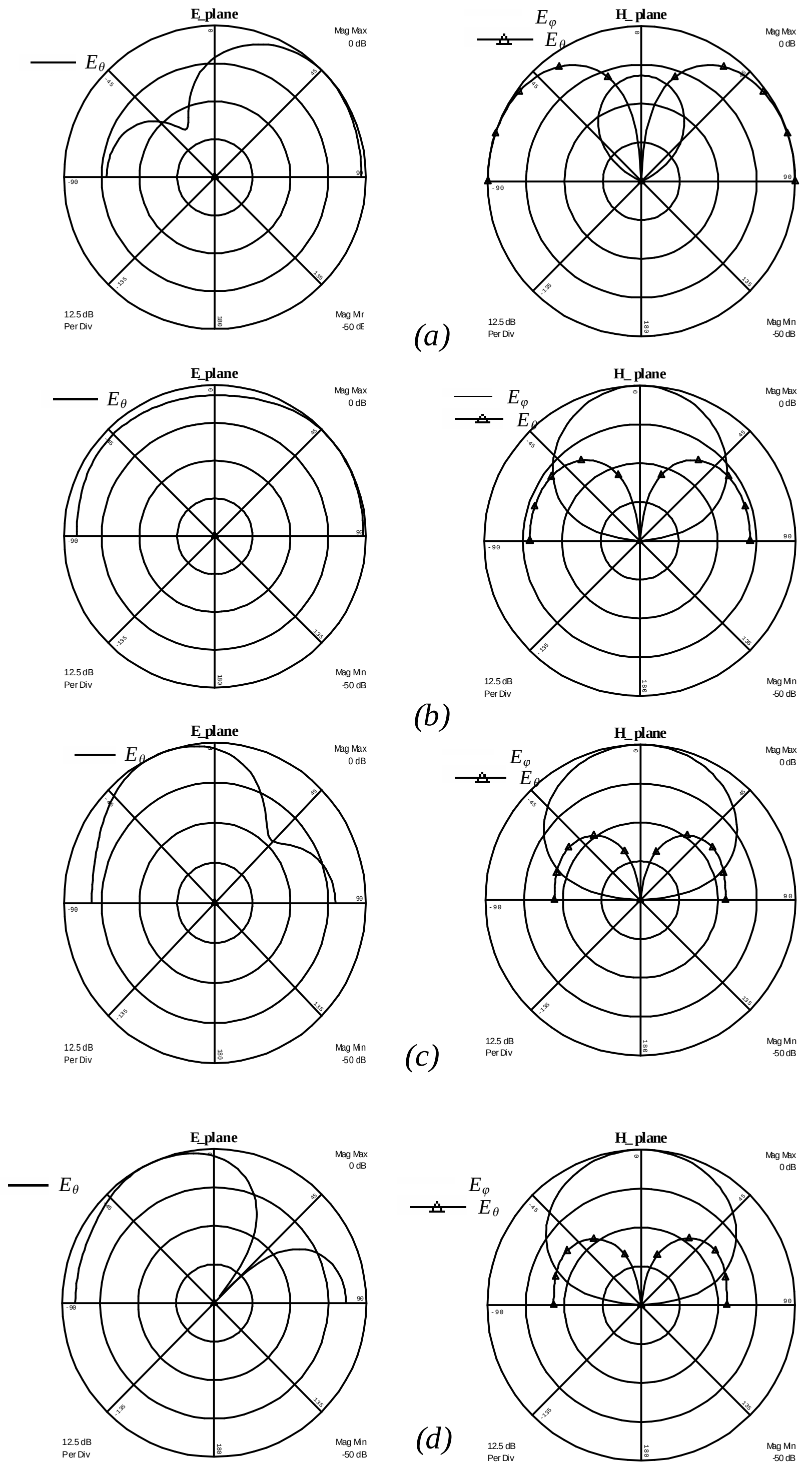

Figure(5.6) E-plane and H–plane radiation patterns of the optimum probe-fed rectangular-slot MPA (set 2) for different frequencies f_r ; (a)f=1.9 GHz,(b)f=2.15 GHz, (c)f=2.45 GHz, and(d)f= 2.54 GHz with parameters: L= 7.03 cm, $(L_s x W_s)=(4.2x0.93)cm^2$, $\varepsilon_r=4.45$,h= 0.96 cm, and $(x_f,y_f)=(0.46cm,3.5cm)$.

5.3 Capacitively-Fed Rectangular-Slot MPA

The capacitive feeding is an excellent feed for single- layer microstrip patch antennas with a thick substrate (thickness=0.1λ_d). Its configuration allows not only a simple mechanical structure but also the effective cancellation of the large reactance due to the long probe by the aid of the capacitive coupling. In this Section a capacitive feeding structure with different capacitor shapes has been presented to improve the bandwidth of the single-layer rectangular-slot MPA (presented in Section 5.2.2).

5.3.1 Simulation Results for Published L-probe MPA

Before starting the design and the simulating of the capacitively-fed rectangular-slot MPA, a published work presented in [65] has been investigated in order to check the computation method. This work consists of a single rectangular patch microstrip antenna faded by L-shape feed(capacitor). The published experimental results of impedance locus and the VSWR were in good agreement with the theoretical results. The configuration of the L-feed antenna is shown in Fig. 5.7. This published work was re-simulated by using the MOP. The package simulation conditions are: (a) the number of divisions=128, (b) the division cell size was x=0.93cm, y=0.81cm, and (c) the top dielectric layer of the enclosure was set to have the properties of air with 10mm in thickness; the antenna was fed with excitation SMA port of 50Ω. The geometric parameters of the published work are presented in table (5.3) with our simulated dimensions produced by the package. The published results of impedance locus and the VSWR were in an excellent agreement with our simulating results. This good agreement between the computed and the published results give a confident in the software operational conditions. Fig. 5.8 clearly illustrates the coincidences of the results.

Table (5.3) The comparison between the published and the simulated geometrical parameters of the L-probe MPA

	W_x(mm)	W_y(mm)	L_h(mm)	L_v(mm)	H(mm)	D(mm)
Published	30	26	10	5	7	2
Simulated	30	26	10.5	5	7	3.25

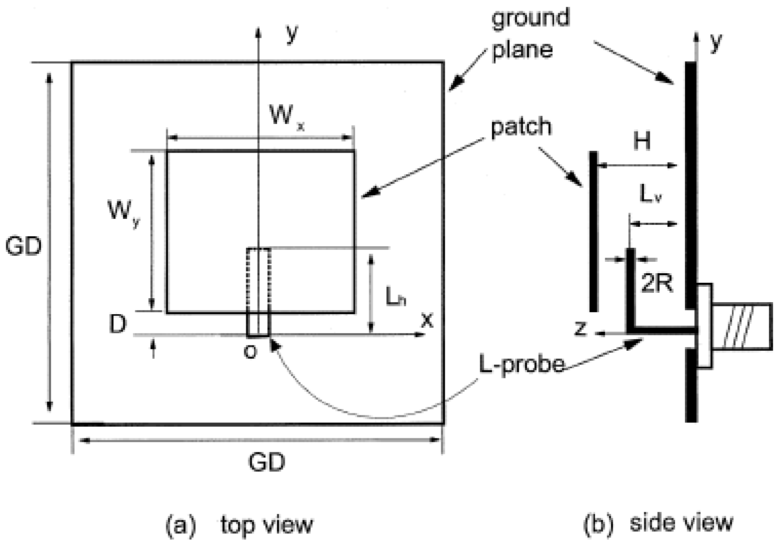

Figure(5.7) The geometry of the L-probe MPA[65]

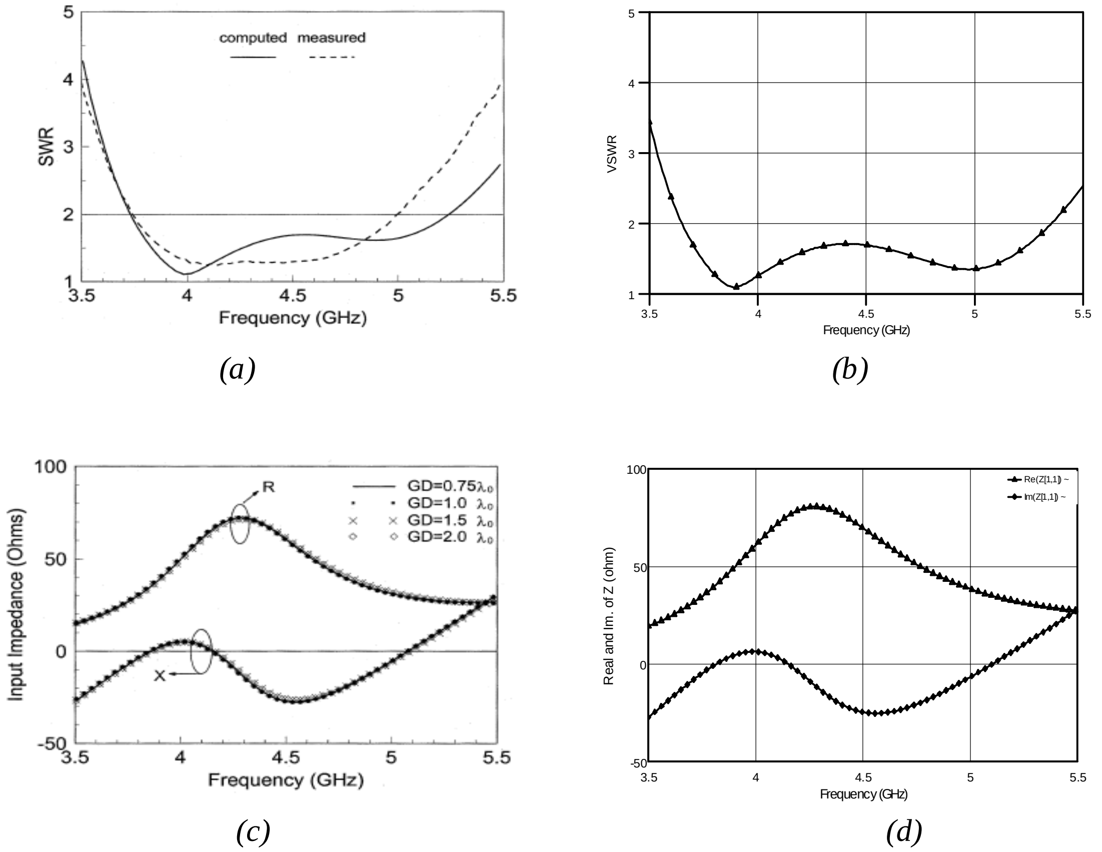

Figure(5.8) VSWR(a and b) and input impedance(c and d) curves of L-probe MPA
(a)and (c)The published results [65]
(b) and (d)The computed results using MOP.

5.3.2 The Configuration of the Capacitively-Fed Rectangular-Slot MPA

The geometry of the capacitively-fed rectangular-slot MPA is shown in Fig. 5.9. It consists of a radiating patch on top of a small capacitor-strip on top of a ground plane with dielectric layers between the radiating patch and the capacitor-strip, ε_{rr}, and between the capacitor-strip and the ground plane, ε_{rc} ,with the same dielectric substrate material, $\varepsilon_{rr} = \varepsilon_{rc} = 4.45$, of thicknesses h_{rc} and h_{cg}

respectively. The capacitor-strip with length L_c, and width W_c was fed by a coaxial feed probe at feed position (x_f=0.46cm,y_f=3.5cm) with respect to radiating patch, the same feed location of the optimum design (set 2) given in table (5.2). The radiating patch is a square slotted MPA with goemetric parameters; L, L_s,*and* W_s, were set at (equal to those values given in table (5.2)) 7.03,4.2, and 0.93 cm respectively. The radiating patch is approximity fed by the capacitor-strip.

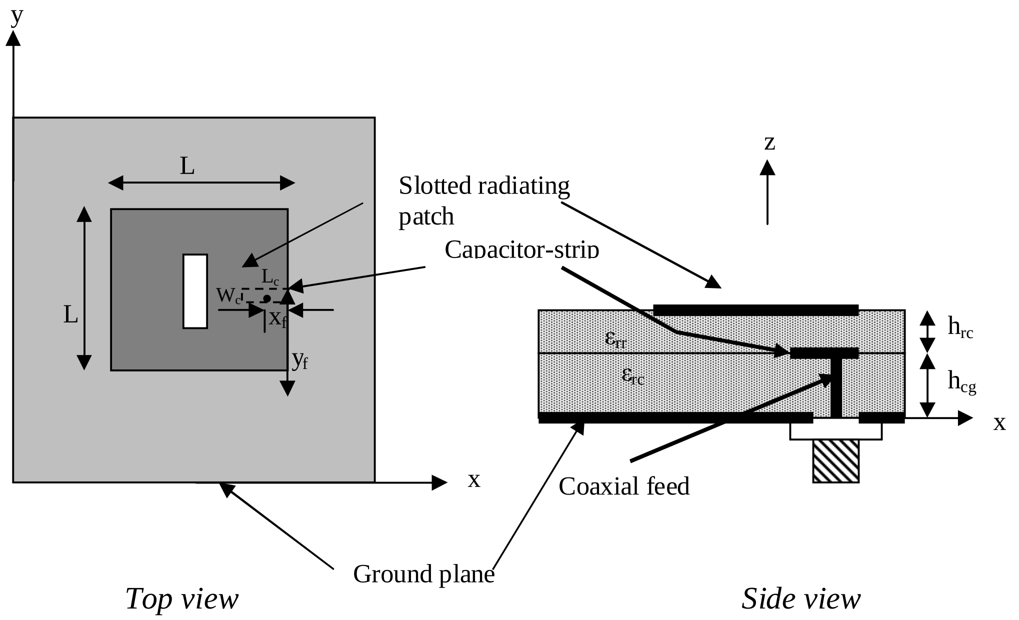

(a)

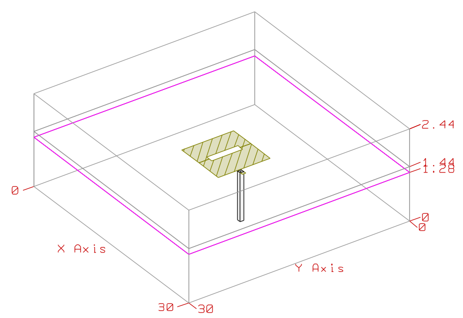

(b)

Figure (5.9) The geometry of the capacitively-fed rectangular-slot MPA: (a) Top and side view (b) MOP view

5.3.3 Simulation and Results of Capacitively-Fed Rectangular-Slot MPA

The geometrical parameters that play an important base to control the wideband behavior of the proposed antenna are the capacitor-strip size, (L_cxW_c), h_{rc}, and h_{cg}. The effect of these parameters on VSWR and input impedance of the capacitively feed square slotted MPA were discussed on the basis of the simulated results by MOP. For all the following designs, the geometric parameters of the radiating patch (L, L_s ,and W_s) and the feed position of the coaxial feed probe were set equals to those values given in table (5.2). The simulation frequency ranged from f_{start}=1.6GHz to f_{final} =3.3GHz. Various configurations have been presented to extend the bandwidth.

First, Fig. 5.10(a) shows the effect of capacitor-strip size on VSWR and input impedance. Table (5.4) shows the capacitor-strip shapes with their dimensions. The capacitor-strip width was set at 0.46cm, its length varying from 0.46-1.87cm forming three shapes (I-, L-, and T-shapes). The spacing between the radiating and the capacitor-strip, h_{rc}, and between the capacitor-strip and the ground plane,h_{cg}, were fixed at 0.16cm and 0.96cm respectively. It can be seen that the best value of the bandwidth was achieved when L_c=0.93cm. Also it is found that the real part of input impedance for the four capacitive strip sizes have the same profile in amplitude and shape while the imaginary part exhibit the same profiles but with different bias values ,it becomes more inductive when L_c increased. Another important note presented in this figure, that there are four resonance frequencies with the obtained bandwidth and the resonance frequency is not sensitive to the capacitor-strip length. Then, with the capacitor-strip size (L_cxW_c) and h_{cg} were fixed at 0.93cmx0.46cm and 0.96cm respectively, the

VSWR and input impedance variations versus frequency for different spacing between the radiating patch and the capacitor-strip, h_{rc}=0.16-0.96cm, are shown in Fig. 5.10(b). It can be seen that the smallest spacing between the two patches gives the best result, this smallest spacing *is* h_{rc}=0.16cm, which means the coupling between them become the best.

Last, the VSWR and input impedance variations versus frequency for capacitor-strip height,h_{cg}, varying from 0.8-1.28cm are shown in Fig.5.10(c) to further optimize the bandwidth of the antenna. The capacitor-strip size and h_{rc} were set at (0.93x0.46), and 0.16cm respectively. Clearly, the input impedance is sensitive to h_{cg}. The real part of input impedance increase when h_{cg} increase and the imaginary part become more inductive. Also it is found that the center frequency decrease when h_{cg} increase. The best value of the bandwidth was achieved when h_{cg} was set at 1.28cm. An overview of the results was given in table (5.5).

Table (5.4) The dimensions and shapes of the capacitor-strips

Dimension(cm^2)	*0.46x0.46*	*0.93x0.46*	*1.4x0.46*	*1.87x0.46*
shape Name	*I-*	*L-*	*T-*	*T-*
Shape	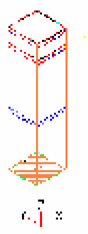	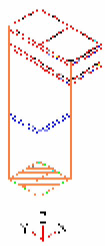	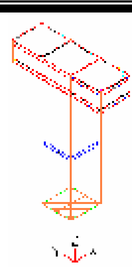	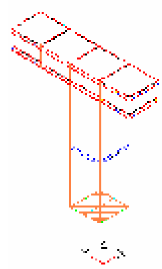

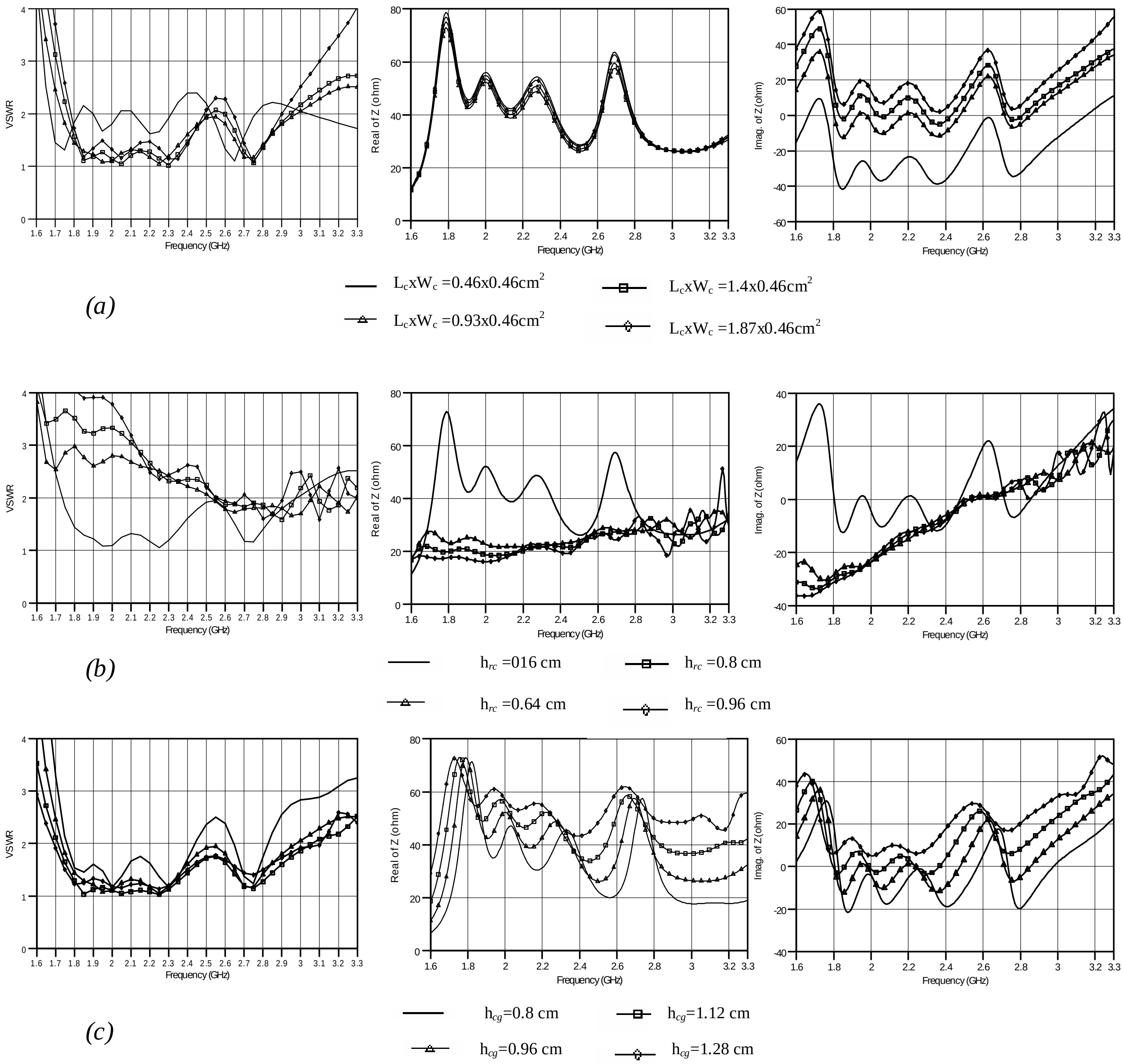

Figure (5.10) VSWR and input impedance (real and imaginary parts) variations versus frequency of a capacitively-fed rectangular-slot MPA with parameters: L=7.03cm, $(L_s x W_s)=(4.2x0.93)cm^2$, and $(x_f,y_f)=(0.46cm,3.5cm)$ for:

(a)Different capacitor-strip size; $L_c x W_c$=0.46x0.46, 0.93x0.46,1.4x0.46, and 1. 87x0.46 cm^2 at h_{rc}=0.16cm and h_{cg}=0.96cm.

(b) Different radiating patch to capacitor-strip spacing; h_{rc}= 0.16,0.64,0.8, and 0.96cm at $(L_c x W_c)=(0.93 x 0.46)cm^2$ and h_{cg}=0.96 cm.

(c) Different capacitor-strip to ground plane spacing; h_{cg}=0.8,0.96,1.12, and 1.28 cm at h_{rc}=0.16cm and $(L_c x W_c)= (0.93 x 0.46)cm^2$

Table (5.5) Effect of capacitor-strip size($L_c x W_c$), h_{rc} and h_{cg}, , on the frequency band of a capacitively-fed rectangular-slot MPA.

Set	*$L_c x W_c$ (cm^2)*	*h_{rc} (cm)*	*h_{cg} (cm)*	*Frequency band (GHz)*
1	0.46x0.46	0.16	0.96	(1.68-1.83)(1.9-2.32)(2.53-2.76)
2	0.93 x.46	0.16	0.96	(1.74-3)
3	1.4 x 0.46	0.16	0.96	(1.77-2.95)
4	1.87 x 0.46	0.16	0.96	(1.78-2.49)(2.65-2.9)
5	0.93 x 0.46	0.64	0.96	(2.55-3.06)(3.16-3.3)
6	0.93x0.46	0.8	0.96	(2.55-2.96)(3.1-3.21)
7	0.93x0.46	0.96	0.96	(2.55-2.9)(3.05-3.15)
8	0.93x0.46	0.16	0.8	(1.76-2.45)(2.65-2.83)
9	0.93x0.46	0.16	1.12	(1.71-3.05)
10	0.93x0.46	0.16	1.28	(1.69-3.11)
11	0.93x0.46	0.16	1.44	(1.67-3.02)
12	0.46x0.46	0.16	1.12	(1.63-4.05)

Figure 5.11(a),(b), and(c) show the radiation patterns (E(x-z),H(y-z), and E(x-y)-planes) at operating frequency 2.15 GHz for various: capacitor-strip size , h_{rc}, and h_{cg} respectively. It can be seen from Fig. 5.11(a) that in general the radiation patterns remain unchanged for the different capacitor-strip size, having symmetrical shape with respect to the zenith, i.e the capacitor-strip size has no effect on the radiation pattern of the antenna. The cross-pol level in the H-plane is considerably high while in the E-plane the cross-pol is vanished. The cross-pol level in the H-plane is higher at angles closer to the endside. From the above results one can conclude that the MPA with capacitive-feed technique dose not affect the shape of the antenna's radiation pattern produced when it is directly-fed by coaxial feed.

It is observed from Fig. 5.11(b) that the co-pol patterns in the E-and H-planes are affected by varying h_{rc}, the co-pol patterns in the E and H-planes patterns decrease and distorted as h_{rc} increase with no cross-pol patterns in the E-plane. The cross-pol level in the H-plane is higher at angles closer to endside, the distortion in the field when h_{rc} increase is due to the decrease in the coupling between the radiating patch and the capacitor-strip and the best result is that when h_{rc} =0.16cm . Fig. 5.11(c) shows that the radiation patterns remain unchanged for the different h_{cg}.

From the above results one can conclude that the best result for obtaining the best antenna performance is that when ($L_c x W_c$), h_{gc}, and h_{cr} were set to (0.46x0.93cm^2 (L-shape), 1.28 cm (0.19λ_d), and 0.16cm (0.024 λ_d)) respectively, as shown table (5.5)(set 10). The antenna characteristics, input impedance(Smith chart and real and imaginary parts) and VSWR variations versus frequency are shown in Fig. 5.12(a,b,and c) respectively. The resultant bandwidth achieved from this design can reach 58% for VSWR≤2, covering the frequency range from 1.69 to 3.11GHz. Also it can be noticed from the Figure that all the frequency range (from 1.6 to 3.3GHz) is concentrated in a small loop near the center of Smith chart but in inductive part. Figure 5.13 shows the radiation patterns for this optimum design (set 10) simulated in both E- and H-planes at specific frequencies within the bandwidth. It can be observed that the co-pol patterns in the E-plane were changed and distorted as the frequency increase. The $HPBW_E^o$ at 2.15GHz ranging from 39.2 to -40^o (having symmetrical shape). There are no cross-pol patterns in the E-plane. Also it can be noticed that in the H-plane the co-pol radiation patterns are very small at lower and higher values of the operating band and with high values near the middle of the band (having symmetrical shape) while the cross- pol pattern is relatively high at lower and

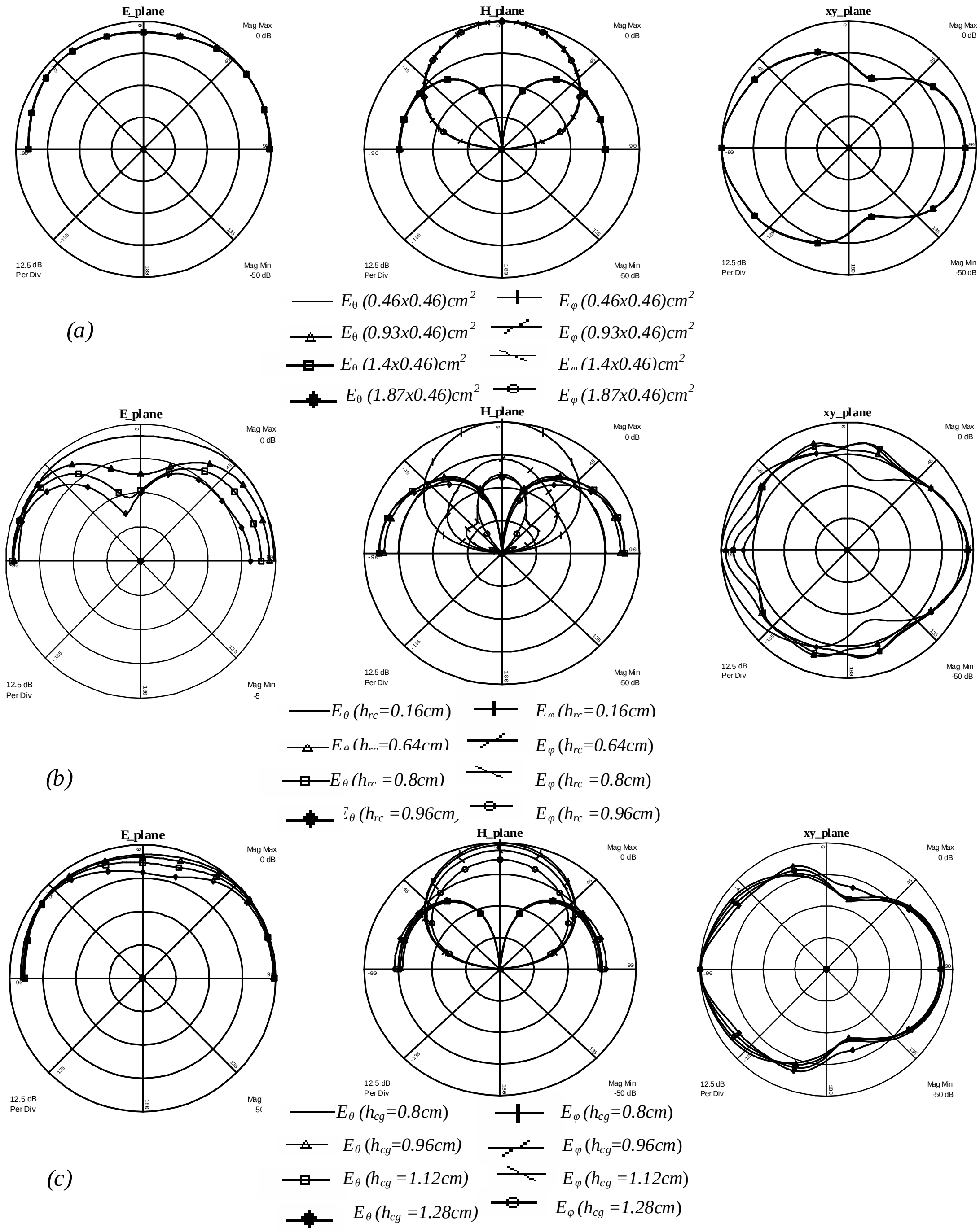

Figure (5.11) E-plane, H-plane, and xy-plane radiation patterns at operating frequency =2.15 GHz of a capacitively-fed rectangular-slot MPA with parameters L=7.03cm, $(L_s\text{x}W_s)$=(4.2x0.93)cm^2, and (x_f,y_f)=(0.46cm,3.5cm) for:
(a)Different capacitor-strip size; $L_c\text{x}W_c$=0.46x0.46, 0.93x0.46,1.4x0.46, and 1.78x0.46 cm^2 at h_{rc}=0.16cm and h_{cg}=0.96cm.
(b) Different radiating patch to capacitor-strip spacing; h_{rc}= 0.16,0.64,0.8, and 0.96cm at $(L_c\text{x}W_c)$ =(0.93 x 0.46)cm^2 and h_{cg}=0.96 cm.
(c) Different capacitor-strip to ground plane spacing; h_{cg}=0.8,0.96,1.12, and 1.28 cm at h_{rc}=0.16cm and $(L_c\text{x}W_c)$= (0.93 x 0.46)cm^2.

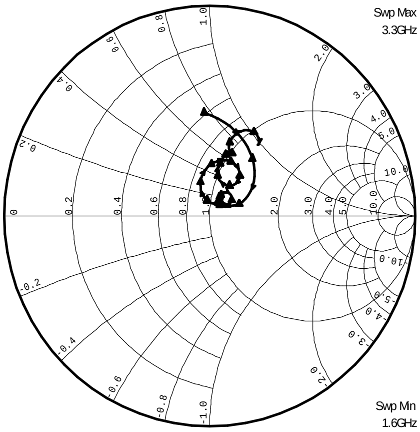

(a)

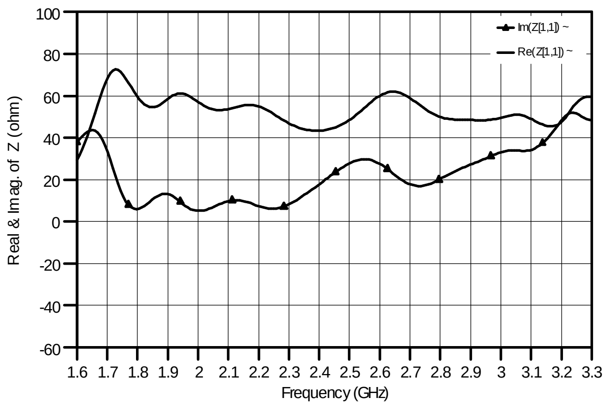

(b)

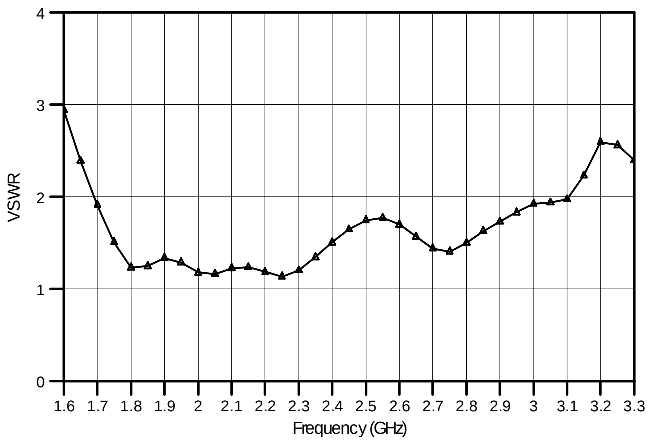

(c)

Figure (5.12) (a) Smith chart, (b) Real and imaginary parts of the input impedance, and(c) VSWR variations versus frequency of a capacitively- fed rectangular-slot MPA (design 10) with parameters: $L=7.03cm$, $(L_s xW_s)=4.2x0.93cm^2$, $h_{rc}=0.16cm$, $h_{cg}=1.28cm$, $(L_c xW_c)=0.93x0.46cm^2$, and $(x_f,y_f)=(0.46cm,3.5cm)$ *simulated by MOP and gives BW of 58%*

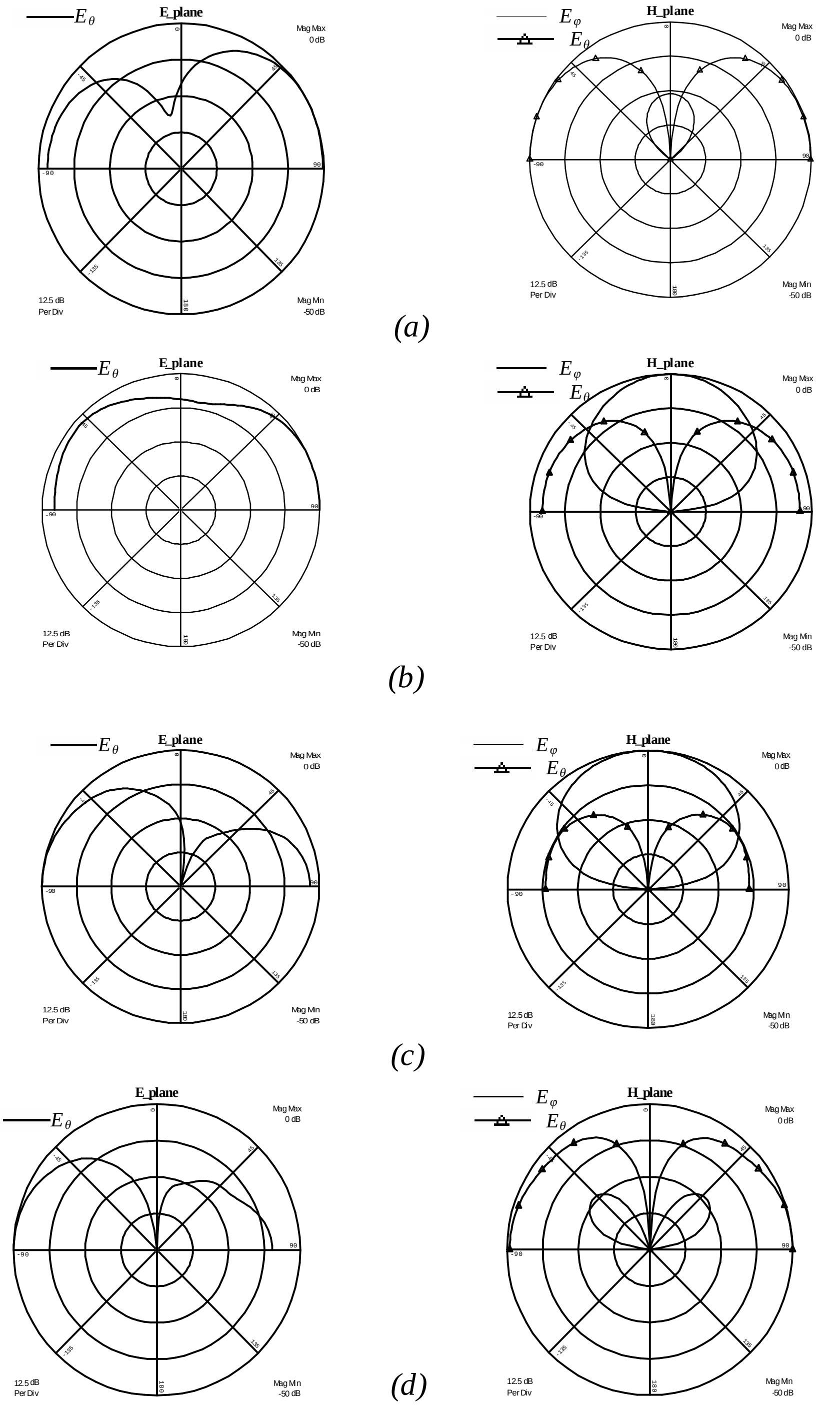

Figure (5.13) E-plane and H-plane radiation patterns of a capacitively-fed rectangular-slot MPA(set10) at different frequencies;(a) f=1.7GHz,(b) f=2.15GHz,(c) f=2.45GHz,and (d) f=3GHz with parameters: L=7.03cm, $(L_s \mathrm{x} W_s)=(4.2\mathrm{x}0.93)cm^2$, $h_{rc}=0.16cm$, $h_{cg}=1.28cm$, $(L_c \mathrm{x} W_c)=(0.93\mathrm{x}0.46)cm^2$,*and*$(x_f,y_f)=(0.46cm,3.5cm)$.

higher values of frequencies and having smaller values near the middle of the band. The $HPBW_H^o$ at 2.15GHz ranging from 24.3 to -24.3^o so that the gain that can produced from this optimum slotted MPA (set 10) at 2.15GHz by applying equation 2.66 is 10.27dB. By comparing the two designs, i.e slotted MPA with direct and indirect feed excitation, it can be observed that the first design has higher gain than the second one, but the BW of the second design having larger value than the first one, nearly two times larger. Also the radiation pattern seems to be unchanged by using this kind of feeding. So that the capacitively-feed excitation technique is seen to be very efficient than the direct coaxial-feed excitation technique.

Another design that can produce a very large bandwidth (85.3% for VSWR $\leq$2), covering the frequency range from 1.63 to 4.05GHz, is shown in Fig 5.14 with geometric parameters given in table (5.5)(set 12). The geometrical parameters of this design have the same values of the first optimum design (set 10) except for the capacitor-strip size and h_{cg} , they are changed. The capacitor-strip size is reduced to exactly the same size of probe feed forming I-shape capacitor-strip and with dielectric substrate thickness h_{cg}=1.12cm(0.17 λ_d) or in other word ,by comparing this design with that directly feed design in table (5.2) , only disconnect the communication between the radiating patch and the feed probe by high dielectric substrate material with small thickness (0.16cm) and by using thicker feeding substrate h_{cg}=1.12cm, one can produce a very large bandwidth . It can be noticed from Fig. 5.14 that all the frequency range, f_{start}=1.6 to f_{final}= 4.1GHz, is located and concentrated at the center of Smith chart, part of the band lay in the capacitive part and the other part is in the inductive part with good matching characteristics.

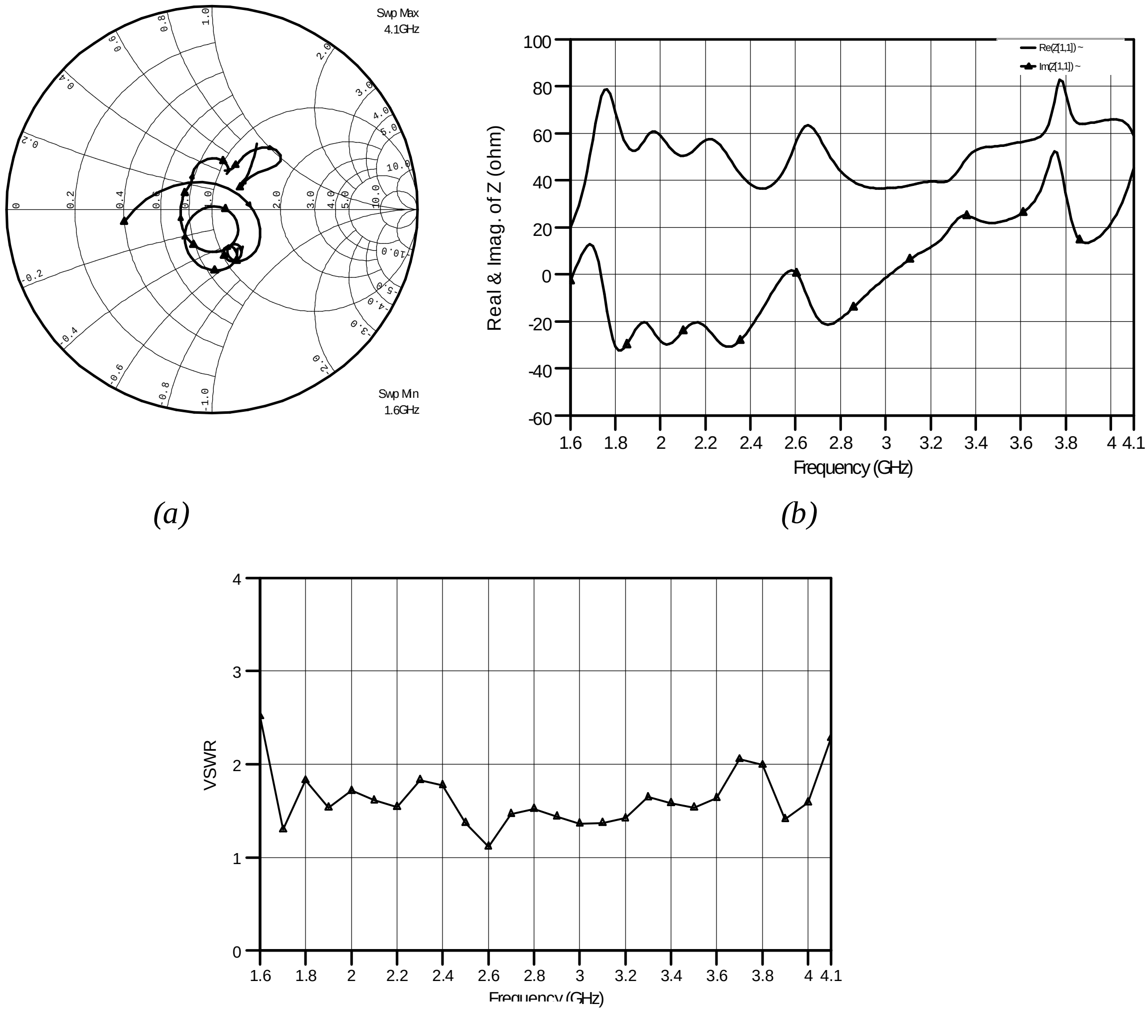

(a) *(b)*

(c)

Figure (5.14)(a) Smith chart,(b) Real and imaginary parts of the input impedance, and (c) VSWR variations versus frequency of a wide band capacitivel- fed rectangular-slot MPA(set12) with parameters:L=7.03cm,(L_s x W_s)=(4.2 x 0.93)cm^2,h_{rc}=0.16cm, h_{cg} =1.12cm, (L_c x W_c)= (0.46 x 0.46)cm^2,and(x_f,y_f)=(0.46cm,3.5cm) simulated by MOP and gives BW of 85%.

Fig. 5.15 shows the simulated radiation patterns for this second optimum design (set 12) in the E and H-planes at different frequencies within the bandwidth. It can be observed that in the E-plane the co-pol patterns were changed with the frequency variation, and the cross-pol pattern was appeared at high value of frequency(f=4GHz) but with very small value at angles closer to endside, nearly zero, and with large value at angles closer to zenith, nearly 18dB. The $HPBW_E^o$ at 2.15GHz is 67.3^o. In the H-plane it is shown that the co-pol radiation patterns are changed with frequency (having symmetrical shape and high value only at 2.15 GHz) while the cross-pol pattern is relatively high at these values of frequencies. The $HPBW_H^o$ at 2.15GHz is 47.6^o, so that the gain that can produced from this optimum capacitively-fed slotted MPA (set 12) at 2.15GHz by applying equation 2.66 is 11.07dB. By comparing this value of gain (which obtained from MPA with capacitive-feed technique) with that produced from MPA with direct feed (14.08 dB) it is smaller but the bandwidth produced from the former design is larger than that produced from the latter, nearly three times larger. In general, it is observed that the bandwidth and the gain produced from MPA of set 12 are better than that from set 10. Table (5.6) gives geometrical parameters and the characteristics for the final optimum designs, set 10, and set 12.

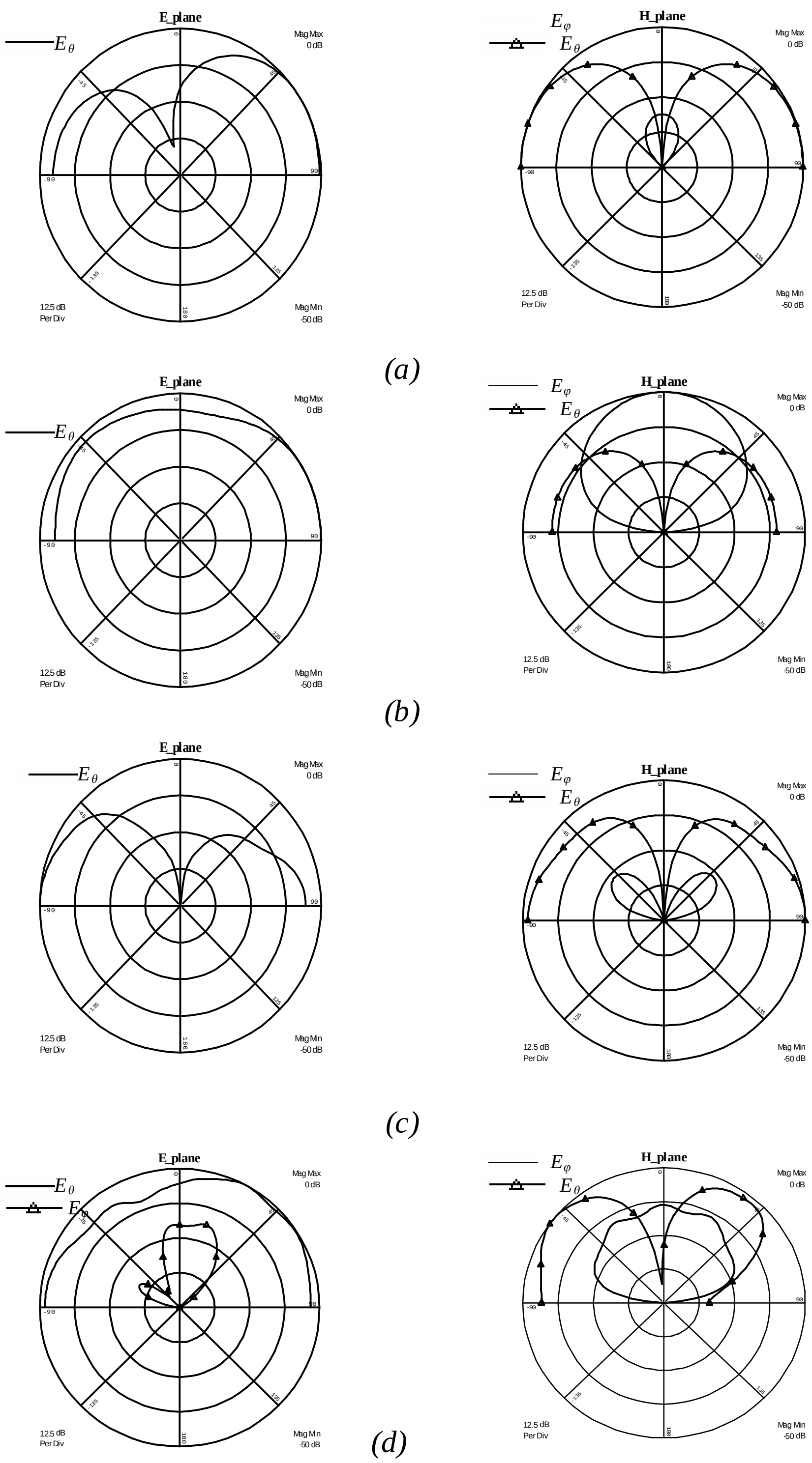

Figure (5.15) E-plane and H-plane radiation field patterns of a wideband capacitivel- fed rectangular-slot MPA (set 12) at different frequencies;(a)f= 1.7GHz,(b) f=2.15GHz,(c) f=2.85GHz,and(d) f=4GHz with parameters:L=7.03cm,$(L_s \times W_s)=(4.2 \times 0.93)cm^2$*,*$h_{rc}=0.16cm$*,* $h_{cg}=1.12cm$*,* $(L_c \times W_c)= (0.46 \times 0.46)cm^2$*,and* $(x_f,y_f)=(0.46cm,3.5cm)$*.*

Table (5.6) The geometrical parameters and the characteristics of the two optimum capacitively- fed rectangular-slot MPA

	Set 10	*Set 12*
L(cm)	7.03	7.03
L_s(cm)	4.2	4.2
W_s(cm)	0.93	0.93
$\varepsilon_{rr} = \varepsilon_{rc}$	4.45	4.45
h_{rc}(cm)	0.16	0.16
$(L_c\mathrm{x}W_c)$ cm^2	(0.93x0.46)	(0.46,0.46)
h_{cg} cm	1.28	1.12
$(x_f$ cm, y_f cm$)$	(0.46,3.5)	(0.46 ,3.5)
f_c GHz	2.45	2.85
Δf (GHz)	1.42	2.42
Capacitor-strip shape	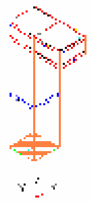	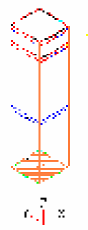
Bandwidth (VSWR$\leq$2)	58%	85%
Gain (dB)	10.27	11.07

5.4 Probe-Fed Stacked Rectangular-Slot MPA

By stacking a parasitic patch on a microstrip patch antenna, the antenna with a wide bandwidth can be realized. In this Section the effect of stacking on the rectangular-slot MPA has been studied.

5.4.1 The Configuration of the Probe-Fed Stacked Rectangular-Slot MPA

The geometry of proposed stacked probe fed antenna is shown in Fig. 5.16, the patch with rectangular-slot designed in Section 5.2.2 was taken and considered as a feeding lower patch ,L_f, which is fed with coaxial cable, a parasitically coupled upper radiating patch,L_r. The radiating and the feeding patches are printed on a dielectric substrate- named by ε_{rr} and ε_{rf} respectively- of the same material $\varepsilon_{rr}= \varepsilon_{rf}$=4.45, the spacing (dielectric substrate thickness) between the radiating and the feeding patches and between the feeding patch and the ground plane are named by h_{rf}, and h_{fg} respectively. The feeding patch is the square slotted patch with geometrical parameters (L_f, L_s, W_s) were set at (7.03cm, 4.2cm, and 0.93cm) respectively, and the feed position of the coaxial feed probe was taken as optimum position at the center of one edge parallel to the length of the rectangular slot (x_f=0, y_f=3.5cm), the radiating patch is a solid square patch with dimension L_r=7.03cm, all these parameters were fixed for all various configurations designed below. The x-axis of the upper patch was shifted from the axis of the lower patch by a distance x_{shift} while the shift in the y-axis is zero.

5.4.2 Simulation and Results of Probe-Fed Stacked Rectangular-Slot MPA

In this type of antenna, an additional parameters to the antenna that can be used to control its impedance, resonant frequency and bandwidth. The wideband characteristic of a probe-fed stacked antenna is the result of coupled resonance. The coupled resonance produces a loop in the impedance locus when plotted on a Smith chart, this loop depends on the degree of mode separation, namely loop becomes larger in area with an increase in mode separation and converges to a point when the mode separation is reduced.

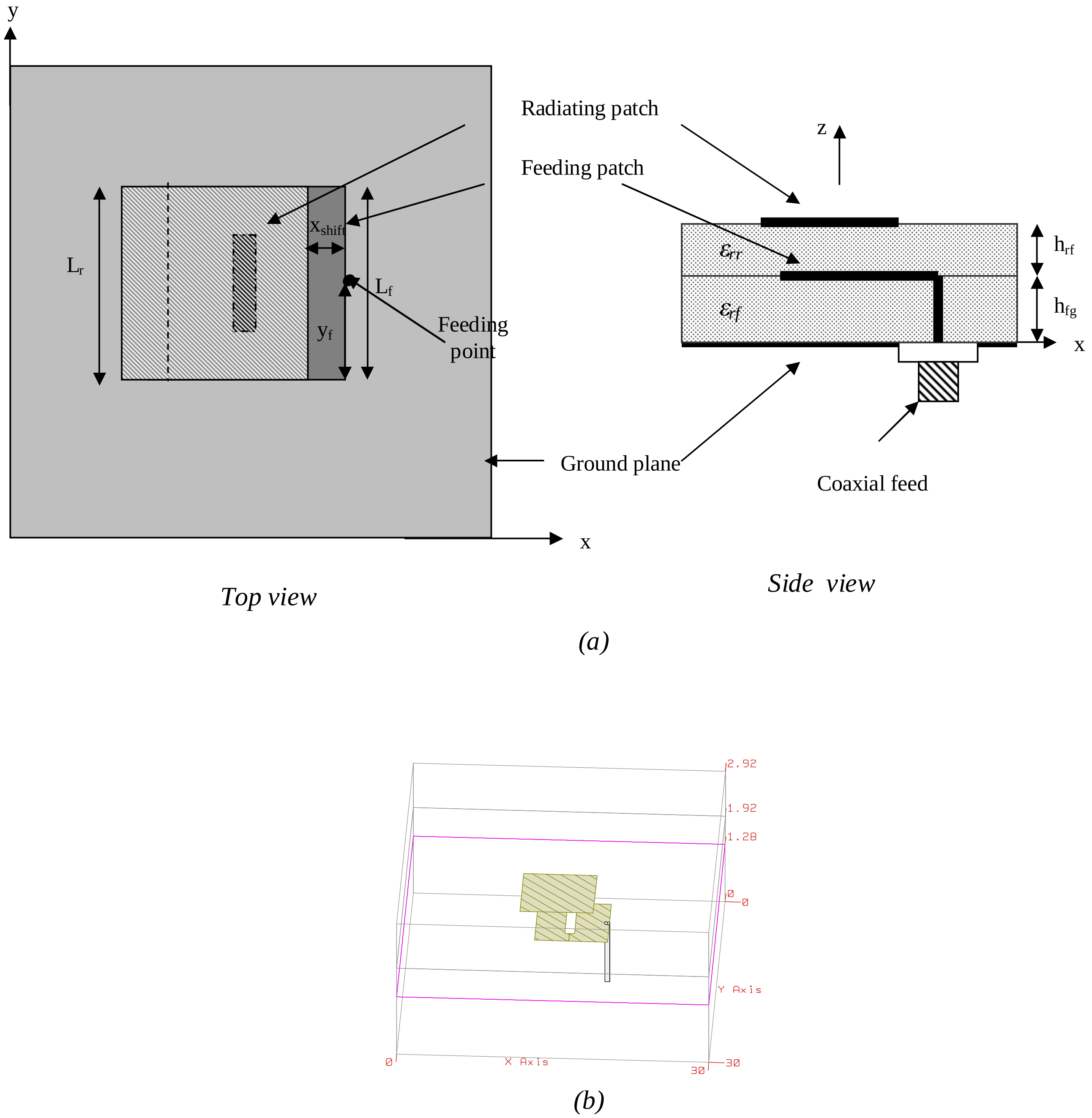

Figure (5.16) The geometry of the probe-fed stacked square slotted MPA (a) Top and side view (b) MOP view

Since the patches in a stacked configuration resonate not independently but due to the strong coupling between the patches, the resonant sizes of the patches should be determined simultaneously. The upper patch is excited only by proximity coupling to the lower patch so its coupling level strongly depends on the separation of the two resonant frequencies. This separation controls the bandwidth of the antenna and is determined by the relative dimensions of the two patches and the separation between them.

The antenna geometric parameters that play an important role to control the wideband behavior of the proposed antenna are, h_{rf}, h_{fg},, and x_{shift}. The effect of these parameters on VSWR and input impedance of the proposed antenna were discussed on the basis of the simulated results by MOP. The simulation frequency ranged from f_{start}=2.1GHz to f_{final} =3.1GHz. Various configurations have been presented to extend the bandwidth.

First, Fig. 5.17(a) shows the effect of the spacing h_{fg} on VSWR and input impedance, h_{fg} varying from 0.64-1.28cm with fixed the other parameters, h_{rf}=0.64 cm, and x_{shift}=1.4cm. It can be seen that the best value of the bandwidth was achieved when h_{fg} =0.96cm which gives bandwidth of 27.7%. Also it is found that as h_{fg} increased the input resistance increases and the input reactance become more inductive.

Then, with the spacing h_{fg} and the shift x_{shift} are fixed at 0.96 cm and 1.4cm respectively, the VSWR and input impedance for different spacing between the radiating and the feeding patches, h_{rf}=0.48-1.12cm, are shown in Fig. 5.17 (b). It can be seen that, the spacing h_{rf}=0.64cm, gives the optimum result for impedance bandwidth (27.7%) which means the coupling between the patches become the best.

Last, the VSWR and input impedance for x_{shift} varying from 0-1.87cm are shown in Fig. 5.17 (c). The spaces h_{rf} and h_{fg} were set at 0.64cm, and 0.96cm

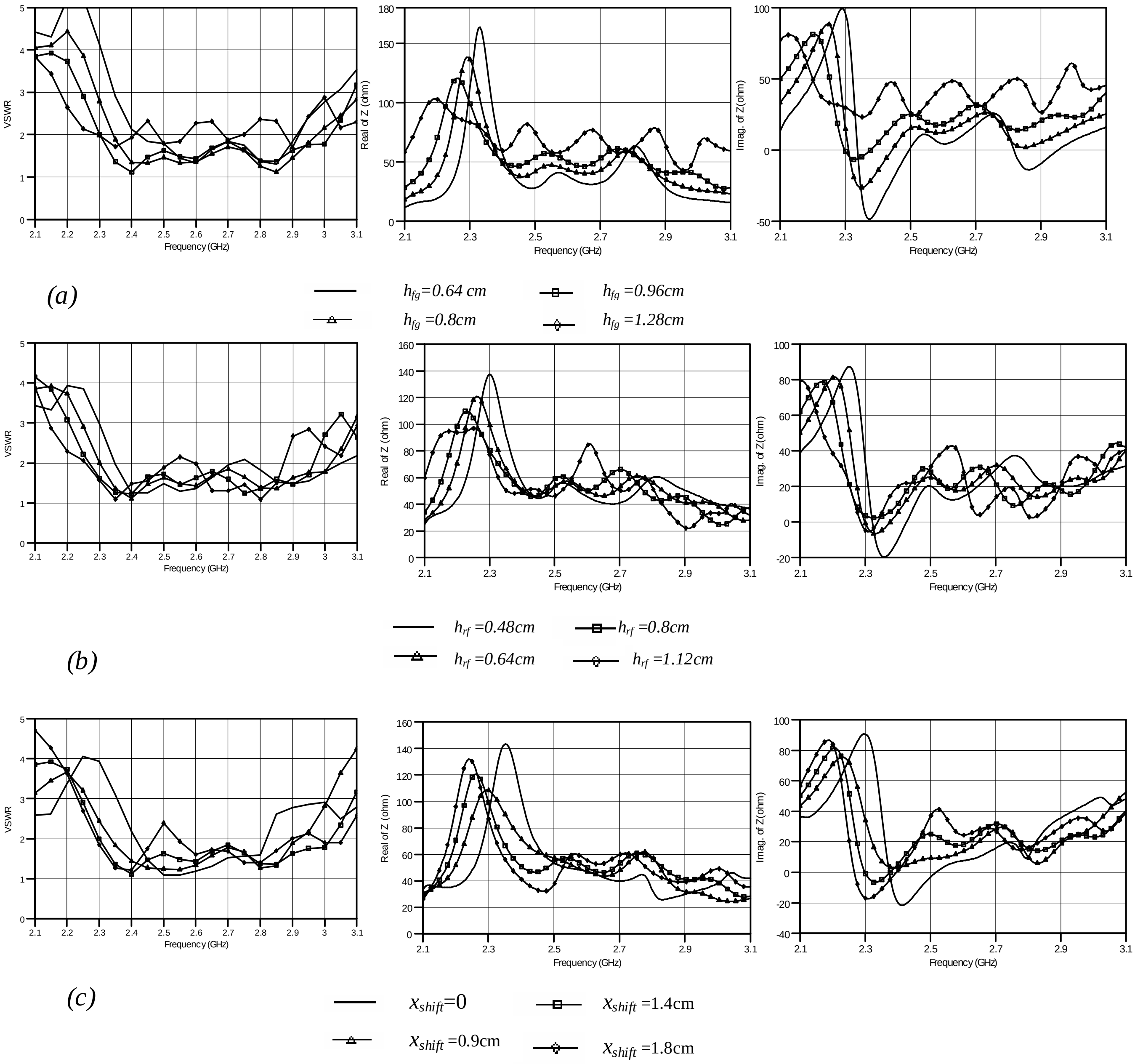

Figure(5.17) VSWR and input impedance (real and imaginary parts) variations versus frequency of a probe-fed stacked rectangular-slot MPA with parameters: L_r=L_f=7.03cm,(L_sxW_s)=(4.2x0.93)cm^2,(x_f,y_f)=(0,3.5cm) for:

(a) Different feeding patch to ground plane spacing: h_{fg}=0.64,0.8,0.96,and 1.28 cm at h_{rf}=0.64 cm and x_{shift}=1.4cm.

(b) Different radiating to feeding patches spacing; h_{rf}=0.48,0.64,0.8,and 1.12 cm at h_{fg} =0.96 cm,and x_{shift}=1.4cm.

(c)Different radiating to feeding patches shift axis; x_{shift} =0,0.9,1.4,and 1.8 cm at h_{rf}=0.64 cm and h_{fg}=0.96cm.

respectively. The best value of the bandwidth was achieved when h_{cg} was set at 1.28cm. An overview of the results was given in table (5.7).

As we have already mentioned, the stacked structure has to be considered as two coupled cavities. The lower cavity is probe coupled and the upper one is approximity coupled. This coupling produces a loop in the impedance locus when plotted on a smith chart as shown in Fig. 5.18. It is seen that more than one coupling loop was appeared in the Smith chart. Fig. 5.18(a) shows impedance locus of the proposed design as a function of h_{fg}. It can be noticed that the loop locus was nearly in the mid of Smith chart (except for h_{fg} =1.28cm which is away from the mid position) which means good matching has been achieved, also it can be seen that the loop becomes smaller when the h_{fg} increased. Fig. 5.18(b) and (c) show the impedance locus as a function of h_{rf} and x_{shift} respectively. It is shown that the loop was not sensitive very well with varying these parameters. This is may be due to interaction of the whole parameters (W_s,L_s, h_{fg} ,etc) with other.

Table (5.7) Effect of x_{shift} , h_{rf}, h_{fg} on the frequency band of a probe-fed stacked rectangular-slot MPA .

Set	x_{shift}	h_{rf}*(cm)*	h_{fg} *(cm)*	*Frequency band (GHz)*
1	1.4	0.64	0.64	(2.4-2.914)
2	1.4	0.64	0.8	(2.35-2.97)
3	1.4	0.64	0.96	(2.3-3.02)
4	1.4	0.64	1.28	(2.3-2.41)(2.48-2.56)(2.69-2.75)(2.87-2.92)
5	1.4	0.48	0.96	(2.35-2.05)
6	1.4	0.8	0.96	(2.26-2.96)
7	1.4	1.12	0.96	(2.26-2.53)(2.6-2.87)
8	0	0.64	0.96	(2.41-2.82)
9	0.9	0.64	0.96	(2.34-2.92)
10	1.87	0.64	0.96	(2.29-2.47)(2.54-2.9)(2.98-3.05)

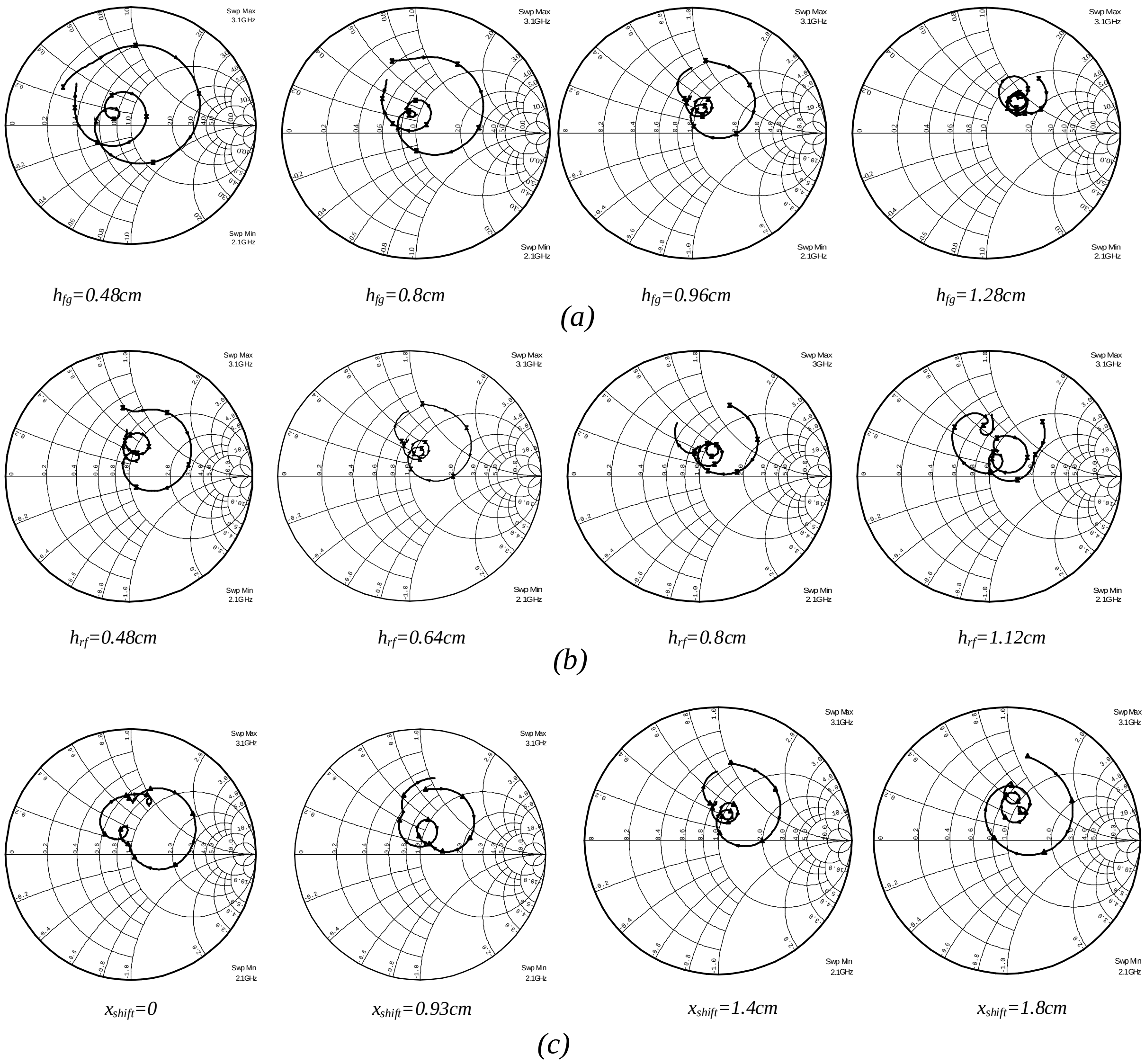

Figure (5.18) Smith chart of a probe-fed stacked rectangular-slot MPA with parameters: $L_r=L_f=7.03$cm,$(L_s \mathrm{x} W_s)=(4.2\mathrm{x}0.93)\mathrm{cm}^2$,$(x_f,y_f)=(0,3.5\mathrm{cm})$ for

(a) Different feeding patch to ground plane spacing: h_{fg}=0.64,0.8,0.96,and 1.28 cm at h_{rf}=0.64 cm and x_{shift}=1.4cm.

(b) Different radiating to feeding patches spacing; h_{rf}=0.48,0.64,0.8,and 1.12 cm at h_{fg} =0.96 cm,and x_{shift}=1.4cm.

(c)Different radiating to feeding patches shift axis; x_{shift} =0,0.9,1.4,and 1.8 cm at h_{rf}=0.64 cm and h_{fg}=0.96cm.

Figure 5.19(a),(b) and(c) display the radiation patterns for these classes of variations (h_{rf}, h_{fg}, and x_{shift}) respectively at operating frequency 2.15 GHz. It can be observed from Fig. 5.19(a) and (b) that in the E-plane patterns, the co-pol patterns were asymmetry around the broadside and their values decreases *as* h_{fg} and h_{rf} increase, with no cross-pol patterns associated with them. In the H-plane, the co-pol patterns shape remain unchanged (having symmetrical shape) with increasing h_{rf} and h_{fg} except for $h_{rf=}$1.12cm and h_{fg} =1.28cm where the co-pol patterns were distorted. The cross-pol patterns have large values and there values decrease slightly with increasing h_{fg} and h_{rf}. The cross-pol is shown to break into two lobes. Figure 5.19(c) shows the effect of x_{shift} on the patterns. It can be noticed that, in the E-plane the co-pol patterns were asymmetry about the broadside. In the H-plane the higher value of the co-pol pattern is that when x_{shift}=1.4cm and the cross-pol remain high for different x_{shift}.

A wide bandwidth can be produced from these designs which can reach nearly 28% for VSWR≤2, covering the frequency range from 2.3 to 3.02GHz when the following geometric parameters (h_{rf}, h_{fg}, and x_{shift}) were set at (0.64cm, 0.96cm, and 1.4cm) respectively as shown in table (5.7) (set 3). Figure 5.20 shows the antenna characteristics for optimum probe-fed stacked square slotted MPA. The coupling loop seen on the Smith chart is due to resonance coupling. All the antenna configurations studied above are to get a coupling loop near the center of Smith chart. Fig. 5.21 shows the computed radiation patterns for this optimum design (set 3) at different frequencies in the E and H-planes at different frequencies within the bandwidth. It can be observed that in the E-plane the co-pol patterns were changed with the frequency variation and have asymmetric shapes. The $HPBW_E^o$ at 2.3GHz ranging from 18.1 to -14.7^o. In the H-plane it is shown that the co-pol radiation patterns are changed with frequency (having symmetrical shape). The cross-pol pattern is relatively high at these values of

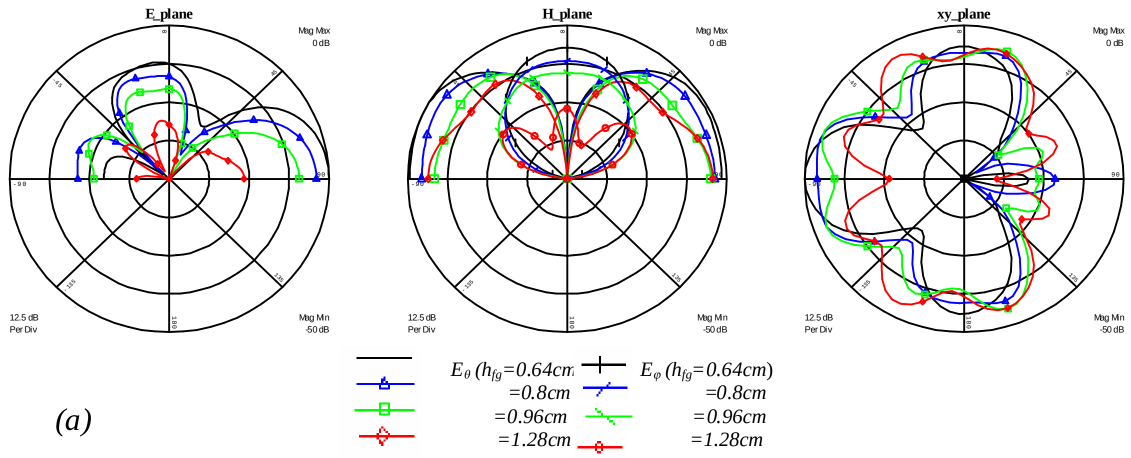

(a)

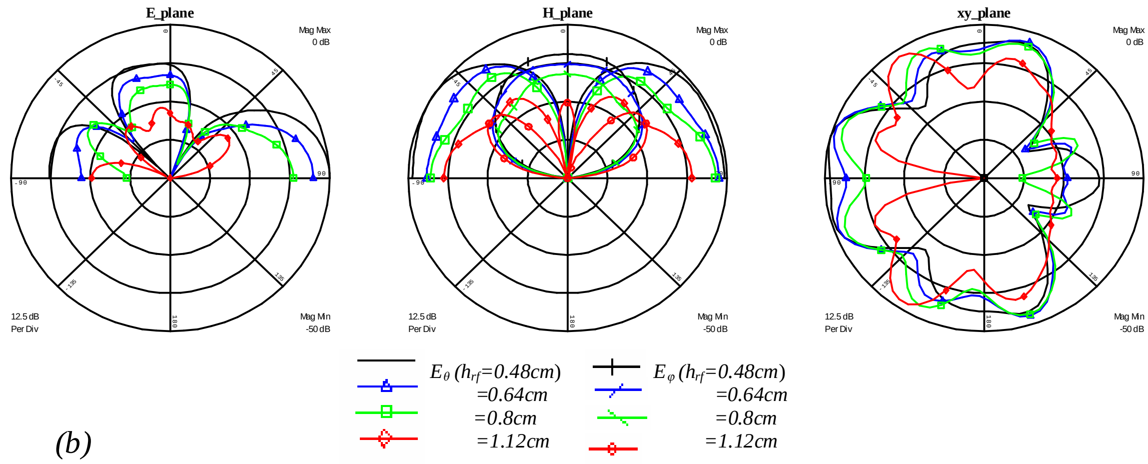

(b)

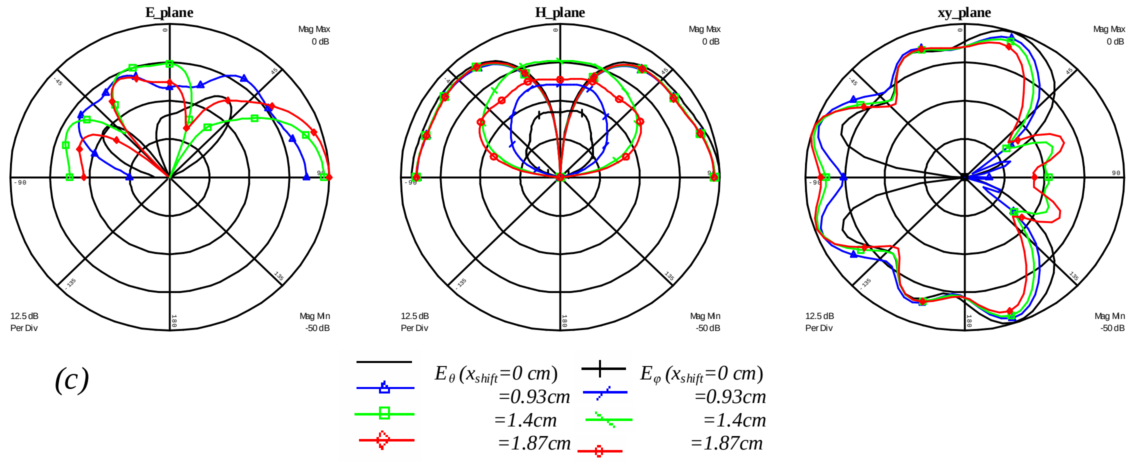

(c)

Figure (5.19) E-plane, H-plane, and xy-plane radiation patterns of a probe-fed stacked rectangular-slot MPA with parameters: $L_r=L_f=7.03cm$, $(L_sxW_s)=(4.2x0.93)cm^2$,and $(x_f,y_f)=(0,3.5cm)$ at center frequency 2.6GHz for:

(a) Different feeding patch to ground plane spacing: h_{fg}=0.64,0.8,0.96,and 1.28 cm at h_{rf}=0.64 cm and x_{shift}=1.4cm.

(b) Different radiating to feeding patches spacing; h_{rf}=0.48,0.64,0.8,and 1.12 cm at h_{fg} =0.96 cm,and x_{shift}=1.4cm.

(c)Different radiating to feeding patches shift axis; x_{shift} =0,0.9,1.4,and 1.8 cm at h_{rf}=0.64 cm and h_{fg}=0.96cm.

frequencies. The $HPBW_H^o$ at 2.3GHz ranging from 26.5 to -26.5^o, so that the gain that can produce from this optimum stacked slotted MPA at 2.3GHz is 13.73dB. Table (5.8) shows the geometrical parameters and the antenna characteristics of the set 3.

Table (5.8) The geometrical parameters and characteristics of the optimum probe-fed stacked rectangular-slot MPA (set 3)

$L_f(cm)$	7.03
$L_s(cm)$	4.2
$W_s(cm)$	0.93
ε_r	4.45
$L_r(cm)$	7.03
$h_{rf}(cm)$	0.64
h_{fg} (cm)	0.96
x_{shift}(cm)	1.4
($x_f$cm , y_f cm)	(0,3.5)
f_c GHz	2.6
Δf GHZ	0.72
Bandwidth (VSWR≤2)	27.7%
Gain (dB)	13.73

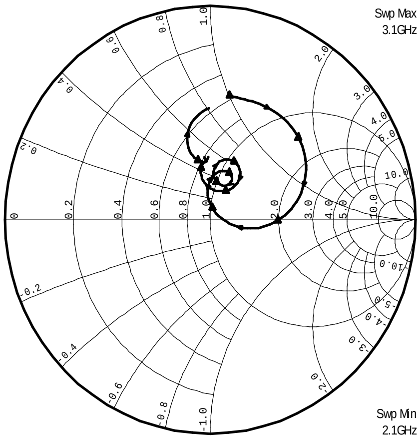

(a)

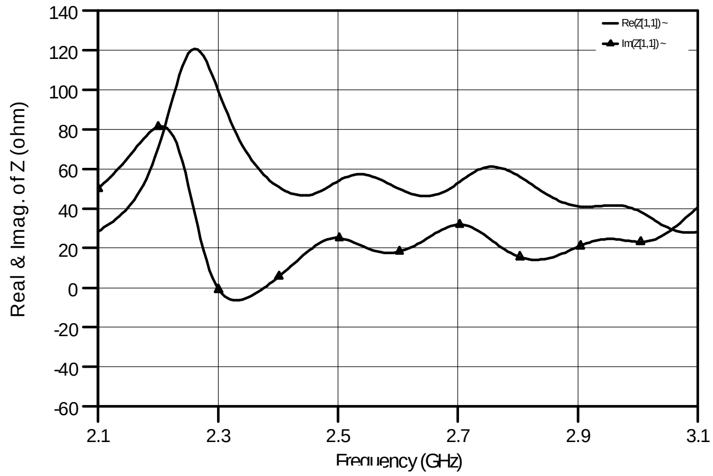

(b)

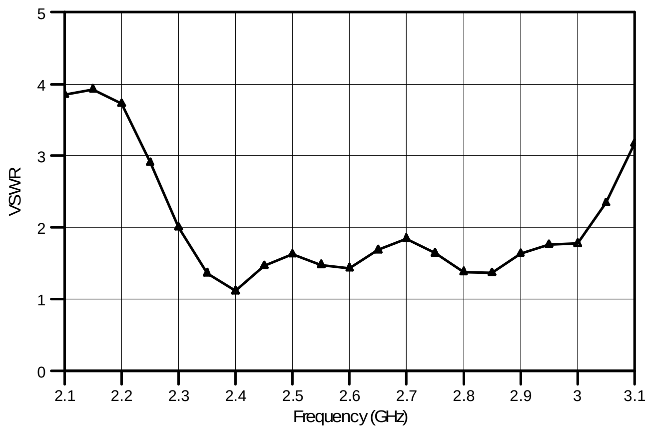

(c)

Figure (5.20) (a) Smith chart, (b) Real and imaginary parts of the input impedance, and (c)VSWR variations versus frequency of the optimum probe-fed stacked rectangular-slot MPA with parameters: $L_r=L_f=7.03cm$, $(L_s xW_s)=(4.2x0.93)cm^2$, $(x_f,y_f)=(0,3.5cm)$, $h_{rf}=0.64cm$, $h_{fg}=0.96cm$, and $x_{shift}= 1.4cm$ simulated by MOP and gives BW of 27.7%.

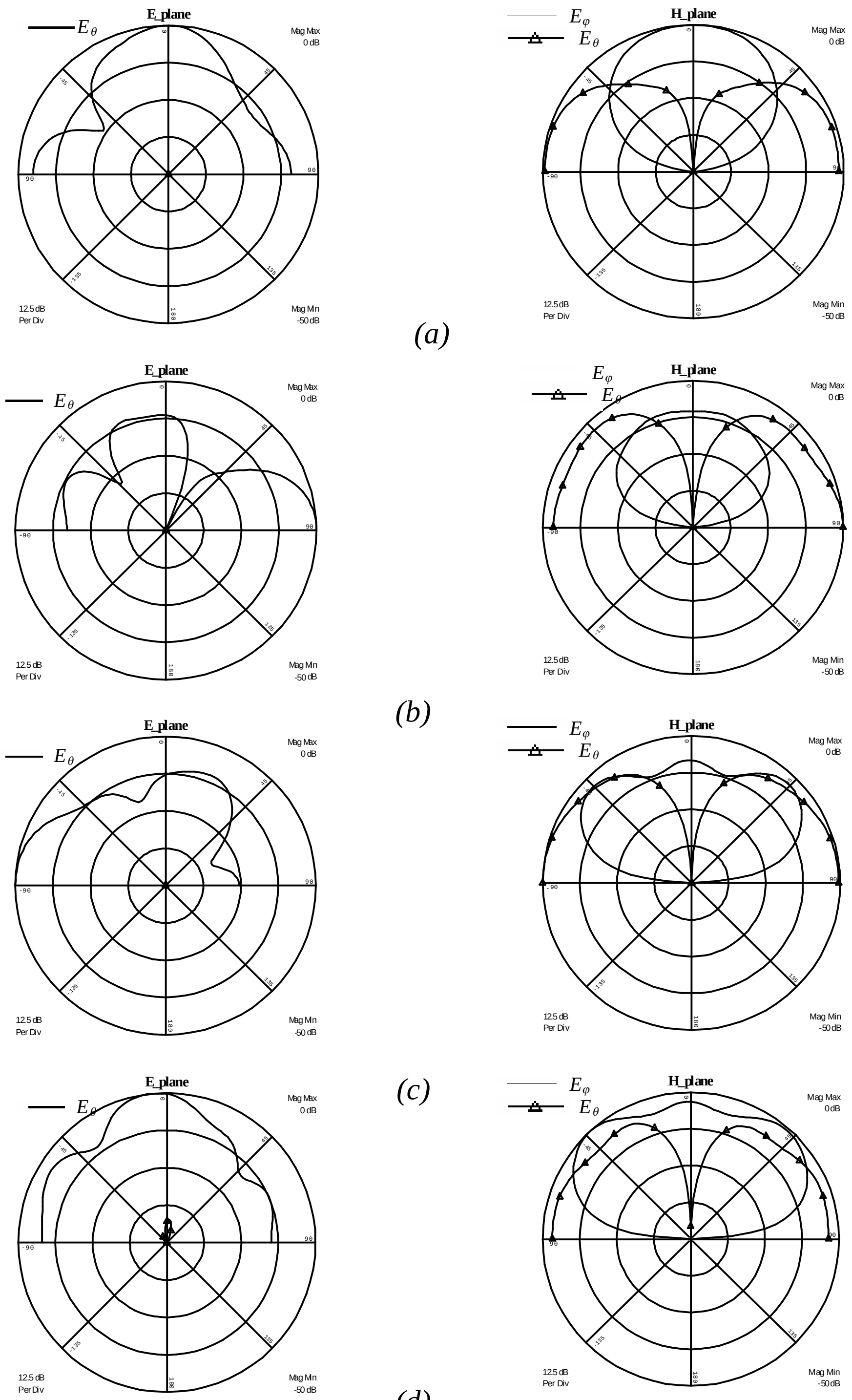

Figure (5.21) E-plane and H-plane radiation patterns of the optimum probe-fed stacked rectangular-slot MPA for different frequencies;(a)f=2.3GHz, (b) f=2.6GHz (c) f=2.8GHz,and(d)f=3GHz,with parameters:L_r=L_f=7.03cm,(L_sxW_s)=(4.2x0.93)cm^2,(x_f,y_f)=(0, 3.5cm), h_{rf}=0.64 cm, h_{fg}=0.96cm, and x_{shift}= 1.4cm.

5.5 Capacitively-Fed Stacked Rectangular-Slot MPA

The effect of indirect feed (capacitively-feed) instead of direct feed(coaxial-feed) on antenna performance of stacked configuration has been studied.

5.5.1 The Configuration of the Capacitively-Fed Stacked Rectangular-Slot MPA

The geometry of the proposed capacitively-fed stacked square slotted MPA is shown in Fig. 5.22. Its consist of a radiating patch on top of a feeding patch on top of a small patch (capacitor-strip) on top of a ground plane with dielectric layers between; the radiating and the feeding patches, ε_{rr} ,between the feeding patch and the capacitor-strip, ε_{rf} ,and between the capacitor-strip and the ground plane, ε_{rc}. All these dielectric layers are of the same substrate material $\varepsilon_{rr}= \varepsilon_{rf}= \varepsilon_{rc}$ =4.45, with their thicknesses named by h_{rf}, h_{fc}, and h_{cg} respectively. The capacitor-strip was fed by a coaxial feed probe at feed position (with respect to the feeding patch) (x_f=0.46cm,y_f=3.5cm). The dimensions of both the radiating and the feeding patches and the shift between them have the same values as that of Section 5.4(table (5.8)). Two coupling are presented here, the first between the radiating and the feeding patches and the second between the feeding patch and the capacitor strip, therefore the bandwidth has been improved.

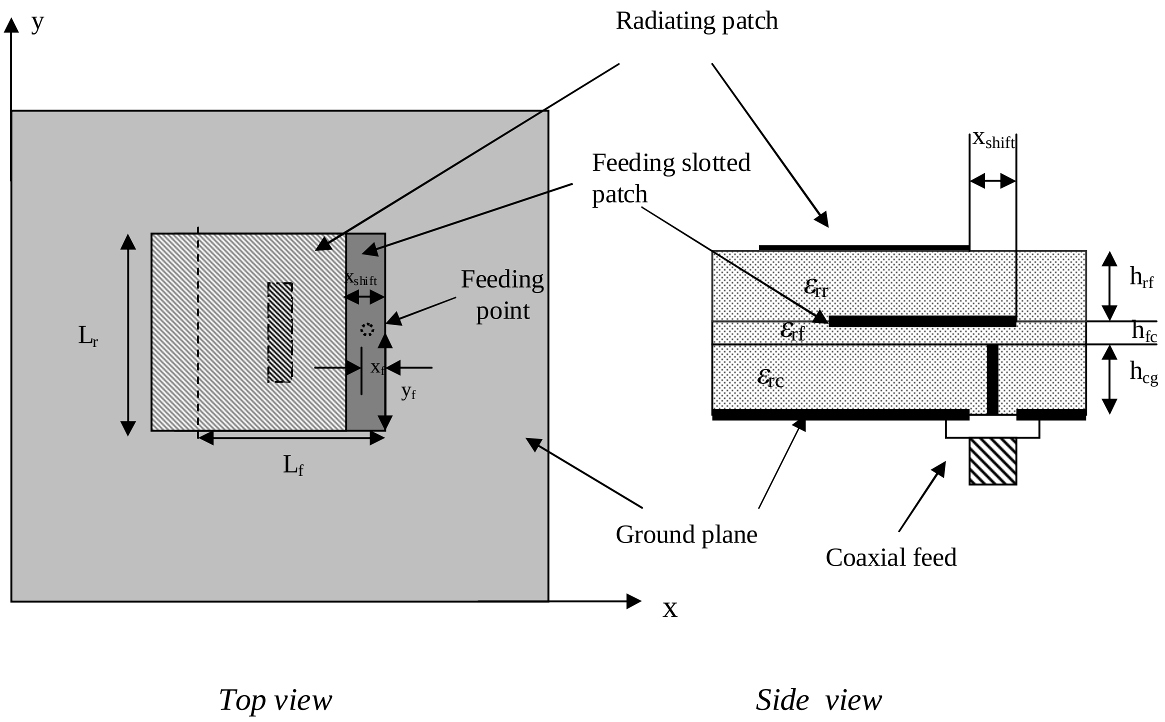

(a)

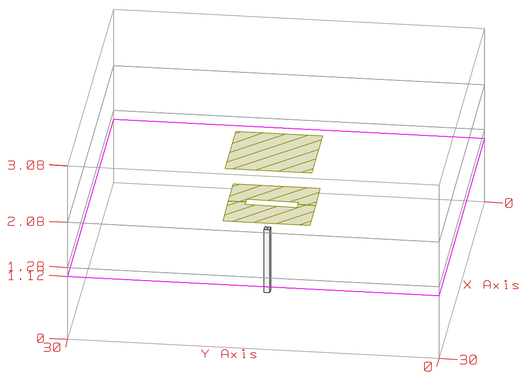

(b)

Figure (5.22) The geometry of the capacitively –fed stacked rectangular-slot MPA: (a) Top and side view (b) MOP view

5.5.2 Simulation and Results of Capacitively-Fed Stacked Rectangular-Slot MPA

In order to enhance the bandwidth of the stacked slotted configuration further a capacitively-fed rather than direct –fed has been applied. It is clear from the structure of the proposed antenna that the structure and the dimensions of the radiating and the feeding patches remain unchanged, i.e. have the same values as in Section 5.4.1. The feed position of the coaxial feed probe, h_{fc}, and h_{rf} are kept fixed for all examples and they are set at (x_f=0.46cm ,y_f=3.5cm), 0.16 and 0.8cm respectively. By adjusting the other parameters such as h_{cg}, and $(L_c x W_c)$, a 2:1 VSWR impedance bandwidth of 33.6%, 46.3%, and 56.7% can be achieved, so that three sets of geometrical parameters have been obtained and they are listed in table (5.9).

Table (5.9) The geometrical parameters and characteristics of the capacitively –fed stacked rectangular-slot MPA

	Set 1	*Set 2*	*Set 3*
L_r(cm)	7.03	7.03	7.03
L_s(cm)	4.2	4.2	4.2
W_s(cm)	0.93	0.93	0.93
$\varepsilon_{rr}= \varepsilon_{rf}= \varepsilon_{rc}$	4.45	4.45	4.45
L_f(cm)	7.03	7.03	7.03
(x_{shift}cm,y_{shift}cm)	(1.4,0)	(1.4,0)	(1.4,0)
(x_f cm, y_f cm)	(0.46,3.5)	(0.46,3.5)	(0.46,3.5)
h_{rf}(cm)	0.8	0.8	0.8
h_{fc} (cm)	0.16	0.16	0.16
h_{cg} (cm)	0.96	1.12	0.96cm
($L_s$cmxW_s cm)	(0.93x0.46)	(0.46x0.46cm^2)	(0.46x0.46cm^2)
f_c(GHz)	2.5	2.7	2.925
Frequency band(GHz)	(2.1-2.94)	(2.04-3.29)	(2.1-3.76)
Δf GHz	(0.84)	1.25	1.65
Bandwidth (VSWR$\leq$2)	33.6%	46.3%	56.7%

Figure 5.23 shows the antenna characteristics of set one. In this design the resultant impedance bandwidth for VSWR=2:1 reaches 33.6%, covering the frequency range from 2.1 to 2.94GHz. In this design the size of the capacitor-strip was set at 0.93cmx0.46cm (L-shape) with dielectric substrate thickness, h_{cg}=0.96cm (0.145λ_d). It can be noticed from this figure that the impedance curve on the Smith chart has three tight impedance loops shifted a small distance from the center of Smith chart with an inductive nature.

To examine the radiation characteristics within the bandwidth for this design (set 1), the co-pol and cross-pol radiation patterns in both principal E- and H-planes are calculated at four frequencies as shown in Fig. 5.24. It can be observed that in the E-plane the co-pol patterns are unchanged (nearly stable) with the frequency variation. In the H-plane it is shown that the co-pol radiation patterns are changed with frequency (having symmetrical shape). The cross-pol pattern is relatively high at these values of frequencies.

To further improve the matching and broaden the bandwidth (set 2), the dimensions of the capacitor-strip is reduced to 0.46cmx0.46cm (I-shape) with the value of h_{cg}=1.12cm. The resultant impedance bandwidth for VSWR=2:1 reaches 46.3%, covering the frequency range from 2.04 to 3.29GHz, as illustrated in Fig 5.25.

Fig. 5.26 shows the calculated radiation patterns in the E and H-planes at different frequencies within the bandwidth for capacitively-fed stacked rectangular-slot MPA (set 2). It can be observed that in the E-plane the co-pol patterns are changed with the frequency variation. In the H-plane it is shown that the co-pol radiation patterns are changed with frequency (having symmetrical shape). The cross-pol pattern is relatively high at these values of frequencies.

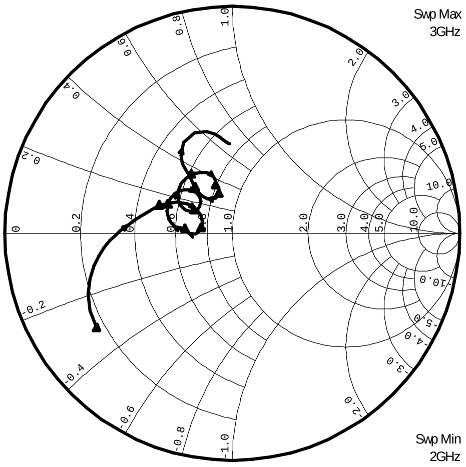

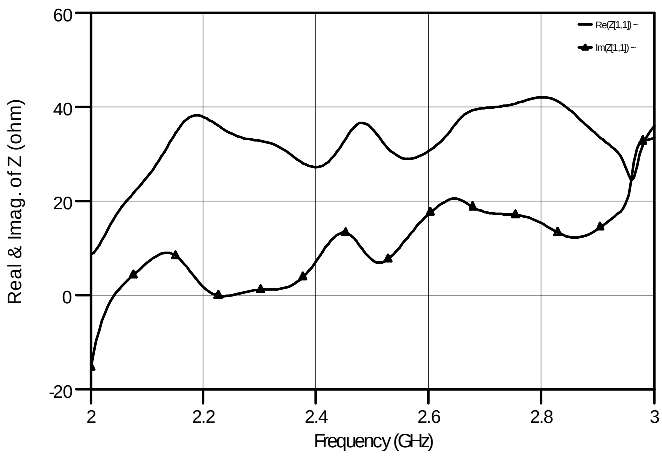

(a) *(b)*

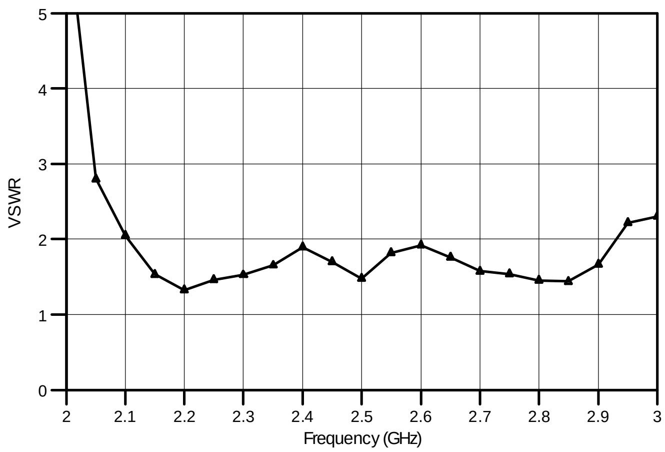

(c)

Figure(5.23) (a) Smith chart, (b) Real and imaginary parts of the input impedance , and(c) VSWR variations versus frequency of a capacitively-fed stacked rectangular-slot MPA (set 1) with parameters: $L_r=L_f=7.03$cm,$(L_s$x$W_s)=(4.2$x$0.93)$cm^2, $x_{shift}=$ 1.4cm ,$(x_f,y_f)=$ (0.46cm,3.5cm), $(L_c$x$W_c)=(0.93$x$0.46)$ cm^2 , $h_{rf}=0.8$cm, $h_{fc}=0.16$ cm, and $h_{cg}=0.96$ cm simulated by MOP and gives BW of 33.6%.

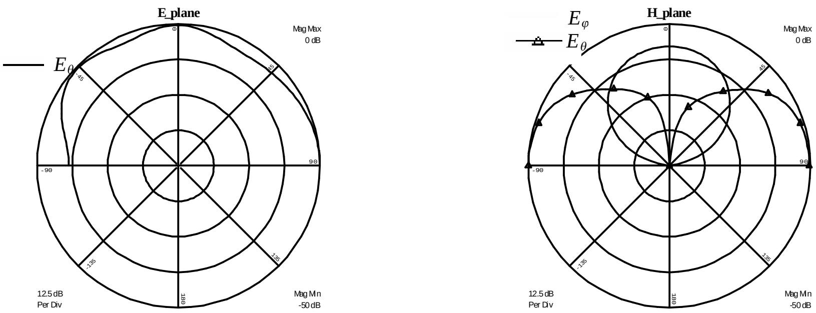

(a)

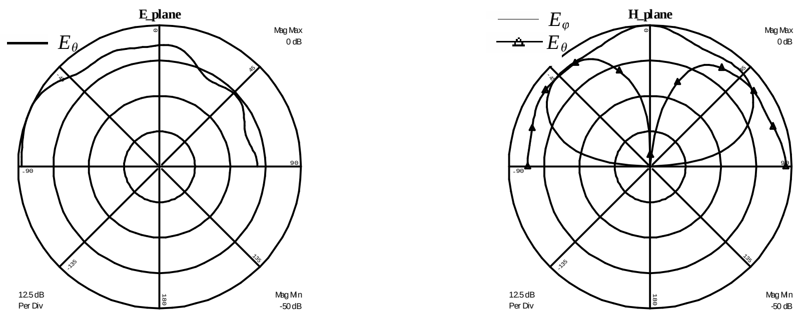

(b)

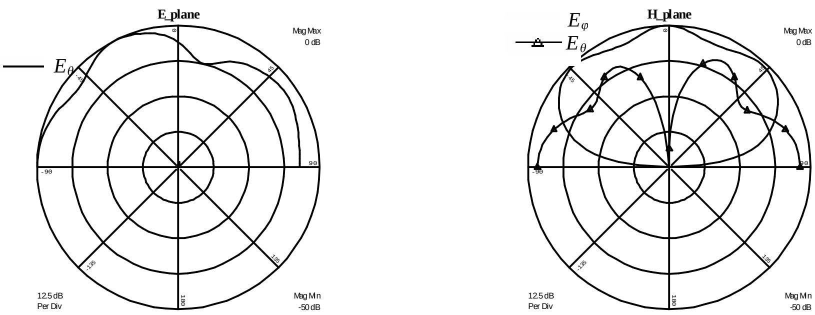

(c)

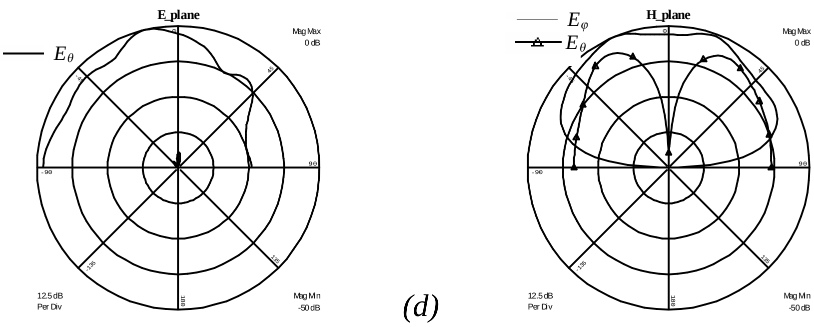

(d)

Figure (5.24) E-plane and H-plane radiation patterns of a capacitively-fed stacked rectangular-slot MPA (set1) for different frequencies;(a) f=2.15GHz, (b)f=2.5GHz, (c)f=2.7GHz, and (d)f=2.9GHz with parameters: $L_r=L_f=7.03cm$, $(L_s x W_s)=(4.2x0.93)cm^2$, $x_{shift}= 1.4cm$, $(x_f,y_f)=(0.46cm,3.5cm)$, $(L_c x W_c)=(0.93x0.46)\ cm^2$, $h_{rf}=0.8cm$, $h_{fc}=0.16\ cm$, *and* $h_{cg}=0.96cm$.

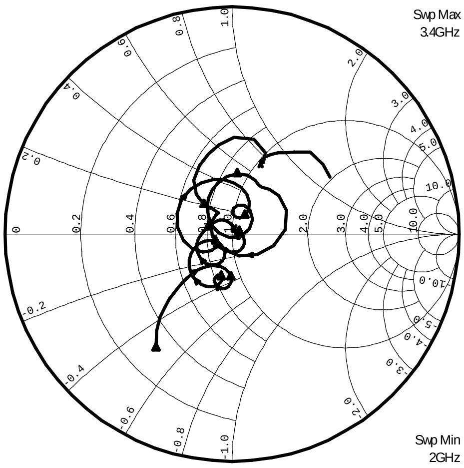

(a)

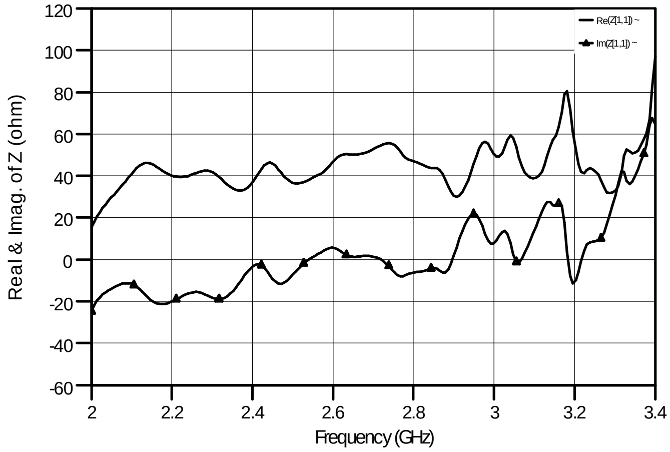

(b)

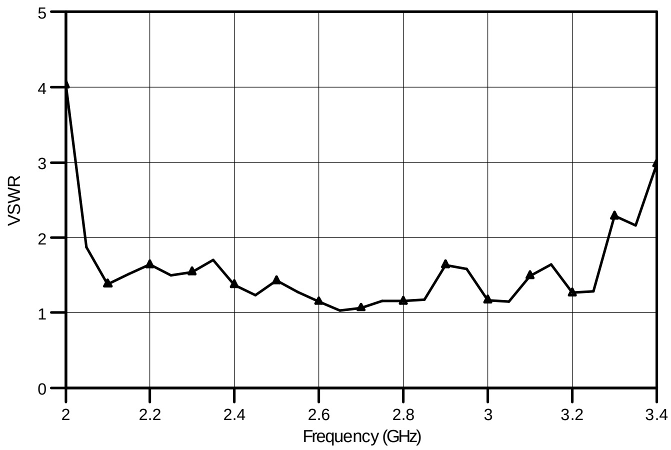

(c)

Figure(5.25) (a) Smith chart , (b) Real and imaginary parts of the input impedance, and (c)VSWR variations versus frequency of a capacitively-fed stacked rectangular-slot MPA(set 2) with parameters: $L_r=L_f=7.03cm$, $(L_s \text{x} W_s)=(4.2\text{x}0.93)cm^2$, $x_{shift}= 1.4cm$,$(x_f,y_f)=(0.46cm,3.5cm)$, $L_c\text{x}W_c=0.46\text{x}0.46\ cm^2$, $h_{rf}=0.8cm$, $h_{fc}=0.16$ cm, and $h_{cg}=1.12$ cm *simulated by MOP and gives BW of 46.3%.*

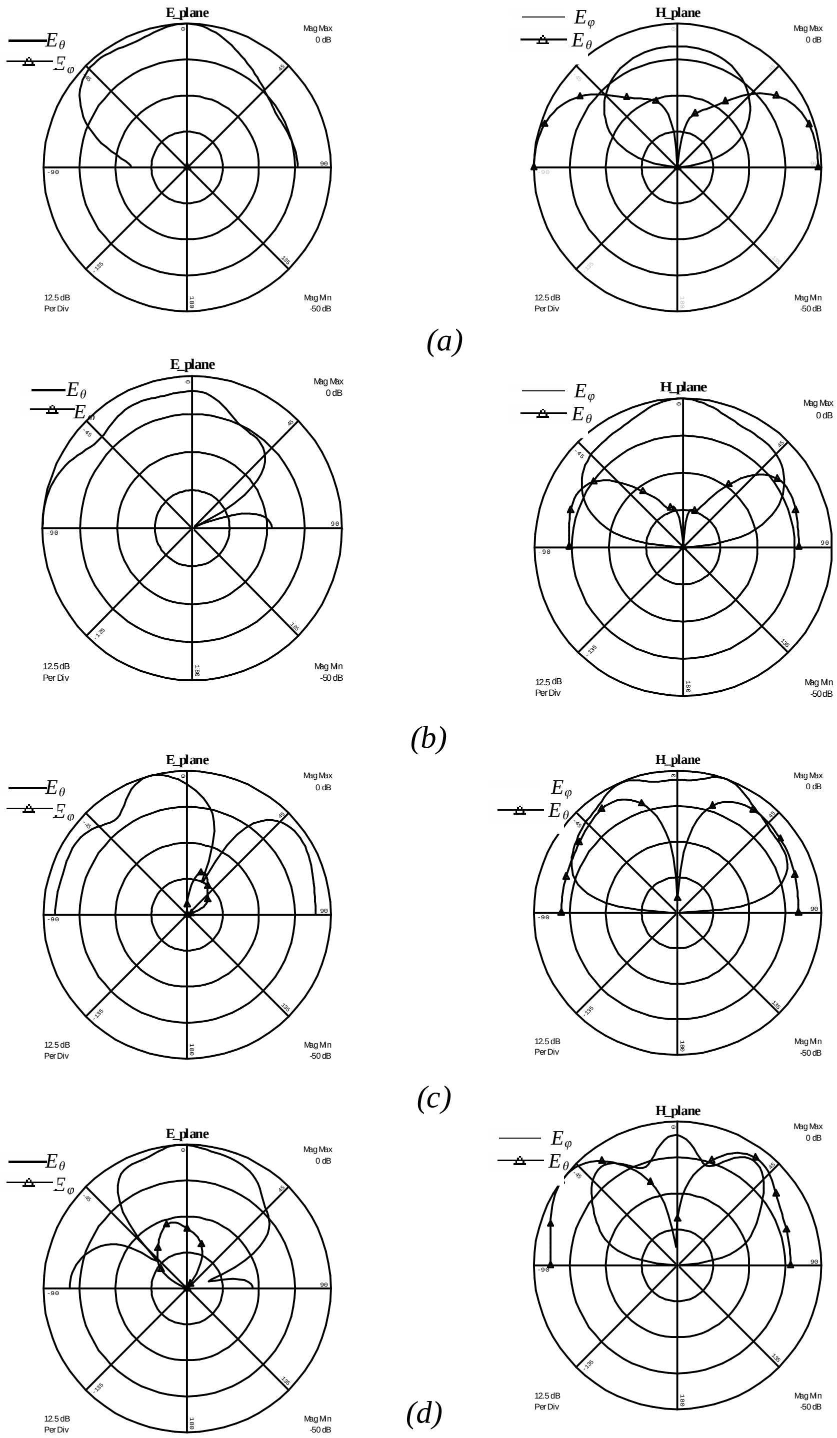

Figure(5.26) E-plane and H-plane radiation patterns of a capacitively-fed stacked rectangular-slot MPA (set 2) for different frequencies; (a)f= 2.15GHz ,(b)f=2.4GHz , (c)f=2.8GHz,and (d) f=3.2GHz with parameters: $L_r=L_f=7.03cm$*,*$(L_s x W_s)=(4.2x0.93)cm^2$*,* $x_{shift}= 1.4cm$ *,*$(x_f,y_f) =(0.46cm, 3.5cm)$*,* $L_c x W_c=0.46x0.46\ cm^2$*,* $h_{rf}=0.8cm$*,* $h_{fc}=0.16\ cm$*,and* $h_{gc}=1.12\ cm$*.*

The input impedance and VSWR of the final capacitively-fed stacked slotted MPA design (set 3) built in order to increase the bandwidth more is shown in Figure 5.27. The resultant impedance bandwidth for VSWR=2:1 reaches 56.7%, covering the frequency range from 2.1 to 3.76 GHz. In this example, all the geometrical parameters were set equal to those of set 2 except h_{cg}, where set equals to 0.96cm. Fig. 5.28 shows the calculated radiation patterns in the E and H-planes at different frequencies within the bandwidth for this design (set 3). It can be observed that in the E-plane the co-pol patterns are changed with the frequency variation. In the H-plane it is shown that the co-pol radiation patterns are changed with frequency (having symmetrical shape). The cross-pol pattern is relatively high at these values of frequencies. Table (5.9) gives an over view for the geometrical parameters and antenna characteristics of these three sets. It can be seen that the bandwidth of the stacked configuration can be improved by using capacitively-fed method, nearly twice times larger than the probe-feed method.

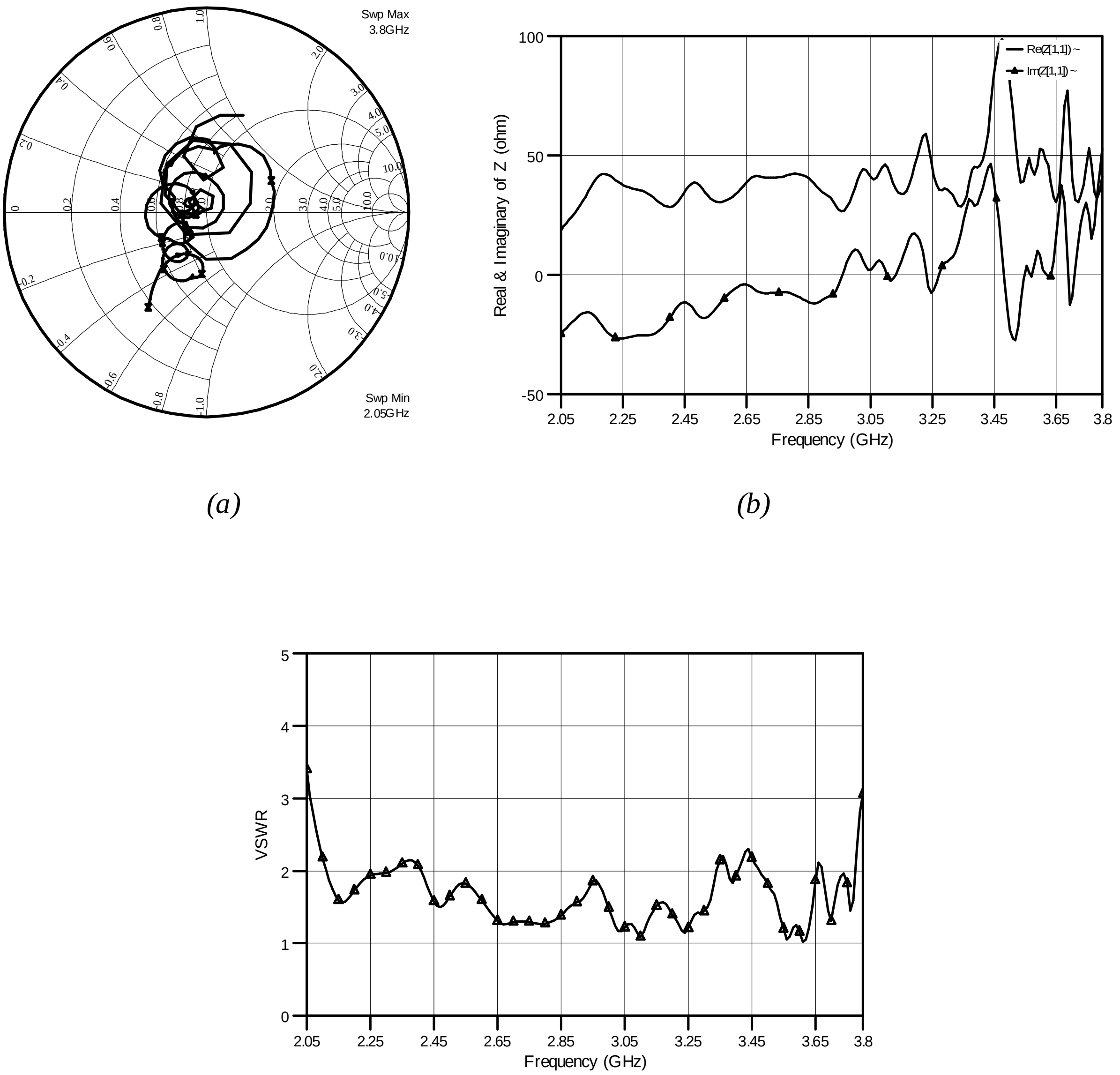

(a) (b)

(c)

Figure(5.27) (a) Smith chart ,(b) Real and imaginary parts of the input impedance,and (c) VSWR variations versus frequency of a capacitively-fed stacked rectangular-slot MPA(set 3) with parameters: L_r=L_f=7.03cm,(L_sxW_s)=(4.2x0.93)cm^2, x_{shift}= 1.4cm ,(x_f,y_f)=(0.46cm,3.5cm), L_cxW_c= 0.46x0.46 cm^2 , h_{rf}=0.8cm, h_{fc}=0.16 cm, and h_{cg}=0.96 cm simulated by MOP and gives BW of 56.7%.

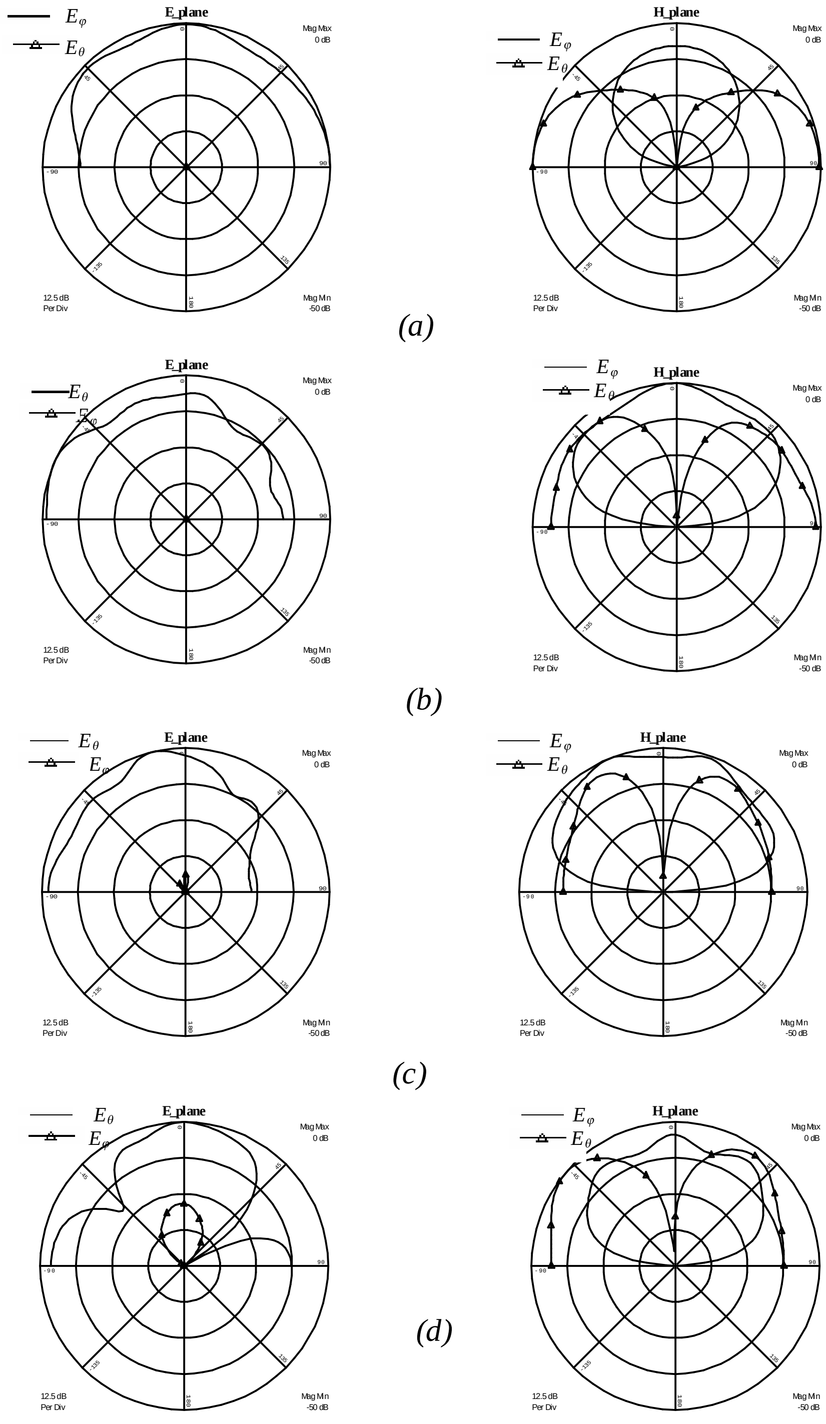

Figure(5.28) E-plane and H-plane radiation patterns of a capacitively-fed stacked rectangular-slot MPA (set3)for different frequencies (a)f=2.15GHz (b)f=2.5GHz ,(c)f=2.9GHz,and (d)f=3GHz with parameters: $L_r=L_f=7.03cm$, $(L_s x W_s)=(4.2x0.93)cm^2$, $x_{shift}=1.4cm$,$(x_f,y_f)=(0.46cm,3.5cm)$, $(L_c x W_c)=(0.46x0.46)\ cm^2$, $h_{rf}=0.8cm$, $h_{fc}=0.16\ cm$, *and* $h_{cg}=0.96\ cm$.

5.6 Probe-Fed Stacked Shorted Rectangular-Slot MPA

Short-circuited microstrip patch antennas can be used as compact wide bandwidth antennas as mensioned in this simulating invistigation. In this section the effect of short walls on the antenna characteristics of stacked slotted MPA has been studied.

5.6.1 The Configuration of the Probe-Fed Stacked Shorted Rectangular-Slot MPA

The goemetry of the proposed probe-fed stacked shorted slotted microstrip patch antenna is shown in Fig. 5.29. The antenna consists of a feeding lower patch,a parasitically coupled upper radiating patch and a common shorting wall (L_{short},W_{short})which connects both patches parallel to the long side of the rectangular slot. The geometric parameters of the feeding patch (L_f, L_s, W_s) were set at (7.03cm, 4.2cm, and 0.93cm) respectively, it is fed by coaxial cable with feed position was set at the center of its edge parallel to the long side of the slot ,(x_f=0,y_f=3.5cm). The radiating and the feeding patches are etched on a dielectric substrate with ε_{rr}= ε_{rf} =4.45, the spacing between the radiating and the feeding patches and between the feeding patch and the ground plane are named by h_{rf}, and h_{fg} respectively. The radiating patch is a solid square patch with dimension L_r of length 8.9cm and it is shifted from the feeding patch by a distance (x_{shift}=0.93cm,y_{shift}=1.4cm).

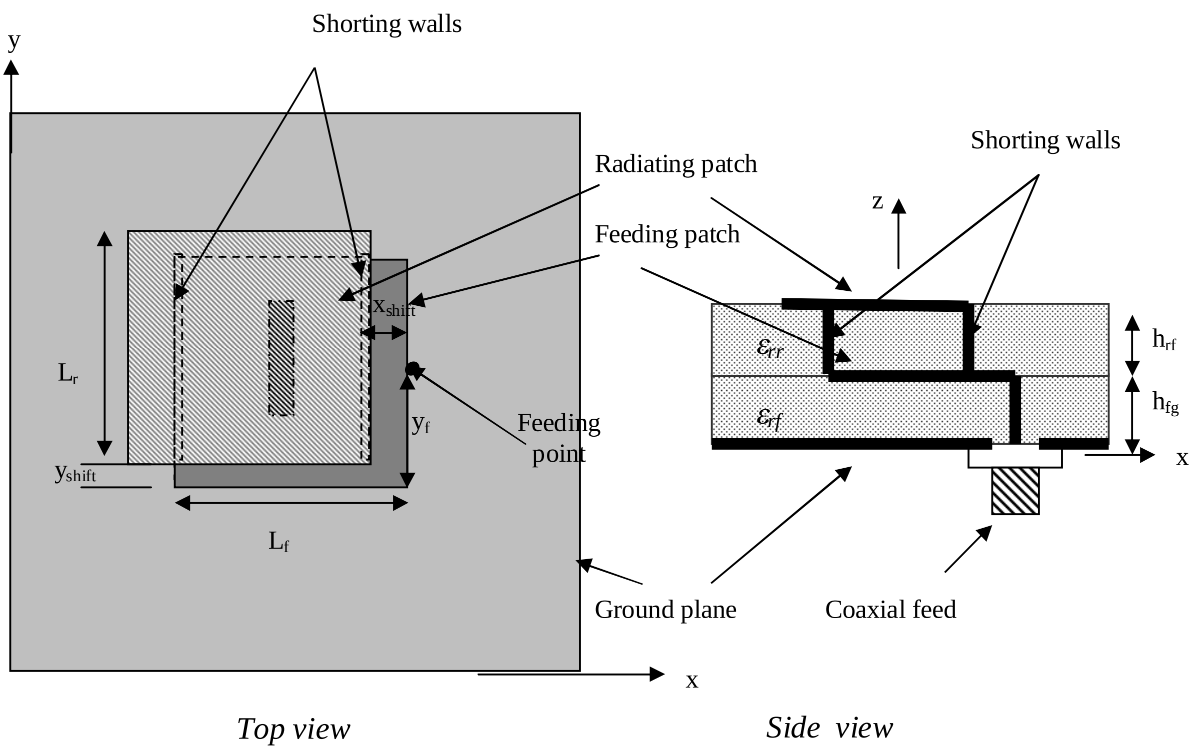

(a)

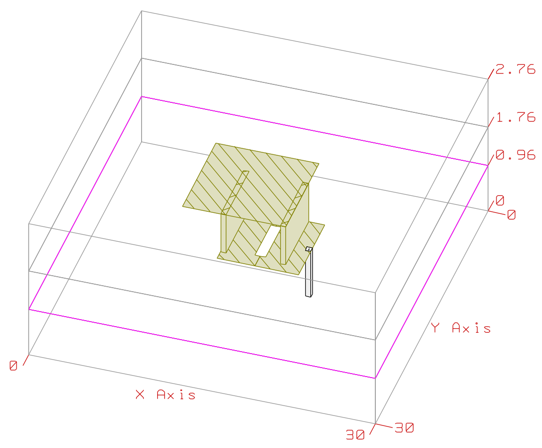

(b)

Figure(5.29) The goemetry of the probe-fed stacked shorted rectangular-slot MPA(a) Top and side view (b) MOP view

5.6.2 Simulation and Resuls of Probe-Fed Stacked Shorted Rectangular-Slot MPA

The effect of shorted wall on probe-fed stacked configuration has been invistigated. The simulation of the proposed antenna has been carried out using MOP. By adjusting the geometrical parameters of this kind of MPA an impedance bandwidth of 30.6%, for VSWR≤2, covering frequency range from 2.15 to 2.9 GHz can be achieved. Figure 5.30 shows the antenna characteristics for this proposed antenna. It can be noticed from Smith chart that the frequency range was located near the center of Smith chart but in the inductive part. The geometric parameters and the antenna characteristics of the proposed antenna are tabulated in table (5.10).

The radiation pattern of probe-fed stacked shorted rectangular-slot MPA in both principal E- and H-planes are computed at four frequencies within the bandwidth as shown in Fig. 5.31. It can be observed that in the E-plane the co-pol patterns were changed and distorted with the frequency variation. The cross-pol pattern is considerably high, the same manner with H-plane.

Table (5.10) The geometrical parameters and characteristics of the probe- fed stacked shorted rectangular-slot MPA.

$L_f(cm)$	7.03
$L_s(cm)$	4.2
$W_s(cm)$	0.93
$\varepsilon_{rr}= \varepsilon_{rf}$	4.45
$L_r(cm)$	8.9
$h_{rf}(cm)$	0.8
$h_{fg}(cm)$	0.96
$(L_{short}\ cm, W_{short} cm)$	(6.09,0.8)
$(x_f cm\ , y_f cm)$	(0,3.5)
$(x_{shift} cm\ , y_{shift} cm)$	(0.93,1.4)
$f_c(GHz)$	2.45
Frequency band(GHz)	(2.15-2.9)
$\Delta f(GHz)$	0.75
Bandwidth (VSWR≤2)	30.6%

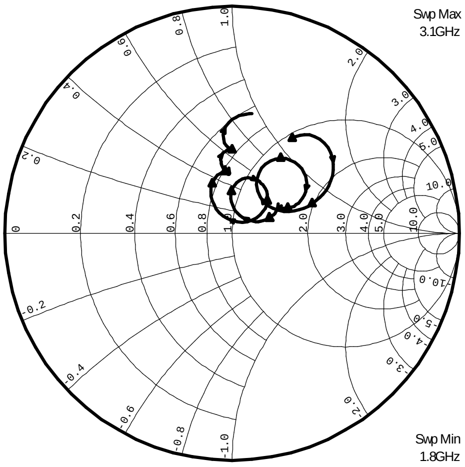

(a)

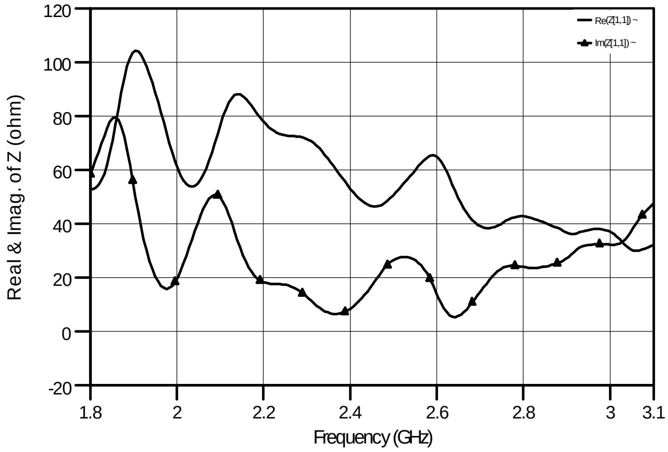

(b)

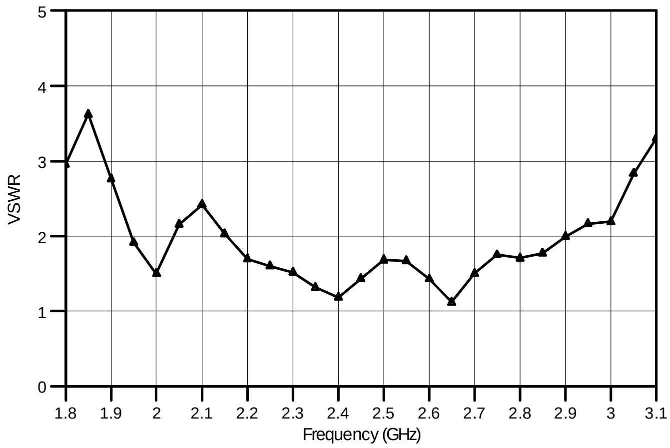

(c)

Figure(5.30)(a) Smith chart ,(b) Real and imaginary parts of the input impedance,and (c) VSWR variations versus frequency of the optimum probe-fed stacked shorted rectangular-slot MPA with parameters: L_f=7.03cm, (L_sxW_s)= (4.2x0.93)cm^2 , L_r=8.9cm ,(x_f,y_f)=(0,3.5cm) ,h_{rf}=0.8cm, h_{fg}=0.96cm, (L_{short}xW_{short}) =(0.8cm, 6.09cm),(x_{shift},y_{shift})=(0.93cm,1.4cm), simulated by MOP and gives BW of 30.6%

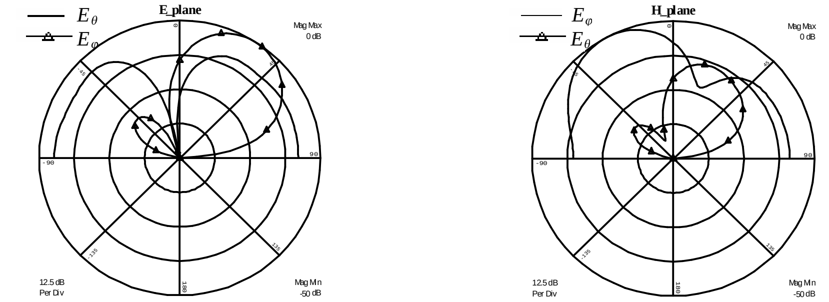

(a)

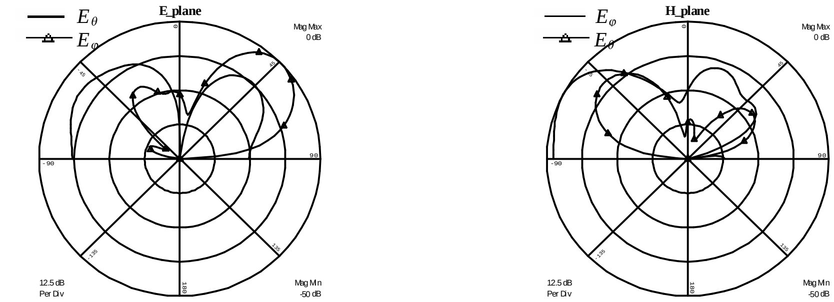

(b)

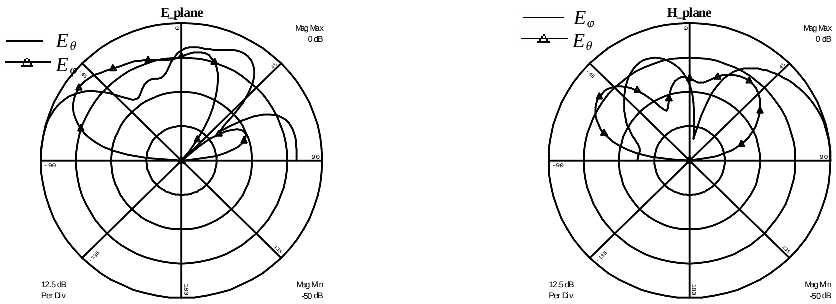

(c)

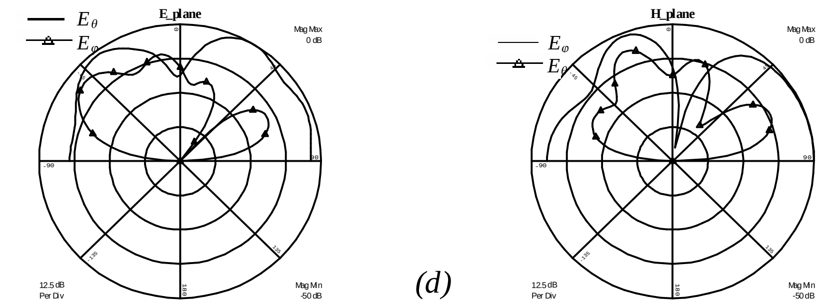

(d)

Figure(6.31) E-plane and H-plane radiation patterns of the optimum probe-fed stacked shorted rectangular-slot MPA for different frequencies; (a)f=2.15GHz, (b)f=2.45GHz ,(c)f=2.7GHz,and(d) f=2.9GHz with parameters L_f=7.03cm ,(L_sxW_s) =(4.2x0.93) cm^2 ,L_r=8.9cm,(x_f,y_f)= (0,3.5cm),h_{rf}=0.8cm,h_{fg}=0.96cm,(L_{short}xW_{short})=(0.8x6.09)cm^2 ,(x_{shift},y_{shift}) =(0.93cm,1.4cm).

5.7 Capacitively-Fed Stacked Shorted Rectangular-Slot MPA

The effect of indirect feed (capacitively-fed) rather than direct feed (coaxial-feed) on the shorted stacked slotted MPA has been studied for bandwidth enhancement purpose.

5.7.1 The Configuration of the Capacitively-Fed Stacked Shorted Rectangular-Slot MPA

The goemetry of the proposed capacitively-fed shorted stacked rectangular-slot MPA is shown in Fig.5.32.

The antenna consists of a feeding lower patch,a parasitically coupled upper radiating patch and a common shorting wall which connects both patches. The geometric parameters of the feeding patch (L_f, L_s, W_s) were set at (7.03cm, 4.2cm, and 0.93cm) respectively, it is fed by approximatly cuopled (indirect feed). The dielectric layers between; the radiating and the feeding patches(ε_{rr}), between the feeding patch and the capacitor-strip(ε_{rf}), and between the capacitor-strip and the ground plane(ε_{rc}) are of the same substrate material, $\varepsilon_{rr}= \varepsilon_{rf} = \varepsilon_{rc}=$ 4.45, with their thicknesses named by h_{rf}, h_{fc}, and h_{cg} respectively and they are set to (0.8, 0.16, and 1.12cm) respectively. The capacitor-strip size is exactly with the same size of probe feed at feed position (x_f=0, y_f=3.5cm) with respect to the feeding patch. The radiating patch is a square patch with dimension of 8.9 cm and it's shifted from the feeding patch by a distance (x_{shift}=0.93cm,y_{shift}=1.4cm).

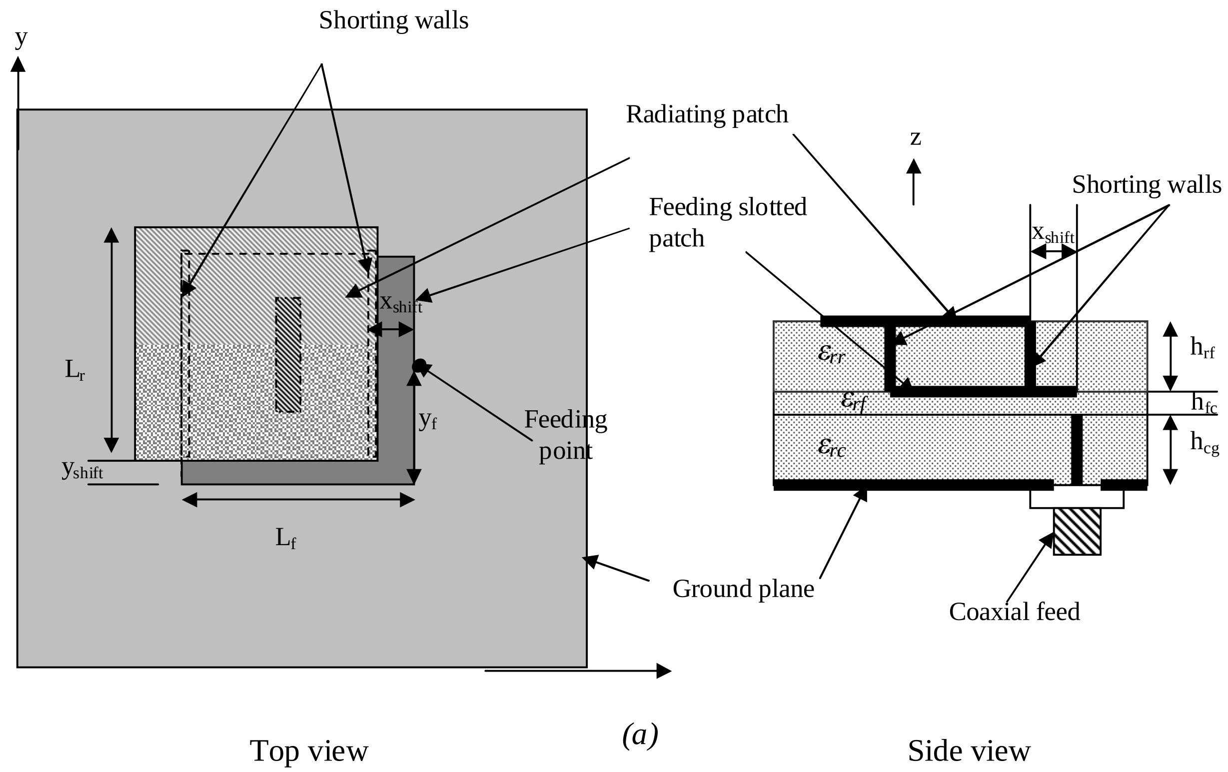

(a)

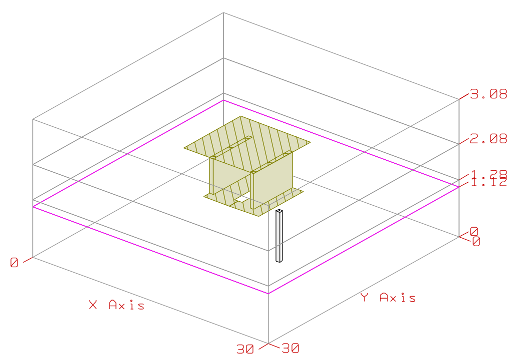

(b)

Figure(5.32) The goemetry of the capacitively-fed shorted stacked rectangular-slot MPA(a) Top and side view (b) MOP view

5.7.2 Simulation and Results of Capacitively-Fed Stacked Shorted Rectangular-Slot MPA

The effect of indirect-fed (capacitively-fed) on the stacked shorted slotted MPA has been established. It is clear from the structure of the proposed antenna that the structure and the dimensions of the radiating and the feeding patches remain unchanged, i.e. have the same values as in Section 5.6. The only change is the type of feeding or in other word only disconnect the communication between the feeding patch and the feed probe by high dielectric substrate material, ε_{rf}, with small thickness (h_{fc}=0.16cm) and by using thicker feeding substrate thickness h_{cg}=1.12cm (0.17 λ_d), one can produce a large bandwidth (67.7%), covering frequency range 1.61 to 3.27GHz, two times larger that direct feed as shown in Fig.5.33.

Fig. 5.33 shows that all the frequency range, f_{start}=1.6 to f_{final}= 3.3GHz, is located and concentrated at the center of Smith chart, part of the band lay in the capacitive part and the other part is in the inductive part with good matching characteristics. Table (5.11) shows the geometrical parameters and the characteristics of capacitively- fed stacked shorted slotted MPA.

The radiation field patterns for both E- and H-plans of the proposed capacitively-fed stacked shorted rectangular-slot MPA are calculated for fifferent frequencies as shown in Fig. 5.34. It can be observed that in both E- and H-planes the radiation field patterns are changed and distorted (have asymmetrical shapes) with the frequency variation.

Table (5.11) The geometrical parameters and characteristics of the capacitively- fed stacked shorted rectangular-slot MPA.

$L_f(cm)$	7.03
$L_s(cm)$	4.2
$W_s(cm)$	0.93
$\varepsilon_{rr}= \varepsilon_{rf}= \varepsilon_{rc}$	4.45
$L_r(cm)$	8.9
$h_{rf}(cm)$	0.8
$h_{fc}(cm)$	0.16
$h_{cg}(cm)$	1.12
$(L_{short}\ cm, W_{short} cm)$	(6.09,0.8)
$(x_f cm\ , y_f cm)$	(0,3.28)
$(x_{shift} cm\ ,y_{shift} cm)$	(0.93, 1.4)
$f_c(GHz)$	2.45
Frequency band(GHz)	(1.61-3.27)
$\Delta f(GHz)$	1.66
Bandwidth (VSWR≤2)	67.7%

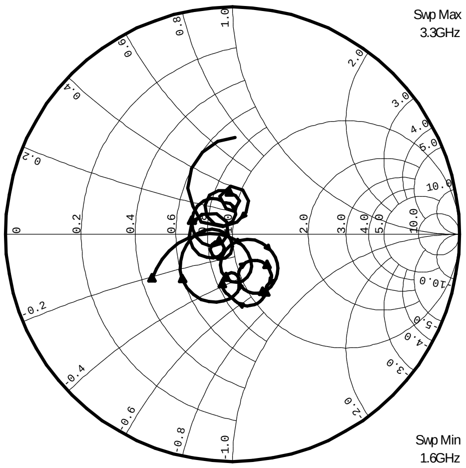

(a)

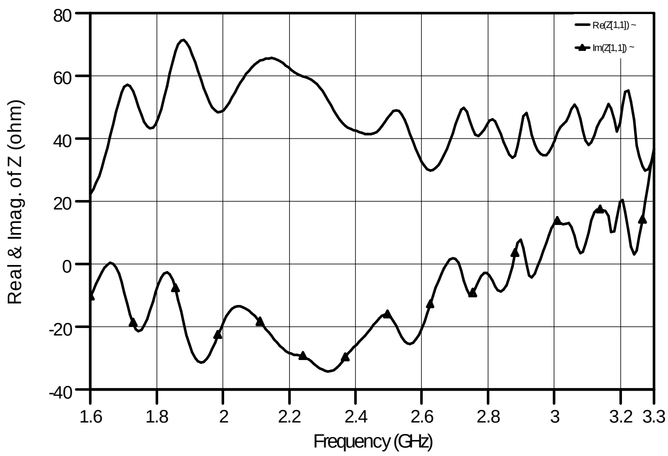

(b)

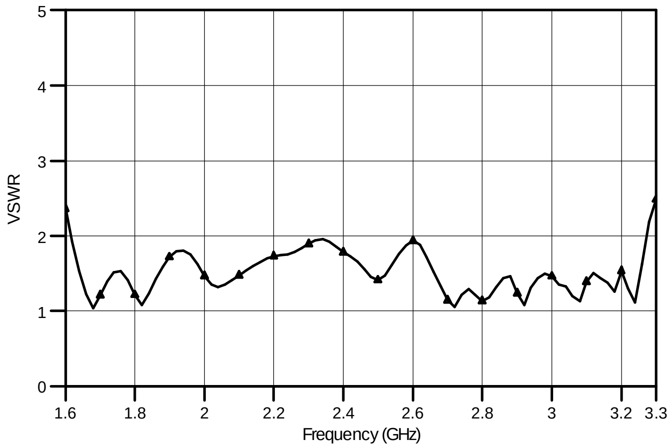

(c)

Figure(5.33) (a) Smith chart ,(b) Real and imaginary parts of the input impedance,and (c) VSWR of the optimum capacitively-fed stacked shorted rectangular-slot MPA with parameters:L_f*=7.03cm,*$(L_s \times W_s)$*=(4.2x0.93)cm*^{2}*,*L_r*=8.9cm,*(x_f,y_f)*=(0,3.5cm),*h_{rf}*=0.8cm,*h_{fc}*=0.16 cm,*h_{cg}*=1.12cm,*$(L_{short} \times W_{short})$*=(0.8x6.09)cm*^{2}*,*$(x_{shift},y_{shift})$*=(0.93cm,1.4cm) simulated by MOP and gives BW of 67.7%.*

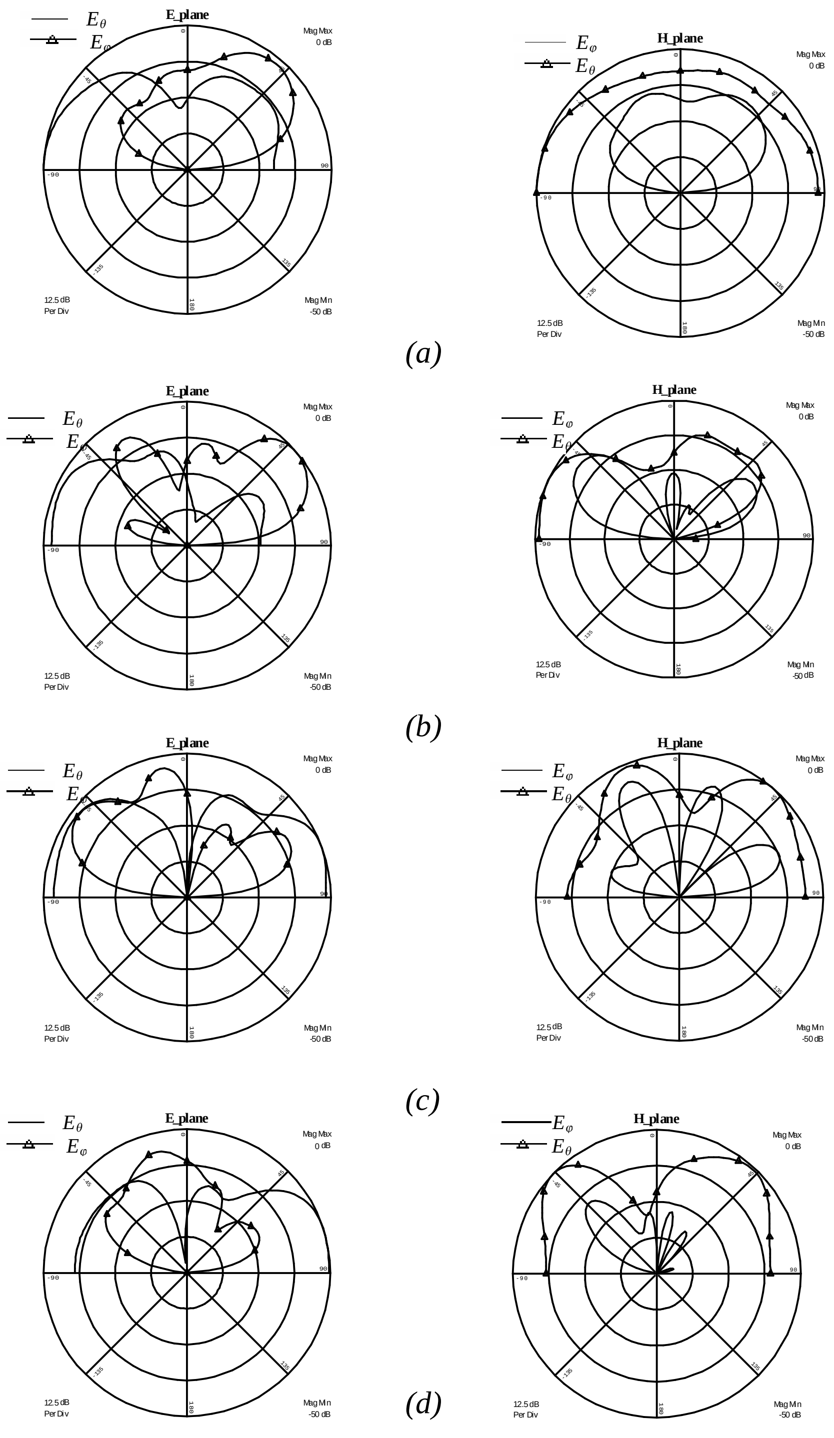

Figure(5.34) E-plane, andH-plane, radiation patterns of the optimum capacitively-fed stacked shorted rectangular-slot MPA for different frequencies;(a)f=2.15GHz,(b)f=2.45 GHz,(c)f=2.8 GHz,and(d)f= 3.2GHz with parameters: L_f*=7.03cm ,(*L_sxW_s*) =(4.2x0.93)cm*^{2}*,* L_r*=8.9cm,(*x_f*,*y_f*)=(0,3.5cm),*h_{rf}*=0.8cm,*h_{fc}*=0.16cm,*h_{cg}*=1.12cm,(*L_{short}xW_{short}*) =(0.8, 6.09) cm*^{2} *,(*x_{shift}*,*y_{shift}*) =(0.93cm,1.4cm)*

Chapter 6

Conclusion and Suggestions for Future Work

6.1 Conclusion

This dissertation is divided into two branches; the first branch includes designing, studying and analyzing single rectangular MPA (operating at different modes) theoretically (using cavity and aperture models). The theoretical results are compared with that produced via simulation (using MOP). The second branch presents several configurations (single patch, single slotted patch, dual-patches, and dual-patches with short walls printed on thick substrates) designed and simulated for bandwidth enhancement purpose which is suitable for use in the S-band.

The major conclusions of the presented work are listed below:

- The theoretical (cavity) formulations derived for single patch microstrip antenna (with the aid of Matlab computation) proves its good performance for analyzing (radiation pattern and input impedance) the single patch microstrip antenna for any m,n mode.

- The narrow bandwidth of single patch microstrip antenna operating at TM_{03} mode excited by 50Ω coaxial feed probe can be increased (22.6%) with relatively high gain (13.5dB) by increasing the thickness of the dielectric substrate with capacitive-feed excitation technique. A uniform broadside radiation pattern with narrow main lobe without cross-pol components has been obtained.

- The non dominant modes (which make deterioration in the radiation pattern) were appeared beside the dominant one in MPA operating at TM_{03} can be eliminated by choosing the proper feed location using MOP. So the MOP demonstrates its ability and performance to produce a pure dominant mode without undesired modes by selecting the optimum feed position. While experimentally it is very difficult to do that.

- The side lobes that appeared beside the narrow main lobe in the H-plane radiation pattern for a single rectangular MPA operating at TM_{03} mode can be eliminated (using the theoretical formulations with the aid of Matlab computation) by increasing size of the MPA (using high dielectric constant, ε_r=9.8, and large aspect ratio, W/L=2).

- A rectangular-slot etched on square patch (with $\lambda_o/2$ length) printed on thick substrate with 50 Ω coaxial feed-probe excitation can produce large bandwidth (~ 28% for VSWR≤2). A good radiation pattern with relative high gain 14.08 dB is achieved.

- A novel rectangular-slot single-patch microstrip antenna with capacitively- fed can produce very wide bandwidth (85%) with uniform radiation patterns and average gain 11.07 dB.

- The bandwidth of a stacked configuration MPA can be increased from 16% for VSWR≤2 with non uniform radiation patterns for solid feeding patch structure to 27.7% with broadside co-pol radiation pattern in the H-plane, and asymmetric co-pol pattern in the E-plane for slotted feeding patch structure.

- A bandwidth of ~57% for VSWR≤2 can be produced for capacitively-fed stacked slotted MPA. The radiation pattern can be improved by this technique with broadside co-pol components for both E- and H-planes.

- Modifying the stacked slot MPA by using short walls with two types of feeding; direct (contact) and indirect (non contact) coaxial probe feed, can improve the bandwidth from 30% (for direct-feed) to 67.7% for (indirect-feed). The radiation patterns for both structures are non uniform.

- From the above results, one can conclude that the slot etched in the patch plays an important role in bandwidth enhancement and in the form of the radiation pattern, also one can conclude that the capacitively-feed excitation technique proofs its performance in producing large bandwidth (in comparison with direct coaxial feed)with keeping the same form of the radiation pattern.

- Basically the MOP built to analyze and simulate the microwave circuits; amplifiers, transmission lines, attenuators, etc. In the presented work the simulating package (MOP) proves its ability and performance for the analysis of the single solid MPA, slotted MPA, capacitive feeding structure of MPA, and stacked MPA with a high degree of accuracy which avoid us to go to the experimental measurements which take more time and it is expensive.

- The confidence in the performance of the MOP comes from its ability and performance with a high degree of accuracy in simulating a wide range of published works in various types of MPAs; single, stacked, stacked with short wall configurations with direct and capacitive feed excitation.

- The presented examples can be used in a wide range of resent application spatially in the communication network which omits the form of the pattern for the frequency band.

6.2 Suggestions for Future Work

- Construct a final designs of this study and then take experimental measurements and comparing with theoretical results of this study.

- Follow the modes generated with change the feed location by taking a thermal photographs to the field pattern on the surface. This gives a deep understanding for the antenna performance spatially when comparing with surface current distributions that calculated by the package.

- Investigate deep studies for the generated modes which gives the possibility of using mode diversity principle in antenna.

- Use the principle of the presence more than one feed in single patch which gives a circular polarization with wide frequency band. This field has important studies in the future; space communication field and other applications.

- Study the bandwidth enhancement by taking other shapes of slots (triangular, circular, etc) and more than one slot.

- Study the stacked configuration but with low dielectric substrate in order to avoid the production of surface waves which deteriorate the radiation pattern.

- Analyze the rectangular slot single patch microstrip antenna by using the FDTD method.

Acknowledgements

I would like to acknowledge my supervisors, Dr. Abdul Kareem A. Ali, Dr. Ahmad K. Ahmad, and Dr. Sabah M. Juma for introducing me into the field of microstrip antenna and their encouragement, assistance, and support. I spatially appreciate the help of Dr. Abdul Kareem A. Ali for his guidance throughout the work.

Thanks are due to the Dean of the College of Science, Head of the Physics Department, and the staff of the Department for their kind attention.

Sincere thanks must also go to my colleagues Ph.D. student Basher J. Al aani, Ammar A. Alrawi, Ahmed Aziz , and Mohammad Khalil for their kind assistance and encouragement.

Last but not least, I would like to extend my thanks to my husband Akeel A. Mohammad, my mother, my father and to all my loved ones for their support and encouragement.

Hind

Abstract

In the present work a design of wideband microstrip patch antennas have been investigated. These antennas were designed to operate in the S-band. Different techniques were followed in order to satisfy this aim; Single solid patch, single slotted patch, stacked, and stacked shorted configurations printed on thick substrate with rather high permittivity (ε_r=4.45). Two types of feeding have been applied; direct (coaxial probe) feed and indirect (capacitive) feed.

Based on the cavity and aperture models, a general method for the analysis of microstrip patch antenna(MPA), for any mode, fed by coaxial probe was introduced.

The performance of the radiation pattern for MPA operating at TM_{03} mode(having narrow main lobe), encourage us to study this mode extensively. This study was focused on eliminate the presence of the side lobes that appeared in the H-plane.

The effect of feed location on eliminates the unwanted modes and keeping only the presence of the wanted one have been studied extensively using the MOP and compared with results obtained by using cavity formulations.

For the design of the antennas a simulation tool Microwave-Office Package (MOP) was used.

In the presented work several techniques for bandwidth (*BW*) enhancement using the MOP have been investigated:

- Bandwidth improvement for single thick rectangular MPA operating at TM_{03} mode with two types of feeding (direct and capacitive feeding techniques) has been investigated. The maximum bandwidth produced is 2.6% for direct and 22.6% for indirect feeding excitation techniques.

- Bandwidth enhancement using stacking structure with three configurations has been investigated. In the first (thin substrate) and second (thick substrate) configurations, an air gap is filled the spacing between the upper and the lower patches. The maximum bandwidth achieved is 3.5% for the first configuration and 11% for the second one with uniform radiation field pattern. In the third configuration, the lower and the upper patches are square. The bandwidth obtained from this structure is 16% with non uniform radiation field pattern.
- Another technique for bandwidth enhancement is presented here. It is based on inductance compensation picture by introducing a capacitor in the antenna structure. This picture is based on cutting a slot in the radiating patch. The maximum bandwidth can be achieved from this design is 27.75% for VSWR≤2 with 14.08dB gain.
- Then another picture of inductance compensation has been combined with the former one in order to increase the bandwidth further. This second picture is based on feeding the slotted radiating patch capacitively. The bandwidth achieved from this combination can be reached 85% for VSWR≤2 and gain of 11.07 dB with uniform radiation field pattern.
- The stacking configuration with the slotted patch as feeding (lower) patch with direct and indirect feeding techniques has been examined. The maximum bandwidth achieved from direct feed stacking configuration is 27.7% while that produced from capacitively-fed stacking configuration is 56.7% for VSWR≤2.
- The stacking configuration presented above has been modified by using short walls also with two types of feedings. The maximum bandwidth achieved from direct feed stacking shorted configuration is 30.6% while that produced from capacitively-fed stacking shorted configuration is 67.7% for VSWR≤2.

Contents   Page No.

List of Symbols

C	Capacitance of the patch
C_A	Capacitive part of the antenna resonant circuit
c	Speed of light
E	Electric field
E_z	Electric field between the rectangular plate and the ground plane
E_o	Maximum amplitude of the E_z field
E_t	Tangential component of the electric field
E_a	Constant electric field over a distance 2a from the edge of the resonator
$E(r)$	Far field
E_θ	θ component of the far field
E_φ	φ component of the far field
H_x	x component of the magnetic field
H_y	y component of the magnetic field
f_c	Center frequency of the band
$(f_r)_{mn}$	Resonance frequency at which the microstrip antennas are to be designed at m,n mode
$(f_r)_e$	Effective resonance frequency
$(f_r)_t$	Resonance frequency of the top patch
h	Height of dielectric substrate
h_{fg}	Dielectric substrate thickness between the feeding patch and the ground plane
h_{rf}	Dielectric substrate thickness between the radiating and the feeding patches
h_{rc}	Dielectric substrate thickness between the radiating patch and the capacitor-strip
h_{cg}	Dielectric substrate thickness between the capacitor-strip and the ground plane
k	Wave number
k_{mn}	Wave number at m,n mode
L	Length of the patch
L_A	Inductive part of the antenna resonant circuit
L_c	Length of the capacitor-strip
L_e	Effective length of the patch
L_{ind}	Inductance of the patch
L_p	Probe inductance
L_r	Length of the radiating (stacking) patch
L_s	Length of the slot
L_t	Length of the top patch

P_c	Power losses in the conductors of the microstrip antenna
P_d	Power losses inside the dielectric
P_r	Power radiated outside the antenna surface
P_T	Total power dissipated by the antenna
Q	Quality factor
Q_T	Total quality factor
R	Resistance of the patch
R_A	Radiation resistance
R_{in}	Input resistance
R_o	Resistance at the radiating edge of the patch
$R(x)$	Resistance at a distance x from the radiating edge of the patch
R_s	Surface resistance
$tand$	Loss tangent of the dielectric
V	Terminal voltage
W	Width of the patch
W_c	Width of the capacitor-strip
W_r	Width of the radiating (stacking) patch
W_T	Total stored energy in the antenna
X_{in}	Input reactance
x_{shift}	Shift in the x-axis between the radiating and the feeding patches
(x_f,y_f)	Coordinates of feed position
y_{shift}	Shift in the y-axis between the radiating and the feeding patches
Z_o	Characteristic impedance of the transmission line
Z_A	Impedance of the patch
Z_{in}	Input impedance of the microstrip antenna
Z_{Total}	Total impedance of the antenna
Γ	Reflection coefficient
Δ	Air gap width between the feeding and the radiating patches
Δl	Line extension
Δl_t	Line extension of the top patch
e_e	Effective dielectric constant
e_r	Dielectric constant of substrate
e_{et}	Effective dielectric constant of the top patch
e_{rf}	Dielectric substrate filled the spacing between the feeding patch and the ground plane
ε_{rr}	Dielectric substrate filled the spacing between the radiating and feeding the patches

e_{rc}	Dielectric substrate filled the spacing between the capacitor-strip and the ground plane
η_o	Intrinsic impedance of free space
l_o	Wavelength of free space
l_d	Wavelength inside the dielectric substrate
μ	Permeability
σ	Conductivity
w	Angular frequency

List of Abbreviations

BW	Bandwidth
HPBW	Half-power beamwidth
$HPBW_E^o$	Half power beam width in E-plane
$HPBW_H^o$	Half power beam width in H-plane
MPA	Microstrip patch antenna
MOP	Microwave-office package
MICs	Microwave integrated circuits
SPAs	Suspended plate antennas
VSWR	Voltage standing wave ratio

List of Figures

List of Tables

Appendix A

Far field calculation

```
% example for calculating the far field of the published work
k=24.86;b=5.71e-002;c=3.8e-002;h=.159e-002;
t=-pi/2:.01:pi/2;
s=0
m=0;n=1;
Ex=[[(-1-(-1)^m)*j.*sin(k*b.*sin(t).*cos(s))+(1-(-1)^m)*cos(k*b*sin(t).*cos(s))].*
sinc(k*h/(2*pi)*sin(t).*cos(s)).*j^n.*[sinc((k*c*sin(t).*sin(s)+n*pi/2)/pi)+(-
1)^n*sinc((k*c*sin(t).*sin(s)-n*pi/2)/pi)]];
Ey=[(-1-(-1)^n)*j.*sin(k*c.*sin(t).*sin(s))+(1-(-1)^n)*cos(k*c*sin(t).*sin(s))].*
sinc(k*h/(2*pi)*sin(t).*sin(s)).*j^m.*[sinc((k*b*sin(t).*cos(s)+m*pi/2)/pi)+(-
1)^m*sinc((k*b*sin(t).*cos(s)-m*pi/2)/pi)];
Etheta=(Ex*cos(s)+Ey*sin(s));
Ephi=-Ex*sin(s).*cos(t)+Ey*cos(s).*cos(t)
polar(t,abs(Ephi))

s2=pi/2
Ex2=[[(-1-(-1)^m)*j.*sin(k*b.*sin(t).*cos(s2))+(1-(-1)^m)*cos(k*b*sin(t).*
cos(s2))].*sinc(k*h/(2*pi)*sin(t).*cos(s2)).*j^n.*[sinc((k*c*sin(t).*sin(s2)+n*pi/2)/pi)+(-
1)^n*sinc((k*c*sin(t).*sin(s2)-n*pi/2)/pi)]];
 Ey2=[(-1-(-1)^n)*j.*sin(k*c.*sin(t).*sin(s2))+(1-(-1)^n)*cos(k*c*sin(t).*sin(s2))].*
sinc(k*h/(2*pi)*sin(t).*sin(s2)).*j^m.*[sinc((k*b*sin(t).*cos(s2)+m*pi/2)/pi)+(-
1)^m*sinc((k*b*sin(t).*cos(s2)-m*pi/2)/pi)];
Et2=(Ex2*cos(s2)+Ey2*sin(s2));
Ephi2=-Ex2*sin(s2).*cos(t)+Ey2*cos(s2).*cos(t);
figure (2)
polar(t,abs(Et2))
```

Appendix B

Input Impedance calculation

```
%example for calculating the input impedance as a function of feed location of the
published work
%W=2c,L=2b
fr=1.19e+009; er=2.62  ;tand=.001;u=4*pi*1e-007;h=.159e-002;xo=5.33e-002;
yo=0.76e-002;m=0;n=1;W=11.43e-002;L=7.62e-002;V=1;
Eo=(h*cos(m*pi*xo/W)*cos(n*pi*yo/L))^-1;
xo=5.33e-002;y1=2.29e-002;
xo=5.33e-002;y2=3.05e-002;

Eo1=(h*cos(m*pi*xo/W)*cos(n*pi*y1/L))^-1;
Eo2=(h*cos(m*pi*xo/W)*cos(n*pi*y2/L))^-1;

E1=h^2*Eo^2*dblquad(inline('([[[[(-1-(-1)^0)*j.*sin(1.42*sin(x).*cos(y))+(1-(-
1)^0)*cos(1.42*sin(x).*cos(y))].*sinc(0.0198/pi*sin(x).*cos(y))* 3.81e-002*j^1.*
[sinc((0.9496*sin(x).*sin(y)+1*pi/2)/pi)+(-1)^1*sinc((0.9496*sin(x).* sin(y)-
1*pi/2)/pi)]].*cos(y)+[[(-1-(-1)^1)*j.* sin(0.9496*sin(x).*sin(y))+(1-(-1)^1)*
cos(0.9496*sin(x).*sin(y))]*5.715e-002*j^0.*sinc(0.0198/pi*sin(x).*sin(y)).*
[sinc((1.42*sin(x).*cos(y)+0*pi/2)/pi)+(-1)^0*sinc((1.42*sin(x).*cos(y)-
0*pi/2)/pi)]].*sin(y)].^2].*sin(x))'),0,pi/2,0,2*pi);

E2=h^2*Eo^2*dblquad(inline('([[-[[(-1-(-1)^0)*j.*sin(1.42*sin(x).*cos(y))+(1-(-
1)^0)*cos(1.42*sin(x).*cos(y))].*sinc(0.0198/pi*sin(x).*cos(y))*3.81e-002*j^1.*
[sinc((0.9496*sin(x).*sin(y)+1*pi/2)/pi)+(-1)^1*sinc((0.9496*sin(x).*sin(y)-
1*pi/2)/pi)]].*sin(y).*cos(x)+[[(-1-(-1)^1)*j.*sin(.9496*sin(x).*sin(y))+(1-(-1)^1)*
cos(.9496*sin(x).*sin(y))]*5.715e-002*j^0.*sinc(0.0198/pi*sin(x).*sin(y)).*
[sinc((1.42*sin(x).*cos(y)+0*pi/2)/pi)+(-1)^0*sinc((1.42*sin(x).*cos(y)-
0*pi/2)/pi)]].*cos(y).*cos(x)].^2].*sin(x))'),0,pi/2,0,2*pi);

Pr=(377)^-1*(fr/3e+008)^2*(E1+E2);
q2=dblquad(inline('cos(0*pi*x/11.43e-002).^2.*cos(1*pi*y/7.62e-002).^2'),0,11.43e-
002,0,7.62e-002);

Pd=2*pi*fr*er*8.85e-012*tand*h*Eo^2*q2/2 ;
q3=dblquad(inline('[1/7.62e-002*cos(0*pi*x/11.43e-002).*sin(1*pi*y/7.62e-002)].^2
+[0/11.43e-002*sin(0*pi*x/11.43e-002).*cos(1*pi*y/7.62e-002)].^2'),0,11.43e-
002,0,7.62e-002);

Pc=-(pi*fr*4e-007*pi/5.7e+007)^.5*(1/(2*fr*4e-007*pi))^2*Eo^2*q3;
Pt=Pr+Pc+Pd;
Wt=Pd/(2*pi*fr*tand);
Qt=2*pi*fr*Wt/Pt;
R=V^2/(2*Pt);
L=R/(2*pi*fr*Qt);
C=Qt/(2*pi*fr*R);
f=1.16e+009:.001e+009:1.22e+009;
for i=1:61
```

```
Zin(i)=1.5/[1/R+j*2*pi*f(i)*C+1/(j*2*pi*f(i)*L)];
end

E11=h^2*Eo1^2*dblquad(inline('([[[[(-1-(-1)^0)*j.*sin(1.42*sin(x).*cos(y))+(1-(-
1)^0)*cos(1.42*sin(x).*cos(y))].*sinc(0.0198/pi*sin(x).*cos(y))* 3.81e-002*j^1.*
[sinc((0.9496*sin(x).*sin(y)+1*pi/2)/pi)+(-1)^1* sinc((0.9496*sin(x).*sin(y)-
1*pi/2)/pi)]].*cos(y)+[[(-1-(-1)^1)*j.*sin(0.9496*sin(x).*sin(y))+(1-(-1)^1)*
cos(0.9496*sin(x).*sin(y))]*5.715e-002*j^0.*sinc(0.0198/pi*sin(x).*sin(y)).*
[sinc((1.42*sin(x).*cos(y)+0*pi/2)/pi)+(-1)^0*sinc((1.42*sin(x).*cos(y)-
0*pi/2)/pi)]].*sin(y)].^2].*sin(x))'),0,pi/2,0,2*pi);

E21=h^2*Eo1^2*dblquad(inline('([[-[[(-1-(-1)^0)*j.*sin(1.42*sin(x).*cos(y))+(1-(-
1)^0)*cos(1.42*sin(x).*cos(y))].*sinc(0.0198/pi*sin(x).*cos(y))*3.81e-002*j^1.*
[sinc((0.9496*sin(x).*sin(y)+1*pi/2)/pi)+(-1)^1*sinc((0.9496*sin(x).*sin(y)-
1*pi/2)/pi)]].*sin(y).*cos(x)+[[(-1-(-1)^1)*j.*sin(.9496*sin(x).*sin(y))+(1-(-
1)^1)*cos(.9496*sin(x).*sin(y))]*5.715e-002*j^0.*sinc(0.0198/pi*sin(x).*sin(y)).*
[sinc((1.42*sin(x).*cos(y)+0*pi/2)/pi)+(-1)^0*sinc((1.42*sin(x).*cos(y)-
0*pi/2)/pi)]].*cos(y).*cos(x)].^2].*sin(x))'),0,pi/2,0,2*pi);

Pr1=(377)^-1*(fr/3e+008)^2*(E11+E21);
Pd1=2*pi*fr*er*8.85e-012*tand*h*Eo1^2*q2/2 ;
Pc1=-(pi*fr*4e-007*pi/5.7e+007)^.5*(1/(2*fr*4e-007*pi))^2*Eo1^2*q3;
Pt1=Pr1+Pc1+Pd1;
Wt1=Pd1/(2*pi*fr*tand);
Qt1=2*pi*fr*Wt1/Pt1;
R1=V^2/(2*Pt1);
L1=R1/(2*pi*fr*Qt1);
C1=Qt1/(2*pi*fr*R1);
f=1.16e+009:.001e+009:1.22e+009;
for i=1:61

Zin1(i)=1.5/[1/R1+j*2*pi*f(i)*C1+1/(j*2*pi*f(i)*L1)];
end

E12=h^2*Eo2^2*dblquad(inline('([[[[(-1-(-1)^0)*j.*sin(1.42*sin(x).*cos(y))+(1-(-
1)^0)*cos(1.42*sin(x).*cos(y))].*sinc(0.0198/pi*sin(x).*cos(y))* 3.81e-002*j^1.*
[sinc((0.9496*sin(x).*sin(y)+1*pi/2)/pi)+(-1)^1*sinc((0.9496*sin(x).*sin(y)-
1*pi/2)/pi)]].*cos(y)+[[(-1-(-1)^1)*j.*sin(0.9496*sin(x).*sin(y))+(1-(-1)^1)*
cos(0.9496*sin(x).*sin(y))]*5.715e-002*j^0.*sinc(0.0198/pi*sin(x).*sin(y)).*
[sinc((1.42*sin(x).*cos(y)+0*pi/2)/pi)+(-1)^0*sinc((1.42*sin(x).*cos(y)-
0*pi/2)/pi)]].*sin(y)].^2].*sin(x))'),0,pi/2,0,2*pi);

E22=h^2*Eo2^2*dblquad(inline('([[-[[(-1-(-1)^0)*j.*sin(1.42*sin(x).*cos(y))+(1-(-
1)^0)*cos(1.42*sin(x).*cos(y))].*sinc(0.0198/pi*sin(x).*cos(y))*3.81e-002*j^1.*
[sinc((0.9496*sin(x).*sin(y)+1*pi/2)/pi)+(-1)^1*sinc((0.9496*sin(x).*sin(y)-
1*pi/2)/pi)]].*sin(y).*cos(x)+[[(-1-(-1)^1)*j.*sin(.9496*sin(x).*sin(y))+(1-(-
1)^1)*cos(.9496*sin(x).*sin(y))]*5.715e-002*j^0.*sinc(0.0198/pi*sin(x).*sin(y)).*
[sinc((1.42*sin(x).*cos(y)+0*pi/2)/pi)+(-1)^0*sinc((1.42*sin(x).*cos(y)-
0*pi/2)/pi)]].*cos(y).*cos(x)].^2].*sin(x))'),0,pi/2,0,2*pi);
```

```
Pr2=(377)^-1*(fr/3e+008)^2*(E12+E22);
Pd2=2*pi*fr*er*8.85e-012*tand*h*Eo2^2*q2/2 ;
Pc2=-(pi*fr*4e-007*pi/5.7e+007)^.5*(1/(2*fr*4e-007*pi))^2*Eo2^2*q3;
Pt2=Pr2+Pc2+Pd2;
Wt2=Pd2/(2*pi*fr*tand);
Qt2=2*pi*fr*Wt2/Pt2;
R2=V^2/(2*Pt2);
L2=R2/(2*pi*fr*Qt2);
C2=Qt2/(2*pi*fr*R2);
f=1.16e+009:.001e+009:1.22e+009;
for i=1:61

Zin2(i)=1.5/[1/R2+j*2*pi*f(i)*C2+1/(j*2*pi*f(i)*L2)];
end
plot(f,Zin);
hold on
plot(f,Zin1,'--');
hold on
plot (f,Zin2,'-.')
hold on
plot(1.19e+009,125,'o')
hold on
plot(1.185e+009,104,'o')
hold on
plot(1.18e+009,60,'o')
hold on
plot(1.172e+009,38,'o')
hold on
plot(1.195e+009,95,'o')
hold on
plot(1.21e+009,20,'o')
hold on
plot(1.18e+009,23,'+')
hold on
plot(1.19e+009,50,'+')
hold on
plot(1.195e+009,32,'+')
hold on
plot(1.205e+009,15,'+')
hold on
plot(1.18e+009,8,'x')
hold on
plot(1.195e+009,13,'x')

%plot(f,imag(Zin1));
figure(2);
plot(f,imag(Zin));
hold on
plot(f,imag(Zin1),'--');
```

```
hold on
plot(f,imag(Zin2),'-.')
hold on
plot(1.175e+009,63,'o')
hold on
plot(1.18e+009,70,'o')
hold on
plot(1.185e+009,50,'o')
hold on
plot(1.19e+009,-20,'o')
hold on
plot(1.195e+009,-57,'o')
hold on
plot(1.21e+009,-38,'o')
hold on
plot(1.18e+009,38,'+')
hold on
plot(1.19e+009,5,'+')
hold on
plot(1.195e+009,-18,'+')
hold on
plot(1.205e+009,-15,'+')
hold on
plot(1.18e+009,18,'x')
hold on
plot(1.19e+009,9,'x')
hold on
plot(1.195e+009,3,'x')
```

<u>Certification</u>

We certify that this thesis entitled "Bandwidth Improvement for Rectangular Microstrip Antennas" is prepared by Hind Subhi Hussain under our supervising at the College of Science of Al-Nahrain University in partial fulfillment of the requirements for the degree of Doctor of Philosophy in physics.

Signature:
Name: ***Dr. Abdul Kareem Abed Ali***
Title: ***Senior Scientific Researcher***
Address: Ministry of Science
Head of Space Observatory and Simulation Research Center, Aeronautics and Space Directorate
Date: ***6 /3/2007***

Signature:
Name: ***Dr. Ahmad K. Ahmad***
Title: ***Assistant Professor***
Address: College of Science
Al- Nahrain University

Date: **6** ***/3/2007***

In view of the available recommendation, I forward this thesis for debate by the examining committee

Signature:
Name: ***Dr. Ahmad K. Ahmad***
Title: ***Assistant Professor***
Address: ***Head of Physics Department***
Date: ***6 /3/2007***

Examining Committee Certificate

We certify that we have read the thesis entitled "Bandwidth Improvement for Rectangular Microstrip Antennas" and as an examining committee, examined the student Hind Subhi Hussain in its contents and what is related to it, and that in our opinion it is adequate for the partial fulfillment of the requirements for the degree of Doctor of Philosophy in physics.

Signature:
Name: **Dr. Raad Sami Fyath**
(Chairman, Professor)
Date: **:** / / 2007

Signature:
Name: **Jamal W. Salman**
(Member, Professor)
Date**:** / / 2007

Signature:
Name: **Dr. Jaber S. Azez**
(Member, Assistant Professor)
Date**:** / / 2007

Signature:
Name: **Dr. Ahmed H. Abood**
(Member, Assistant Professor)
Date**:** / / 2007

Signature:
Name: **Dr. Hussain Juma Abbas**
(Member, Assistant Professor)
Date**:** / / 2007

Signature:
Name: **Dr. Abdul Kareem Abed Ali**
(Supervisor, Senior Scientific Researcher)
Date**:** / / 2007

Signature:
Name: **Dr. Ahmad K. Ahmad**
(Supervisor, Assistant Professor)
Date**:** / / 2007

Signature:
Name: Sabah M. Juma
(Supervisor, Professor)
Date**:** / / 2007

I here by certificate upon the decision of the examining committee

Signature:
- Name: **Dr. LAITH ABDUL AZIZ AL-ANI**
Title: Assistant Professor
(Dean of the college of science)
Date**:** / / 2007

الاسم: هند صبحي حسين محمد الراوي
العنوان:بغداد – الغزالية- محلة ٦١٤ – زقاق ١- رقم الدار ٢٦
الهاتف: ٠٧٧٠٢٥٧١٠٤١
البريد الالكتروني: hindalrawi@yahoo.com
عنوان الأطروحة: تحسين عرض الحزمة للهوائيات الشريطية المستطيلة

References

[1] F.R. Connor, "Antennas," printed in Great Britain by the Pitman Press, Bath, 1972.

[2] G.A. Dechamps, " Microstrip microwave antenna, " *3rd USAF Symposium on Antenna*, 1953.

[3] R.E. Munson, "Conformal microstrip antennas and microstrip phase arrays, " *IEEE Trans. Antennas Propaga.*, vol. AP-22, pp.47-78, 1974.

[4] D. C. Chang, "Special issue, " *IEEE Trans. Antennas Propaga.*, vol. AP-29,1981.

[5] I.J. Bahl and P. Bhartia, " Microstrip antennas," Artech Hous Inc.,1980.

[6] R. C. Johnson, "Antenna engineering handbook, " McGraw-Hill, 3rd ed. Inc.1993.

[7] T.A. Milligan, "Modern antenna design, " John Wily& Sons Inc., 2nd ed 2005.

[8] J. R. James and P. S. Hall, "Handbook of microstrip antennas," *IEE Electromagnetic Waves* Series 28, Peter Peregrinus Ltd, London,1989.

[9] D. Guha, "Broadband design of microstrip antennas: recent trends and developments, " *Mechanics, Automatic Control and Robotics*, vol.3, no.15, pp. 1083-1088, 2003.

[10] Z. N. Chen, M.Y.W.Chia, " A Novel center-slot-fed suspended plate antenna, " *IEEE Trans. Antennas Propaga.*, vol. 51, no. 6, pp.1407-1410, 2003.

[11] Z. N. Chen, M. Y. W. Chia, " Broadband suspended plate antennas fed by double L-shaped strips," *IEEE Trans. Antennas Propaga.*, vol. 52, no. 9, pp. 2496-2500, 2004.

[12] F. Yang, X. Zhang, X.Ye, and Y. Rahmat-Samii, “ Wide-band E-shaped patch antennas for wireless communications, ” *IEEE Trans. Antennas Propaga.*, vol. 49, no. 7, pp.1094-1100, 2001.

[13] N. Herscovici, “ New considerations in the design of microstrip antennas, ” *IEEE Trans. Antennas Propaga.,* vol. 46, no. 6, pp. 807-8012, 1998.

[14] N. Herscovici, “ A wide-band single-layer patch antenna, ” *IEEE Trans. Antennas Propaga.,* vol. 46, no. 4, pp. 471-474, 1998.

[15] A. Kuchar, “Aperture-coupled microstrip patch antenna array,” M. Sc. Thesis,Technischen Universität Wien , Deutsch-Wagram,1996.

[16] A.G. Derneryd , “ A Theoretical investigation of the rectangular microstrip antenna element,” *IEEE Trans Antennas Propagat.,* vol. AP-26, no. 4, pp. 532-535, 1978.

[17] D. M. Pozar, “Input impedance and mutual coupling of rectangular microstrip antennas,” *IEEE Trans. Antennas Propogat.,* vol. AP-30, no. 6, pp. 1191-1196, 1982.

[18] Z.N. Chen M.Y.W. Chia, “Center fed microstrip patch antenna,” *IEEE Trans. Antennas Propaga.*, vol. 51, no. 3, pp. 483-487, 2003.

[19] V. Voipio, “Wideband patch array techniques for mobile communications,” M.Sc. Thesis, Helsinki University of Technology, 1998.

[20] D. S. Hernandez and I.D. Robertson, “A survey of broadband microstrip patch antennas,” *Microwave Journal*, pp. 60-84, 1996.

[21] A. Hussein , “Microstrip backfier antenna, ” M.Sc. Thesis, College of Science , Al-Nahrain university (Formerly Saddam University), Baghdad, Iraq,1995.

[22] E. Chang, S. A. Long and W. F. Richards, “An experimental investigation of electrically thick rectangular microstrip antennas,” *IEEE Trans. Antennas Propagat*., vol. AP-34, no. 6, pp. 767-772, 1986.

[23] K.F. Lee, R.Q. Lee, T.Talty, "Microstrip subarray with coplanar and stacked parasitic elements, " *Electron. Lett.*, vol.26, no.10, pp.668-669,1990.

[24] G.Vandenbosh and A.V. Capelle, " A study of the effect of the top patch in rectangular dual patch microstrip antenna," *Ann. Telecommun.*, vol 47, n 3-4,1992.

[25] P.K. Singhal, B. Dhaniram, and S. Banerjee, " A stacked square patch slotted broadband microstrip antenna," *Journal of Microw. Optoelectron.*, vol 3, no.2,pp. 60-66,2003.

[26] Z. N. Chen, M. Y. W. Chia, and C. L. Lim, "A stacked suspended plate antenna," *Microw. Opt. Technol. Lett.*, vol. 37, no.5, pp. 337-339, 2003.

[27] C.S. Lee, V. Nalbandian, and F. Schwering, " Planar dual-band microstrip antenna," *IEEE Trans. Antennas Propagat.*, vol. 43, no. 8, pp. 892-894, 1995.

[28] J.Ollikainen, M.Fischer, and P.Vainikainen, " Thin dual-resonant stacked shorted patch antenna for mobile communications, " *Electron. Lett.*,vol.35,no.6, pp. 437-438, 1999.

[29] J.T.Rowley, and R. B. Waterhouse, " Performance of shorted microstrip patch antennas for mobile communications handsets at 1800 MHz, " *IEEE Trans. Antennas Propagat.*, vol. 47, no.5, pp. 815-822, 1999.

[30] R.L. Lee, G.de Kean,M.M.Tentzeris, and J.Laskar, " Development and analysis of a folded shorted-patch antenna with reduced size, " *IEEE Trans. Antennas Propagat.*, vol. 52, no.2, pp. 555-560, 2004.

[31] H.F.Pues and A.R. Van de Capelle, "An impedance matching technique for increasing the bandwidth of microstrip antennas," *IEEE Trans. Antennas Propagat.*, vol. 37, no. 11, pp. 1345-1354, 1989.

[32] H. An, B.K.J.C.Nauwelaers, and A.R. Van de Capelle, "Broadband microstrip antenna design with the simplified real frequency technique," *IEEE Trans. Antennas Propagat.*, vol. 42, no. 2, pp. 129-136, 1994.

[33] D.de Haaij, J.W. Odendaal, and J.Joubert, "Increasing the bandwidth of a microstrip patch antenna with a single parallel resonant circuit," *in Procee. of the IEEE Africon 2002 Conf.*, vol.2, George, South Africa, pp. 527-529, 2002.

[34] Z. N. Chen and M.Y.W. Chia, "Design of broadband probe-fed plate antenna with stub," *IEE Procee. Microw. , Antennas Propagat.*, vol.148, no.4, pp. 221-226, 2001.

[35] C.L.Make, K.M. Luk, K.F.Lee, and Y.L.Chow, " Experimental study of a microstrip patch antenna with an L-shape probe," *IEEE Trans. Antennas Propagat.*, vol. 48, no. 5, pp. 777-783, 2000.

[36] J.Park, H.Gina, and S.H. Baik, "Design of a modified L-probe fed microstrip patch antenna, " *IEEE Trans. Antennas and Wireless Propagat. Lett.*, vol. 3, pp.117-119, 2004.

[37] Z. N. Chen and M.Y.W. Chia, " Broadband probe-fed L-shaped plate antenna," *Microw. and Opt. Technol. Lett.*, vol.26, no.3, pp. 204-206, 2000.

[38] G.A.E.Vandenbosch, " Network model for capacitively fed microstrip element, " *Electron. Lett.*, vol.35, no.19, pp. 1597-1599, 1999.

[39] Z. N. Chen and M.Y.W. Chia, " Broadband suspended plate antenna with probe-fed strip," *IEE Procee. on Microw., Antennas Propagat.*, vol.148, no.1, pp.37-40, 2001.

[40] M.A. Gonzalez de Aza, J.Zapata, and J.A. Encinar, " Broad-band cavity-backed and capacitively probe-fed microstrip patch arrays, " *IEEE Trans. Antennas Propagat.*, vol. 48, no. 5, pp. 784-789, 2000.

[41] J.W. Jang, " Characteristics of a large bandwidth rectangular microstrip-fed inserted triangular patch in a circular slot antenna," *Microwave Journal*, vol.45, no.5,pp. 288-298,2002.

[42] K.F. Tong, K.M.Luk, K.F.Lee, and R.Q.Lee, " A Broad-band U-slot rectangular patch antenna on a microwave substrate, " *IEEE Trans. Antennas Propagat*., vol. 48, no. 6, pp. 954-960, 2000.

[43] X.X.Guo, K.M.Luk, and K.F.Lee, " A Quarter-wave U-shaped patch antenna with two unequal arms for wideband and dual frequency operation, " *IEEE Trans. Antennas Propagat*., vol. 50, no. 8, pp. 1082-1086, 2002.

[44] W.F. Richards, Y.T. Lo, and D.D. Harrison, "An improved theory for microstrip antennas and applications," *IEEE Trans. Antennas Propagat*., vol. AP-29, no. 1, pp. 38-46, 1981.

[45] Y. T. Lo, D. Solomon and W. F. Richards, "Theory and experiment on microstrip antennas," *IEEE Trans Antennas Ppropagat.*, vol. AP-27, no. 2, pp. 137-145, 1979.

[46] E. H. Newman, P. Tulyathan, "Analysis of microstrip antennas using moment method," *IEEE Trans. Antennas Propaga.*, vol. AP-29, no. 1, pp.47-53, 1981.

[47] A. G. Derneryd, and A. G. Lind, "Extended analysis of rectangular microstrip resonator antennas," *IEEE Trans. Antennas Propagat*., vol. AP-27, no.6, pp. 846-849, 1979.

[48] G. P. Gauthier and G. M. Rebeiz, "Microstrip antennas on synthesized low dielectric-constant substrates," *IEEE Trans. Antennas Propagat*., vol. 45, no. 8, pp. 1310-1313, 1997.

[49] V. Gupta, S.Sinha, S.K.Koul, and B.Bhat, "Wideband dielectric resonator loaded suspended microstrip patch antennas," *Microw. Opt. Technol. Lett.* ,vol.37, no.4,pp. 300-302, 2003.

[50] R. K. Mishra and T. Milligan, "Cross-polarization tolerance requirements of square microstrip patches, " *IEEE Antennas Propagat*. magazine, vol. 38, no. 2, pp. 56-58, 1996.

[51] M. N. O. Sadiku , " Elements of electromagnetics," A division of Holt, Rinehart and Winston,Inc.1989.

[52] P. Hammer, D. V. Bouchaute, D. Verschraeven, and A. V. Capelle , " A model for calculating the radiation field of microstrip antennas," *IEEE Trans. Antennas Propagat*., vol. AP-27, no.2, pp. 267-270, 1979.

[53] W. L. Stutzman and G. A. Thiele, "Antenna theory and design,"John Wily & Sons, 1981.

[54] A. A. Abdul Karim, "Theoretical and experimental investigation of circular-shaped microstrip antennas," Ph.D. Thesis, Department of physics, College of Science, Al-Nahrain University, 1996.

[55] Z.F. Lui, P.S. Kooi, L.W. Li, M.S. Leong, and T.S. Yeo, " A method for designing broad-band microstrip antennas in multilayered planar structures," *IEEE Trans. Antennas Propagat*., vol. 47, no.9 ,pp. 1416-1420, 1999.

[56] J. Huang, "The finite ground plane effect on the microstrip antenna radiation patterns," *IEEE Trans. Antennas Propagat*., vol. AP-31, no.4, pp. 649-653, 1983.

[57] A.A. Mohammed, H. Subhi, A.K. Ahmad, S.M. Juma, " Cavity model analysis of rectangular microstrip antenna operating in TM_{03} mode", International conference on Information & communication technologies: from theory to application- ICTTA'06, 24-28 April, Damascus, Syria.

[58] L.I. Basilio, A. Khayat, J. T. Williams, and S. A. Long, " The dependence of the input impedance on feed position of probe and microstrip line-fed patch antennas," *IEEE Trans. Antennas Propogat.*, vol. 49, no. 1, pp. 45-47, 2001.

[59] K.R. Carver and J.W. Mink, " Microstrip antenna technology," *IEEE Trans. Antennas Propagat*., vol. Ap-29, pp. 2-24, 1981

[60] R.B.Waterhouse ," Design of probe-fed stacked patches," *IEEE Trans. Antennas Propagat*., vol. 47, no.12, pp. 1780-1784, 1999.

[61] Y.X. Guo, C.L. Make,K.M. Luk, and K.F.Lee,“ Analysis and design of L-probe proximity fed-patch antennas,” *IEEE Trans. Antennas Propagat.*, vol. 49,no.2, pp. 145-149, 2001.

[62] Y.X. Guo, K.M Luk, and K.F. Lee, “ Broadband dual polarization patch element for cellular-phone base stations, ” *IEEE Trans. Antennas Propagat.*, vol. 50,no.2, pp. 251-253, 2002.

[63] K. F. Lee, K. M. Luk, K. F. Tong, S. M. Shum, T. Huynh, and R. Q. Lee, “Experimental and simulation studies of coaxially fed U-slot rectangular patch antenna,” *Inst. Elect. Eng. Proc. Microwave Antennas Propagat.*, vol. 144, pp. 354–358, 1997.

[64] S.Gao, J.Li,“ FDTD analysis of a sized-reduced, dual frequency patch antenna,” *Progress In Electromagnetics Research, PIER* 23, 59-77,1999

[65] Y. X. Guo, K. M. Luk, and K. F. Lee,“ L-probe fed thick-substrate patch antenna mounted on a finite ground plane,” *IEEE Trans. Antennas Propagat*, vol. 51, no. 8, pp.1955-1963, 2003.

Republic of Iraq
Ministry of Higher Education and Scientific Research
Al-Nahrain University
College of Science

BANDWIDTH IMPROVEMENT FOR RECTANGULAR MICROSTRIP ANTENNAS

A THESIS
SUBMITTED TO THE COLLEGE OF SCIENCE OF Al-NAHRAIN UNIVERSITY IN PARTIAL FULFILLMENT OF THE REQUIREMENTS FOR THE DEGREE OF DOCTOR OF PHILOSOPHY
IN

PHYSICS

By

Hind Subhi Hussain Al-Rawi

(B.Sc. 1993)

(M.Sc. 1996)

Shawal 1427A.H.
November 2006 A.D.

الخلاصة

فـي العمـلِ الحـالي تـم تصـميم ودراسـة هوائيـات شـريطية ذات حزمـة ترددية واسـعة صُمّمتْ للإشتِغال في حزمةS-band .عدة تقنيات اتبعت لتحقيق هذا الهدف: هوائي شريطي ذو رقعه مفردة صلبة(لاتحتوي على فتحة) ، هوائي شريطي ذو رقعه مفردة تحتوي على فتحة في المنتصف،هوائي شريطي متعدد الرقع، هوائي شريطي متعدد الرقع ذو جدار موصل يصل بين رقعة التغذية والرقعة المشعة. جميع هذه الرقع مطبوعة على مادة عازلة سميكة ذات ثابت عزل عالي نوعا ما (ε_r=4.45). نوعين من التغذية تم تطبيقه في هذا العمل:تغذية مباشرة بواسطة مجس التغذية المحوري و تغذية غير مباشرة بواسطة اضافة متسعة اسفل رقعة التغذية للحصول على تغذية نوع capacitively.

اعتماداً على نموذ جي الفجوة و الفتحة تم اشتقاق طريقة عامة لتحليل هوائيات الرقعة المفردة(لاي نمط) والتي يتم تغذيتها بواسطة مجس التغذية المحوري

ان اداء هيكل الاشعاع لهوائي شريطي يعمل بنمط TM_{03}(يمتلك فص اساسي ضيق) تشجعنا لدراسة هذا النمط بصورة واسعة. هذه الدراسة ركزت على الغاء وجود الفصوص الجانبية التي تـ ـهر في هيكل الاشعاع عند المستوي H.

تم دراسة تأثير موقع التغذية للتخلص من الانماط غير المرغوب فيها والأحتفاظ بوجود النمط الأساسي بإستخدام برنامج MOP ومقارنتها مع النتائج التي تم الحصول عليها بإستخدام معادلات الفجوة .

ان برنامج المحاكاة الذي تم استخدامه في تصميم الهوائيات هو Microwave-Office (MOP)Package.

في هذا العمل تم تحقيق عدة تقنيات لزيادة عرض الحزمة الترددية بإستخدام برنامجMOP:

- تم زيادة عرض الحزمة لهوائي شريطي ذو رقعة مفردة يعمل عند النمطTM_{03} مع نوعين من تقنيات التغذية: تغذية مباشرة وغير مباشرة بواسطة مجس التغذية المحوري. عرض الحزم الترددية التي تم الحصول عليها للتغذية المباشرة وغير المباشرة على التوالي هي 2.6% و 22.6% .

- تم تحقيق زيادة عرض الحزمة بإستخدام هيكليلية الرقع المتعددة. ثلاث هيكليات قدمت ودرست.في الهيكلية الاولى (عازل خفيف)والهيكلية الثانية (عازل سميك) . ان فجوة هواء تفصل الفراغ بين الرقعتين العليا والسفلى. اعلى عرض حزمة تم الحصول عليه هو 3.5% للهيكلية الاولى و11% للهيكلية الثانية بهيكل مجال اشعاع منتظم. في الهيكلية الثالثة ، كلا الرقعتين العليا والسفلى مربعة .عرض الحزمة التي تم الحصول عليها من هذا التركيب هو 16 % مع هيكل مجال اشعاع غير منتظم.
- تقنية اخرى لتحسين عرض الحزمة مقدمة هنا. انها مبنية على صورة معادلة الحث باضافة متسعة الى تركيب الهوائي. هذه الصورة مبنية على قطع فتحة في الرقعة المشعة. عرض الحزمة الذي تم الحصول عليه من هذا التصميم هو% 27.75عند $VSWR \leq 2$ بكسب 14.08.dB.
- صورة اخرى لمعادلة الحث اندمجت مع السابقة لغرض زيادة عرض الحزمة اكثر. هذه الصورة الثانية مبنية علي تغذية الرقعة المفتوحة المشعة سعوياً. عرض الحزمة المنجز من هذا الدمج يمكن ان يصل الى % 85 عند $VSWR \leq 2$ وبكسب 11.07 dB مع هيكل مجال اشعاعي منتظم.
- تم استخدام هيكلية الرقع المتراصة باستخدام الرقعة المفتوحة كرقعة تغذية(السفلى). أُخذت مع نوعين من تقنيات التغذية: تغذية مباشرة وغير مباشرة. اقصى عرض حزمة تم الحصول عليه من التغذية المباشرة هو % 27.7 بينما تلك التي تم الحصول عليها من التغذية السعوية لهيكلية التراص هو% 56.7 عند$VSWR \leq 2$.
- تم تطوير هيكلية التراص المقدمة مسبقاً باستخدام جدار توصيل بين الرقعتين (رقعة التغذية والرقعة المشعة) ايضاً باستخدام نوعين من تقنيات التغذية(مباتشرة وغير مباشرة). اقصى عرض حزمة تم الحصول عليه من التغذية المباشرة لهيكلية التراص ذات جدار التوصيل هو % 30.6 عند $VSWR \leq 2$. بينما تلك التي تم الحصول عليها من نفس التصميم ولكن ذي تغذية سعوية هو %67.7 عند $VSWR \leq 2$.

بسم الله الرحمن الرحيم

وَعَلَّمَكَ مَالَمْ تَكُن تَعْلَمُ وَكَانَ فَضْلُ اللَّهِ عَلَيْكَ عَظِيمًا

صدق الله العظيم

النساء الآية(١١٣)

جمهورية العراق
وزارة التعليم العالي والبحث العلمي
جامعة النهرين
كلية العلوم

تحسين عرض الحزمة للهوا ئيات الشريطية المستطيلة

رسالة
مقدمة الى كلية العلوم في جامعة النهرين
وهي جزء من متطلبات نيل درجة
دكتوراه فلسفة
في
الفيزياء

اعداد
هند صبحي حسين الراوي

(بكالوريوس ١٩٩٣)
(ماجستير ١٩٩٦)

شوال 1427
تشرين الثاني 2006